NUMERICAL AND EXPERIMENTAL STUDY OF EQUILIBRIUM SWELLING OF STIMULI RESPONSIVE COMPOSITE HYDROGELS

Nader Hamzavi Zarghani

(*M.Eng.*, NUS)

A THESIS SUBMITTED

FOR THE DEGREE OF DOCTOR OF PHILOSOPHY

DEPARTMENT OF MECHANICAL ENGINEERING

NATIONAL UNIVERSITY OF SINGAPORE

2015

Declaration

I hereby declare that the thesis is my original work and it has been written by me in its entirety. I have duly acknowledged all the sources of information which have been used in the thesis.

This thesis has also not been submitted for any degree in any university previously.

Nader Hamzavi Zarghani

13 August 2015

Acknowledgments

First and foremost, I would like to express my gratitude to my supervisors Professor VPW Shim, Dr. Alex Gu, and A/Professor Erik Birgersson. I appreciate their efforts and supports towards pursuit of my aspiration throughout this PhD journey. My primary thanks goes to Dr. Park Woo Tae and Prof. Shim for offering me PhD admission. I would like to thank Prof. Shim who taught me the importance of communication skills. I also thank Dr. Alex Gu who encouraged me to conduct my research on hydrogels. I am grateful of A/Prof. Birgersson as an exemplary advisor, who helped me shape up my character as an independent researcher.

I was lucky to collaborate with prolific researchers around the world from different disciplines. Thanks to Dr. John Tsang who helped to expand my academic network. I wish to thank Professor Aleksey Drozdov who hosted me in Denmark during my research attachment in Danish Technological Institute (DTI), and whose contribution to my research work is noteworthy. Thanks to my dear friend, Dr. Jean-Yves Dewavrin with whom I made a successful collaboration on soft hydrogels. I learned it from him that when there is an obstacle in research, I should face it today, otherwise it will face me tomorrow. I am also grateful of my teammates in Singapore-Stanford Biodesign module who made it possible to convert a concept to a real design to address a clinical need.

It was an unforgettable pleasure to daily meet my dearest friends and colleagues in NUS; Dr. Amir, Dr. Saeid, Emmanuel and and Fleur, Mohammad, Dr. Sarah, Dr. Kyrin, Dr. Chen Yang, Dr. Habib, Dr. Kianoosh, Dr. Long bin, Dr. Jia Shun, Dr. Liu

Jun, Nigel, and Nhan Tien; and also my colleagues in DTI, Dr. Peter, Jose, and Pia. I truly appreciate their valuable inputs and contributions to my research work.

I gratefully thank the kind assistance provided by lab officers of Impact Mechanics Lab: Mr. Joe Low Chee Wah and Mr. Alvin Goh Tiong Lai.

I would like to thank my dear friends in Singapore and Denmark whose presence and fun-loving spirit made the otherwise grueling experience tolerable for me: Reza and Sahba, Omid and Maryam, Ramin and Marjan, Atieh, Soheil and Tannaz, Behdad and Azadeh, Peter and Susan, and Lennart and Ca.

My sincere thanks belong to my parents Hossein and Nezhat and my brothers Navid and Nima through all these years for always being with me when I needed them even if they are thousands of miles away. I would like to acknowledge and extend my heart-felt gratitude to my dearest wife, Ladan, who have made the completion of this thesis possible with her care and love specially during my difficult times.

This thesis would not have been possible without the excellent infrastructure and facilities of NUS, and the generous financial support of A*STAR Graduate Academy.

Contents

Summary

This study addresses the large deformation and transport phenomena of composite gels subjected to swelling with two constituent polymers which have different sensitivity to external stimuli. It is desired to investigate the effect of external stimuli on the equilibrium swelling of two kinds of composite hydrogels: core/shell hydrogels and a natural/synthetic gel.

In the theoretical model, a hydrogel is assumed to be a multi-phase medium including polymer network, solvent and solutes (for the case of ionic hydrogels). Governing equations and constitutive relations are described by means of the free energy imbalance relation. The theoretical model is extended to analyze the equilibrium swelling of core/shell hydrogels which are stimuli-responsive.

The influence of temperature, pH, and ionic strength are studied. First, numerical simulations are provided for the equilibrium swelling of a doubly temperature-sensitive core/shell hydrogel. The equilibrium swelling of poly (N-isopropyl acrylamide)/ poly (N-isopropyl methacrylamide) core/the shell with different volume phase transition temperature (VPTT) for each domain has been determined by finding the mutual interaction between core and shell. A homogeneous swelling of the core, and a radial inhomogeneous swelling of the shell have been predicted at different temperatures. Verification with the experimental data from dynamic light scattering reveals that increasing the shell thickness develops a two-step transition behavior in the swelling-temperature curves which attribute to the VPTTs of the core and shell polymer network. In contrary, hydrogels with thin shells exhibit only one transition point attributed to the VPTT of

the core.

Next, the equilibrium swelling of a dual pH- and temperature-sensitive core/shell hydrogel is studied. This hydrogel includes the poly (N-isopropyl acrylamide)-co-Arylic Acid in the core and poly (N-isopropyl acrylamide) in the shell. In agreement with observations, swelling ratio decreases with temperature and shows two transition points akin to the VPTT of the core and shell at higher pH values. The model predicts the decrease of the degree of ionization in the core with temperature showing a similar trend as the swelling ratio. Furthermore, the maximum radial stress occurs at the core/shell boundary when both domains collapse. Moreover, the main mechanism for swelling in an acidic bath is determined to be the induced pressure by the electrostatic repulsion between bound charges rather than the ionic pressure.

Finally, a natural/synthetic composite gel is synthesized for swelling experiments when solution pH varies from very low to very high. A homogeneous swelling is assumed for this hydrogel based on its observed morphology. A non-monotonic dependence of swelling ratio on pH is observed. A theoretical model accounting for the effect of pH and ionic strength is utilized to elucidate this phenomenon by establishment of ion pairs between fixed ions of functional groups and mobile ions. The influence of constituent polymers of the composite gel on its swelling ratio is investigated. The swelling and the mechanical stiffness of AC composite hydrogels can be adjusted by the concentration of carbopol and agarose, respectively. It is suggested that the swelling of carbopol may be hindered by the stiffness of agarose.

Perface

This thesis presents a numerical and experimental study of equilibrium swelling of stimuli-sensitive composite hydrogels. The following publications are carried out for this doctoral thesis

Journals and Conferences:

1. N. Hamzavi, A.D. Drozdov, Y. Gu, E. Birgersson, 2015, *Modeling equilibrium swelling of temperature-sensitive core/shell gels*, In preparation.

2. N. Hamzavi, A.D. Drozdov, Y. Gu, E. Birgersson, 2015, *Equilibrium swelling of coupled* pH- *and temperature-sensitive core/shell gels*, In preparation.

3. N. Hamzavi, A.D. Drozdov, Y. Gu, E. Birgersson, 2015, *A* pH-*sensitive natural/synthetic composite hydrogel: Numerical simulation and swelling experiments on Agarose-Carbopol*, In preparation.

4. N. Hamzavi, A.D. Drozdov, V.P.W. Shim, Y. Gu, 2014, *Micromechanics of Composite Hydrogels*, 24th International Workshop on Computational Mechanics of Materials (IWCMM 24), Madrid, Spain.

Other works:

1. J.Y. Dewavrin, N. Hamzavi, V.P.W. Shim, M. Raghunath, 2014, *Tuning the architecture of three-dimensional collagen hydrogels by physiological macromolecular crowding*, Acta biomaterialia, 10 (10), 4351-4359.

2. N. Hamzavi, W.M. Tsang, and V.P.W. Shim, 2013, *Nonlinear elastic brain tissue model for neural probe-tissue mechanical interaction*, 6th International IEEE/EMBS conference on neural engineering (NER), San Diego, USA.

3. N. Hamzavi, A. Sharma, K.M. Sum, C. Wanpei, H. Kai, T.Y. Ling, L. Wan'E, C. Chan, 2012, *Nasogastric tube introducer device*, U.S. Patent 61/725,178, Issued in Nov. 2012.

4. N. Hamzavi, W.M. Tsang, V.P.W. Shim, 2012, *Investigating the mechanical interaction between neural electrode and brain tissue*, International Conference on BioElectronics, BioSensors, BioMedical Devices, BioMEMS/NEMS and Applications (Bio4Apps), Singapore.

5. N. Hamzavi, W.M. Tsang, V.P.W. Shim, 2012, *The effect of neural electrode insertion speed on tissue strain during implantation – A study based on brain phantom material and image correlation*, International conference on medical and biological engineering (ICMBE), Singapore.

List of Figures

List of Symbols

α	Degree of ionization
$\bar{r}$	radius of a spherical gel in the reference state
ε	Permittivity of material
Γ	Rate of production of mobile ions
Φ	Potential energy of the electric field in the actual state
$\boldsymbol{\nabla}$	Gradient vector in the actual state
$\mathbf{E}$	Electric field in the initial state
$\mathbf{e}$	Electric field in the actual state
$\mathbf{T}_{\mathrm{M}}$	Maxwell stress
K_a	Dissociation constant of functional groups
R	Charge density in the initial state
r	Charge density in the actual state
^{C}	Core
^{S}	Shell
C_b	Concentration of total bound charges
k	Molarity of water
Q	Swelling ratio in the actual state
R	radius of a spherical gel in the initial state
r	radius of a spherical gel in the actual state
T_Θ	Cauchy stress in tangential direction
T_R	Cauchy stress in radial direction

V Volume of a spherical gel in the actual state

X Concentration of counter ions in the gel

β Fraction of neutral groups to total number of functional groups

χ Florry-Huggins parameter

μ Chemical potential energy

Π Largrange multiplier

Ψ Specific free energy

$\mathbf{B}_{\mathrm{e}}$ The right Cauchy-Green tensor

$\mathbf{C}_{\mathrm{e}}$ The left Cauchy-Green tensor

$\mathbf{J}$ Solvent flux in the initial state

$\mathbf{j}$ Solvent flux in the actual state

$\mathbf{S}$ First Piola-Krichhoff stress tensor

$\mathbf{T}$ Cauchy stress tensor

φ_{net} Volume fraction of polymer network

φ_{sol} Volume fraction of solvent

$^{\mathsf{T}}$ Transpose sign

C Number of solvent molecules per unit volume in the initial state

c Number of solvent molecules per unit volume in the actual state

C_0 Number of solvent molecules per unit volume in the reference state

D Diffusivity

e Charge of an electron

f Coefficient of volume expansion

G Shear modulus

J_{e} Principal invariants of the Cauchy-Green tensors

k_B Boltzmann's constant

Q_0 Swelling in the reference state

T	Temperature
v	Volume of a water molecule
W_e	Elastic strain energy
$\mathbf{D}$	Rate-of-strain tensor
$\mathbf{F}$	Deformation gradient for transformation from initial to actual state
$\mathbf{f}$	Deformation gradient from initial to reference state
$\mathbf{F}_\mathrm{e}$	Deformation gradient for elastic deformation from reference to actual state
$\mathbf{H}$	Electric displacement in the initial state
$\mathbf{h}$	Electric displacement in the actual state
E	Young's modulus

Chapter 1

Introduction and background

An exclusive class of polymer materials are hydrogels, which are colloidal materials with a mixing behavior of solids and liquids. When a polymer network swells in water and forms a polymer gel, it is called a hydrogel. Hydrogels are wet and soft materials which exhibit biocompatibility and physiochemical similarity with natural tissue and extracellular matrix [1]. Their high water content can be more than one thousand times of their dry weight [2] without dissolution of polymer network due to the existence of crosslinks. Crosslinks keep the three dimensional structure of swollen hydrogels by chemical bonds (for example, covalent bonds), or physical bonds (for example, hydrogen bonds, electrostatic interactions, van der Waals forces, or physical entanglements) [3].

The ability of hydrogels to change their volume when they are brought in contact with water is called swelling. Swelling is described as a chemical interaction between water molecules and polymer network in the microscopic scale leading to macroscopic

deformation. After discovering this energy transformation (chemical energy to mechanical energy) for swollen polymer gels in 1950s [4, 5], hydrogels are entitled as mechanochemical systems [6] and novel applications are proposed afterwards.

The initial application of gels for medical use has been started in the 1950s when Otto Wichterle and Drahoslav Lím invented Poly(hydroxyethyl methacrylate) (pHEMA) to develop soft contact lenses [7]. Hydrogels have also been used as superabsorbent materials to enhance water preservation in soils in the 1960s. The interest in developing hydrogels for biomedical applications has grown further, after Tanaka discovered a new class of polymer gels in the mid-1970s [8]. Despite conventional hydrogels, they exhibit a fast and considerable volume transition from collapsed to swollen state by a small change in external environment or external stimuli. These stimuli-responsive hydrogels have become promising candidates for various practical applications such as biosensors, soft actuators, drug delivery carriers, scaffolding biomaterials, bioimplants, and microfluidics [9–15].

Recently, composite hydrogels have become a focus of interest in some studies since they can combine properties of two or more polymer hydrogels [16–18]. Composite hydrogels may include functional and stimuli-responsive particles (for instance, rigid particles, micro or nanogels) embedded in a hydrogel [19, 20]. Multiple sensitivity is an important feature of composite hydrogels, which may result in stepwise or non-monotonic swelling behavior in response to an external stimulus.

Modeling the swelling behavior of composite hydrogels and verification of numerical results with experimental data are challenging problems. This study aims to delve

deeper into the equilibrium analysis of composite hydrogels comprising two polymer networks. It is desired to 1) numerically analyze the anisotropic swelling of core/shell composite hydrogels which are responsive to pH and temperature and validate the results with experimental data, and also, 2) to explain non-monotonic swelling of a natural/synthetic composite gel at a wide range of pH values, observed in our swelling experiments on this composite hydrogel. This study may lead to further development of composite hydrogels for the engineering of hydrogel-based devices whose swelling can be controlled by constituent polymer gels which are stimuli-responsive.

1.1 Classification of Hydrogels

Hydrogels can be categorized into different types based on various parameters [21, 22]. They might be natural or synthetic hydrogels based on the type of polymer constituents; or physical or chemical hydrogels with permanent or transient crosslinks, respectively based on the type of crosslinks; or neutral or ionic gels based on whether side groups attached to the backbone of polymer chains are neutral or functional, respectively; or aerogels, lyopic gels or hydrogels based on whether their solvent constituent is air, oil or liquid, respectively; or macrogels, microgels and nanogels based on the size of colloids.

1.1.1 Stimuli-responsive hydrogels

One of the main families of hydroges is stimuli-responsive hydrogels which absorb a pronounced amount of water and reconfigure their polymer network in response to

physical and chemical stimuli. Physical stimuli include temperature, pressure, solvent composition, light, sound, electric or magnetic fields, while chemical stimuli comprises pH, ionic strength, enzymes, alcohol and specific solutes [23–25]. These hydrogels with intelligent properties are called smart hydrogels which have been used in numerous applications, such as in sensing-actuation mechanisms, in on-line process monitoring, in the immobilization of cells, in drug delivery and tissue engineering [9, 14, 26–30]. Temperature, pH and ion are three stimuli whose influence on swelling behavior of hydrogels are investigated in this thesis.

1.1.1.1 Temperature sensitivity

The most common type of responsive gels are temperature-sensitive gels which demonstrate phase transformation between swollen and collapsed states by changing temperature. Poly N-isopropyl acrylamide (pNIPAM) was the first hydrogel reported to have a volume-phase transition behavior in pure water [31] and has become the most typical temperature-sensitive gel. pNIPAM swells when temperature drops below the lower critical solution temperature (LCST) of the linear polymer which is around 32-35 °C – which is close to the volume phase transition temperature (VPTT) of pNIPAM hydrogels [32]. Hydrophobic groups of pHEMA and their interaction with solvent which are sensitive to temperature, are responsible for dependence of swelling on temperature. At lower temperatures, water molecules surround the hydrophobic solutes and non-polar segments become solvable in water by making hydrogen bonding. At higher temperatures, hydrophobic interactions becomes stronger as water molecules move away from

hydrophobic groups, and this results in shrinkage of hydrogels [33].

There is another type of temperature-sensitive hydrogels – copolymers of poly(acrylamide) – which exhibit an increase in swelling when temperature increases above an upper critical solution temperature (UCST) [9]. Moreover, a combination of these two behaviors – swelling with temperature followed by shrinkage – is also observed in some kind of temperature-sensitive hydrogels [34].

1.1.1.2 pH sensitivity

Another special class of stimuli-responsive hydroges is ionic polymer gels (polyelectrolyte gels) containing functional groups – acidic: such as, carboxylic COOH and sulphonic acid SO_3H, or basic: such as, amine NH_2 groups – which deprotonate or protonate in response to changes of pH values. Polyelectrolyte (PE) gels are classified as anionic, cationic or ampholytic gels if their functional groups are acidic, basic or both (acidic and basic), respectively [35]. Swelling of PE gels occurs when the solution pH reaches pK_a (acid dissociation constant) which results in the dissociation of functional groups and the production of mobile ions and bound ions. Fig.1.1 demonstrates a molecule of polyacrylic acid (AAc) in a coiled structure when it is dry. When molecules of AAc are hydrated with hydrogen chloride in a bath, swollen hydrogels are obtained after deprotonation of functional and uncoiling of polymer chains.

Polytelectrolyte gels show relatively higher swelling with a faster rate compared to neutral gels [36]. Two mechanisms are proposed to explain this behavior [37–39]: (i) increased osmotic pressure resulting from excess counter ions intake; and (ii) re-

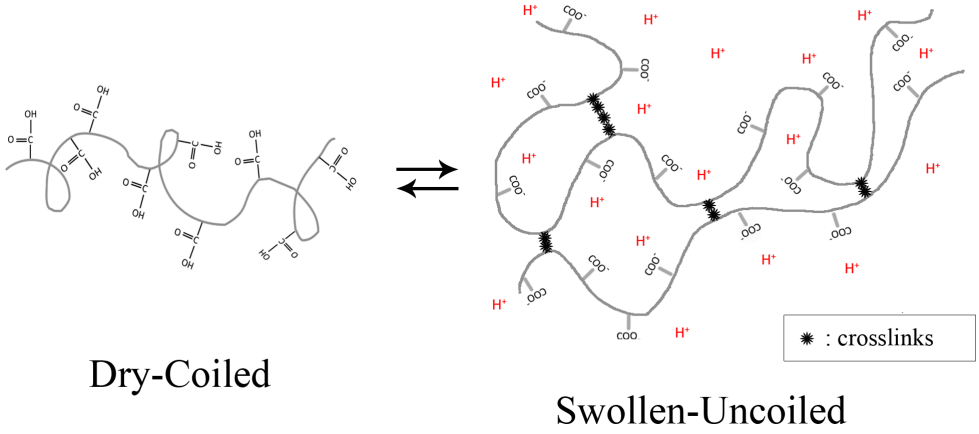

Figure 1.1: Schematic of polyacrylic acid molecule in dry state has coiled structure and when hydrated with hydrogen chloride becomes deprotonated and make an uncoiled structure.

pulsion between bound charges. The former is conventionally assumed to be the main mechanism for swelling of PE gels. Among numerous commercial and industrial applications [40], PE gels are actively used in biomedical research as carriers in controlled drug delivery systems [41] and also, as biosensors and permeation switch [42].

1.1.1.3 Ion sensitivity

Salt addition to a bath influences the equilibrium swelling of PE gels to reduce pronouncedly by two to three orders of magnitude. This shrinking behavior can be explained qualitatively by ionic pressure decrease together with the Donnan's equilibrium law, although quantitative comparison between calculations and experimental results fails to be achieved only by this mechanism [43]. Three mechanisms are suggested to improve predictions: (i) screening charged functional groups [44, 45], (ii) formation of ion-pairs between free counter-ions and bound charges [45–47], (iii) increasing chemical potential of solvent [48, 49].

1.1.2 Natural and synthetic hydrogels

Polymer network of hydrogels can be natural or synthetic polymers which provide specific properties specially for designing and fabricating scaffolds to support cell adhesion, migration and growth, and also to assist nerve regeneration [50, 51].

1.1.2.1 Natural hydrogels

Natural hydrogels include proteins (e.g. collagen and gelatin) and polysaccharides (e.g. agarose and hyaluronic acid (HA)). These hydrogels have low toxicity, good biocompatibility, and similar chemical structure to polymers within the body [52]. Natural polymer gels can facilitate cell proliferation by providing cell-scaffold adhesion. The shortcoming of these gels is their biodegradation via enzymatic action, which may affect the mechanical integrity, although it may be desirable to diffuse some cells into the hydrogel [53].

1.1.2.2 Synthetic hydrogels

Synthetic hydrogels have consistent properties (physical and chemical) compared to natural gels, and this reproducibility is crucial for tissue engineering applications [54]. Generally, synthetic hydrogels are biologically inert and therefore, have weak cell adherence. An example of these synthetic gels is poly(2-hydroxyethyl methacrylate) or pHEMA which has been implemented into cortical lesion cavities and showed astrocyte and axon ingrowth in a hydrogel scaffold [55]. The shortcomings of pHEMA gels which are cell attachment and proliferation, has been rectified by its assembly with

other monomers [56, 57].

1.1.3 Composite hydrogels

Composite hydrogels are prepared by combination of at least two individual polymer gels in an attempt to combine properties of constituent polymers. Some composite hydrogels are developed to reproduce motions in plants in a self-shaping mechanism (such as opening of chiral seed pods [58]). The 2D layered structure of a composite gel can deform to a 3D complex structure – cylinder, helical or even cone – during anisotropic swelling [59, 60]. Moreover, composite gels may be interpenetrating hydrogels (IPNs), semi-IPN hydrogels, doubly crosslinked microgels, and double-network hydrogels [22].

A special kind of composite gels are prepared with a core/shell structure which has polymer networks in core and shell domains. The first core/shell microgel – polystyrene in the core and pNIPAM in the shell – is reported in [61]. Composite core/shell hydrogels with multi-responsiveness to more than one stimulus (e.g. temperature and pH) have been studied since 1990 [37, 62–66].

In a series of studies [66], a dual thermo-sensitive core/shell microgel – poly(N-isopropyl acrylamide) pNIPAM as the core, and poly(N-isopropyl methacrylamide) pNIPMAM as the shell – has been synthesized with different volume phase transition temperatures (VPTT) for each domain. This composite microgel is desirable for drug delivery applications since it exhibits a rapid swelling which can be controlled by the human body temperature which is in between the VPTTs of two domains. Later, another series of dual-responsive pNIPAM-co-AAc hydrogels are synthesized in the

form of microgels [38,67,68] and also, macrogels [69–72]. These composite hydrogels are produced by adding polyacrylic acid (AAc) to the base hydrogel which is pNIPAM. Therefore, the swelling behavior of these hydrogels is a function of pH and temperature.

Composite hydrogels may be composed of synthetic and natural hydrogels (also known as hybrid hydrogels) in order to make bioactive polymers which has advantages over its individual compartments in terms of easier preparation and more functionality. In synthetic/natural composite gels which are developed for tissue-engineering scaffolds, the synthetic block adjusts the structural integrity of the scaffold and the natural block provides its biological properties to enhance its bioactivity [54]. Numerous natural biopolymers – for instance, chitosan, heparin, alginate, collagen, and hyaluronic acid – are combined with synthetic polymers – for instance, pNIPAM, polyethylene glycol (PEG), polyacrylamide (PAAm) and polyvinyl alcohol (PVA) to make composite gels [73–75]. Fo instance, alginate-polyacrylamide hydrogels are introduced as potential candidates to replace cartilage, since their they have high toughness and stiffness at the same time [76]. The novel dissipation mechanism in this hydrogel results in a high fracture energy of 9000 J m^{-2} [77] which is almost nine times higher than the fracture energy of articular cartilage [78].

1.2 Characterization techniques

Physical and mechanical properties of hydrogels are important features in investigating usefulness as a matrix for tissue-engineering scaffolds and drug delivery systems, wound healing, and cartilage replacement [79, 80]. An important physical property is

swelling ratio and water content which can be characterized by submerging a dry hydrogel in a bath and measuring its weight after soaking. Accordingly, the swelling ratio is expressed by

$$Q = \frac{W_s - W_0}{W_0}, \tag{1.1}$$

where W_s and W_0 are the weight of the hydrogel specimen in the fully swollen state and in the dry state, respectively. In a swollen state, hydrogel network expand to accommodate more water molecules (as shown in Fig. 1.2) until network elasticity reaches an equilibrium with osmotic pressure. Special techniques are also developed which show fast kinetic swelling in hydrogels, for instance dynamic light scattering (DLS) and small angle neutron scattering (SANS). DLS and SANS have been utilized to measure the size of microgel particles during swelling and polymer density within core and shell domains, respectively [81].

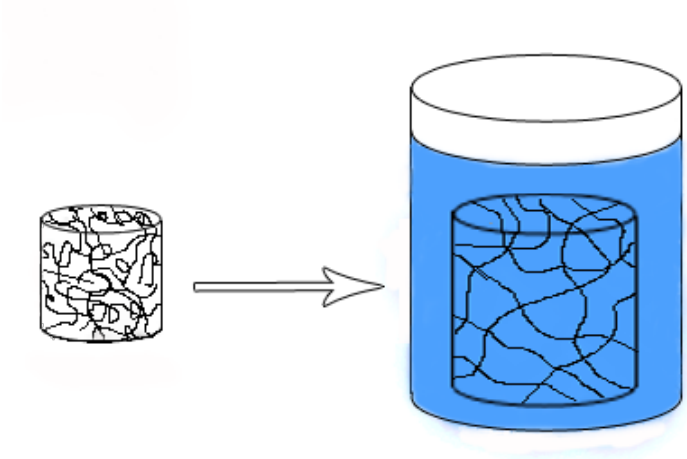

Figure 1.2: Schematic of a cylindrical hydrogel in dry state and in swollen state when subjected to swelling in water bath.

There are different techniques to characterize the structure of hydrogels. The internal structure of macroscopic gels can be observed by scanning electron microscopy

(SEM) from freeze-dried samples. It should be noted that freeze-drying is supersensitive to cooling process and the actual structure of hydrogels in wet condition may not be preserved after freeze-drying unless proper techniques are used [82]. The surface morphology of hydrogels can be observed by small angle neutron scattering (SANS), SEM, and also, atomic force microscopy (AFM). AFM is widely used in liquid or semi-

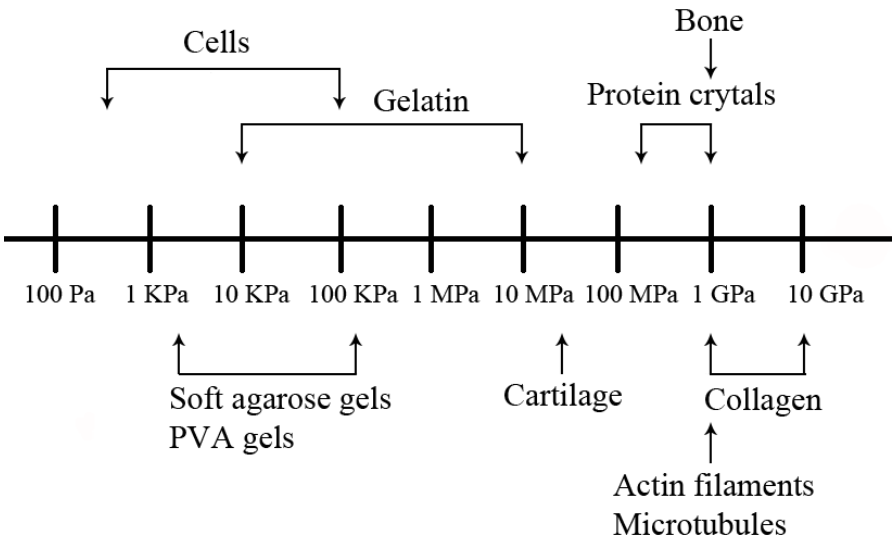

Figure 1.3: Elastic modulus for a wide range of soft materials is shown.

solid environments to capture the morphology, the elasticity and the pore size of hydrogels [77, 83–85].

AFM is well suited to characterize many biological systems with low elastic modulus demonstrated in Fig. 1.1. However, it requires considerable expertise to deal with comparatively slow and tedious set-up and measurement process. AFM is also successfully utilized to measure viscoelasticity of soft materials by observing any change in amplitude and phase of retraction force compared to indentation force [86]. Adhesion property of polymer gels needs to be quantified in terms of viscoelasticity which is an-

other key feature for designing matrix and scaffolds [87]. Rheology is another test to measure viscoelasticity of soft materials by applying a shear stress to samples and measuring storage modulus and loss modulus which describe elasticity and viscoelasticity, respectively. Rheology methods have been developed further to measure the elastic modulus of very soft materials in the range of 10^{-3} to 10^{5} Pa [88]. Slippage should be prevented between hydrogel and the walls of rotating/fixed tools of rheometer.

1.3 Modeling swelling behavior of hydrogels

Swelling of hydrogels is migration of solvent molecules into polymer network and reconfiguration of the network in response (see Fig. 1.2). After a hydrogel is immersed in a solvent, polymeric chains start to stretch and imbibe solvent molecules. During this transient swelling process, solvent molecules start to distribute through network and thereafter, the volume of hydrogels changes with time until hydrogels reaches an equilibrium state and swelling kinetics stops. In the equilibrium state, solvent molecules distribute homogeneously within the network and the chemical potential of the internal and the external solvents become equal. Theoretical models are developed to analyze the swelling behavior of polymer gels [89, 90].

1.3.1 Mono-phase model

Single-phase model is developed to capture large deformation of hydrogels by considering them as swollen elastomer and using "eight-chain" model instead of Gaussian

chain model of Flory-Rehner theory. In this model which is known as Arruda-Boyce or Flory-Erman [91], swelling is contributing to both volume expansion and netwrok extension by prescribing swelling stretch rather than determining it based on the state of stress. This phenomenological model may predict hydrogel behavior under compression, tension and simple shear; however it can not describe the coupling effect of solvent diffusion and network deformation and to determine transient chemo-mechanical responses of hydrogels.

1.3.2 Models based on mixture theory

This approach is based on continuum mixture of two phases – a solid and a fluid – initiated by Tanaka and co-workers [92] based on the mixture theory. The biphasic mixture theory is applied with the concept of volume fraction in composite materials to solve field equations (conservation of mass, momentum, energy and etc.) using physical properties (i.e. mass and displacement) of each phase at microscale and to consider the contribution of each phase by its volume fraction at continuum level.

Both the fluid and the solid are assumed to be incompressible considering no mass exchange between two phases. The stress of mixture is decomposed into hydrostatic pore pressure of the fluid and average stress of the solid network. The displacements of solid and fluid are defined individually and the interaction between them is generally excluded. Basically in comparison with the displacements of the network, the displacements of the fluid is considered to be small, and at the equilibrium condition, the fluid motion is assumed to be zero. This theory has limitations to prescribe boundary con-

ditions on fluid phase. There are some studies who show an agreement between the thermodynamic models and the modified models derived from mixture theory [93].

1.3.3 Thermodynamic model

Theory of gel swelling has been used in many studies to capture the mechanochemical response of hydrogels to the surrounding environment [89, 94]. Gibbs [95] developed a thermodynamic model for a porous solid filled with fluid based on statistical theories, and Biot [96] used the thermodynamic model and incorporated it with Darcy's law for fluid diffusion.

In these theories, non-specific free energy functions are used to predict the equilibrium state of the hydrogels subjected to thermal and chemical stimuli. The first specific free energy function for polymer gels is introduced by Flory and Rehner [97] based on the assumption of a Gaussian distribution of polymer chains [98]. Flory-Rehner theory determines the thermodynamical equilibrium of polymer gels by introducing a free energy function for neutral gels to incorporate the influence of the entropy of stretching network, and the entropy and the enthalpy of mixing polymer network and solvent. Flory-Rehner theory has been modified to describe the behavior of various types of hydrogels (such as ionic polymer gels) [89].

In the last decade, numerous constitutive models have been developed in the thermodynamic framework to express solvent diffusion and elastic response of neutral gels considering three-dimensional finite strains [99–108]. The swelling of stimuli-responsive hydrogels has also been the focus of theoretical models. Advanced contin-

uum models are provided to determine three-dimensional finite swelling deformation of temperature-sensitive gels [109–113]. The most common approach is to employ the Flory-Huggins parameter as a function of temperature and polymer density [31, 114]. Furthermore, theoretical models are proposed to study pH-sensitive gels which exhibit higher swelling with a faster rate compared to neutral gels [115–122]. Most constitutive models account for the contribution of ionic pressure arising from the gradient of ion concentration inside and outside the polymer network of PE gels.

A new challenge for modeling is inhomogeneous swelling of hydrogels which have a geometry constraint [123] or a modulated network [124]. Numerous continuum models have been developed to describe this behavior [125–132]. An example of a mechanical constraint is core-shell structure existing in some hydrogels due to the gradient of crosslinks in microgels [133] or the creation of two distinct domains in core/shell composite gels [134]. The inhomogeneous swelling of neutral core/shell gels has been predicted by many theoretical models [128–130, 135–139]. Simplification of the interaction between core and shell domains is considered in some studies to find approximate results [129, 140]. Thus, the intention is to include the mutual interaction between swelling and mechanical forces of core and shell domains in order to predict swelling accurately. Moreover, few studies are focused on the influence of more than one stimulus on core/shell hydrogels. There is room for further research on coupled effect of temperature and pH on core/shell hydrogels

1.4 Objectives

Mechanics and physics of hydrogels has become an exciting area of research for scientists to explore new materials for novel applications. Complex swelling behavior has been observed in composite hydrogels comprising two or more polymer networks which respond differently to a change in external environment. Modeling the swelling behavior of stimuli-responsive composite hydrogels in order to predict experimental results accurately, is a challenge.

In this study, the equilibrium swelling – which is the equilibrium between the swelling forces and the mechanical forces – of composite hydrogels including two polymer gels, is studied. This study attempts to understand the swelling mechanism of composite gels in response to multi external stimuli, and to provide a tool for simulation analysis and prediction of their swelling deformation leading to fabrication of novel hydrogel-based devices.

The objectives of this study can be listed as:

1. *To predict the equilibrium swelling of temperature-sensitive core/shell composite hydrogels*: A thermodynamic model is applied to derive constitutive relations for solvent diffusion and elastic deformation of temperature-sensitive core/shell hydrogels. The model is extended to analyze the equilibrium swelling of a core/shell hydrogel with deformable core and shell domains, and furthermore, the effect of temperature and shell thickness on its swelling is investigated.

2. *To determine the equilibrium swelling of dual responsive core/shell composite hy-*

drogels in response to changes in temperature and pH: A thermodynamic model is applied to describe the swelling of a pH-sensitive hydrogel which is consisted of three phases including polymer network, solvent, and solutes under mechanical and chemical equilibrium conditions. The model is able to account for ionic pressure and electrostatic repulsion between fixed charges of functional groups in the analysis of equilibrium swelling. The model is then extended to determine the equilibrium analysis of core/shell composite hydrogels which are responsive to both temperature and pH. The coupled effect of pH and temperature is considered to validate simulation results with experimental data, and to investigate the influence of pH on deprotonation of functional groups and volume phase transition temperature.

3. *To study the swelling behavior of a natural/synthetic composite gel experimentally and to model its equilibrium swelling at a wide range of* pH *values*: An experimental study on the swelling behavior of a natural/synthetic composite hydrogel is conducted to study its swelling behavior over a wide range of pH values, from highly acidic to highly basic. The effect of different compositions of constituents swelling behavior at different pH values is also investigated. Then, a constitutive model is adapted to explain the dependence of the equilibrium swelling on pH accounting for the effect of pH and ionic strength. Furthermore, the contribution of the swelling of constituent polymers to equilibrium swelling of the composite hydrogel is also studied and discussed.

1.5 Exposition of the thesis

The exposition is organized as follows: chapter one presents an introduction to hydrogels and their applications, classification of hydrogels, a summary of theoretical models for swelling behavior of gels, followed by objectives of the thesis. Mathematical formulation is then described in chapter two. The equilibrium swelling of core/shell composite hydrogels is analyzed by accounting for the effect of temperature in chapter three, and the coupled influence of pH and temperature is addressed in chapter four. Chapter five presents an experimental study on swelling behavior of a natural/synthetic composite hydrogel, and in Chapter six, a theoretical model is applied to determine the swelling behavior of this hydrogel considering the effect of pH and ionic strength. Conclusion and recommendation for future works are formulated in chapter seven.

Chapter 2

Mathematical formulation

In this chapter, mathematical formulation for three-dimensional deformation of polymer gels is presented. Constitutive relations are applied with the aid of free energy inequality relation to describe the coupled solvent diffusion and large deformation of a hydrogel following earlier studies [102,141,142]. These relations are extended further to describe deformation of core/shell hydrogels subjected to swelling.

2.1 Constitutive relations

A continuum model is applied to study the deformation of a hydrogel under mechanical and swelling forces. A continuum volume of a hydrogel comprises two phases: a polymer network and a solvent. Solvent diffusion into polymer network is allowed, but without any mass exchange between these two phases.

2.1.1 Kinematics

Macro-deformation of a hydrogel has been described in three individual states which are assumed in the thermodynamic framework of this work. First, the initial state of a hydrogel is assumed to be the same as its dry undeformed state. Second, the reference state for deformation of a hydrogel is considered to match with its as-prepared state after polymerization process. Third, the actual state of a hydrogel is its highly swollen state. Deformation gradient $\mathbf{F}$ maps the deformation from the initial state to the actual state. The multiplicative decomposition of deformation gradient $\mathbf{F}$, is described in terms of deformation gradient for elastic deformation $\mathbf{F}_{\mathrm{e}}$ and deformation gradient for partial swelling $\mathbf{f}$:

$$\mathbf{F} = \mathbf{F}_{\mathrm{e}} \cdot \mathbf{f} \,. \tag{2.1}$$

For an isotropic polymer network, $\mathbf{f}$ describes the expansion of a dry gel to its partially swollen state and it reads

$$\mathbf{f} = f^{\frac{1}{3}} \cdot \mathbf{I} \,, \tag{2.2}$$

where f is the coefficient of volume expansion which describes the evolution of reference state, and $\mathbf{I}$ is the identity tensor. Therefore,

$$\mathbf{F} = f^{\frac{1}{3}} \mathbf{F}_{\mathrm{e}} \,. \tag{2.3}$$

The Cauchy-Green tensors for elastic deformation reads

$$\mathbf{B}_\mathrm{e} = \mathbf{F}_\mathrm{e} \cdot \mathbf{F}_\mathrm{e}^\intercal, \quad \mathbf{C}_\mathrm{e} = \mathbf{F}_\mathrm{e}^\intercal \cdot \mathbf{F}_\mathrm{e}, \tag{2.4}$$

where $^\intercal$ stands for transpose sign. Velocity gradients are derived by differentiating Eq. 2.1 as follows

$$\mathbf{L} = \dot{\mathbf{F}} \cdot \mathbf{F}^{-1}, \quad \mathbf{L}_\mathrm{e} = \dot{\mathbf{F}}_\mathrm{e} \cdot \mathbf{F}_\mathrm{e}^{-1}. \tag{2.5}$$

Differential equations for principal invariants of the Cauchy-Green tensors ($J_{\mathrm{e}1}$, $J_{\mathrm{e}2}$, $J_{\mathrm{e}3}$) are obtained:

$$\dot{J}_{\mathrm{e}1} = 2\mathbf{B}_\mathrm{e} : \mathbf{D}_\mathrm{e}, \quad \dot{J}_{\mathrm{e}2} = 2(J_{\mathrm{e}2}\mathbf{I} - J_{\mathrm{e}3}\mathbf{B}_\mathrm{e}^{-1}) : \mathbf{D}_\mathrm{e}, \quad \dot{J}_{\mathrm{e}3} = 2J_{\mathrm{e}3}\mathbf{I} : \mathbf{D}_\mathrm{e}, \tag{2.6}$$

where $\mathbf{D}$ as the rate-of-strain tensor reads,

$$\mathbf{D} = \frac{1}{2}(\mathbf{L} + \mathbf{L}^\intercal) \,, \quad \mathbf{D}_\mathrm{e} = \frac{1}{2}(\mathbf{L}_\mathrm{e} + \mathbf{L}_\mathrm{e}^\intercal) \,, \quad \mathbf{D} = \mathbf{D}_\mathrm{e} + \frac{\dot{f}}{3f}\mathbf{I} \,. \tag{2.7}$$

When f is a time-invariant parameter, Eqs. 2.6. are simplified to

$$\dot{J}_{\mathrm{e}1} = 2\mathbf{B}_\mathrm{e} : \mathbf{D}, \quad \dot{J}_{\mathrm{e}2} = 2(J_{\mathrm{e}2}\mathbf{I} - J_{\mathrm{e}3}\mathbf{B}_\mathrm{e}^{-1}) : \mathbf{D}, \quad \dot{J}_{\mathrm{e}3} = 2J_{\mathrm{e}3}\mathbf{I} : \mathbf{D}. \tag{2.8}$$

2.1.2 Molecular incompressibility

The change in volume per unit volume in the reference state ($\det\mathbf{F}-1$) is assumed to be due to only the uptake of solvent molecules. The solvent uptake is determined by

$$Q = Cv, \tag{2.9}$$

where Q denotes the degree of swelling and C is the concentration of solvent molecules – number of solvent molecules per unit volume of a hydrogel in its initial state – and v is the volume of a single solvent molecule. So, the molecular incompressibility implies that,

$$\det\mathbf{F} = 1+Q. \tag{2.10}$$

Moreover, φ_{net} and φ_{sol} as the volume fraction of polymer network and solvent, respectively, are given by

$$\varphi_{sol} = \frac{Q}{1+Q}\,, \quad \varphi_{net} = \frac{1}{1+Q}. \tag{2.11}$$

2.1.3 Kinetic relations

A kinetic law is used to describe the diffusion of solvent molecules into an isotropic network and is given by

$$\mathbf{j} = -\frac{Dc}{k_B T}\nabla\mu, \tag{2.12}$$

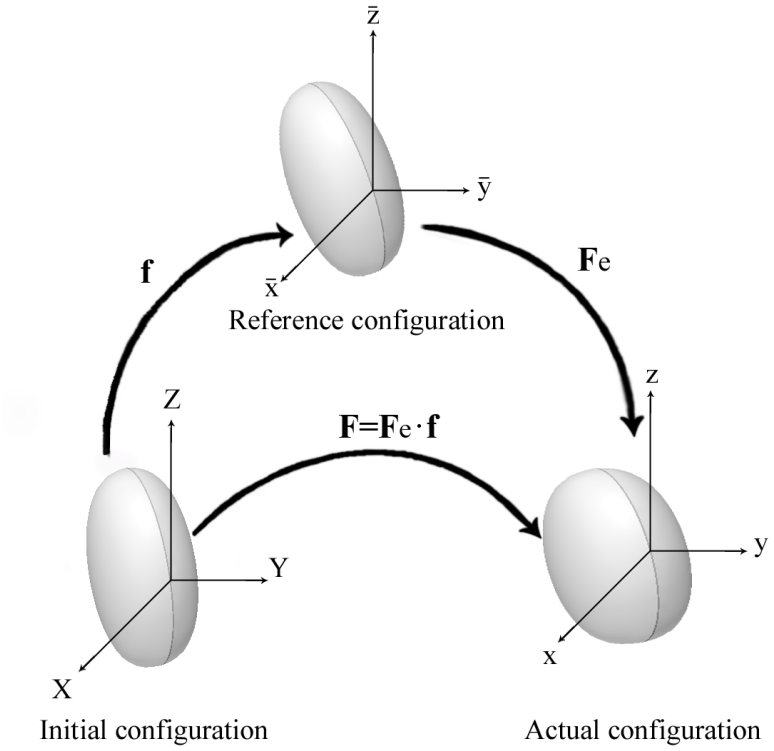

Figure 2.1: The reference configuration is obtained from the initial configuration by changes in swelling ratio of hydrogels during polymerization process. The deformation gradient from initial to actual configuration $\mathbf{F}$ is decomposed into elastic part $\mathbf{F}_e$ and initial swelling part $\mathbf{f}$.

where D is diffusivity, k_B is Boltzmann's constant, T is temperature, and $c = C/\det\mathbf{F}$ denotes number of solvent molecules per unit volume in the actual state. Solvent flux $\mathbf{j}$ and the gradient of chemical potential energy $\nabla\mu$ are expressed by

$$\mathbf{j}_0 = (\det\mathbf{F})\mathbf{F}^{-1}\cdot\mathbf{j}\,, \quad \nabla_0\mu = \nabla\mu\cdot\mathbf{F}\,, \tag{2.13}$$

where ∇_0 and $\mathbf{j}_0$ are gradient operator and solvent flux vector in the initial state, respectively. Insertion of Eq. 2.13 into Eq. 2.12 results in

$$\mathbf{j}_0 = -\frac{DC}{k_BT}\mathbf{F}^{-1}\cdot\nabla_0\mu\cdot\mathbf{F}^{-1}\,. \tag{2.14}$$

When there is no external source to inject solvent molecules, conservation law for solvent molecules reads

$$\dot{C} + \nabla_0\cdot\mathbf{j}_0 = 0. \tag{2.15}$$

$\dot{C}$ is expressed by insertion of Eq. 2.14 into Eq. 2.15 as follows

$$\dot{C} = \nabla_0\left(\frac{DC}{k_BT}\mathbf{F}^{-1}\cdot\nabla_0\mu\ \cdot\mathbf{F}^{-1}\right). \tag{2.16}$$

2.1.4 Free energy density of a neutral hydrogel

A simple free energy is used to approximately describe the behavior of a neutral hydrogel. Following Flory and Rehner [97], the specific free energy Ψ in the actual state, is described by the summation of the free energy of network stretch, and the mixing

energy of polymer-solvent interaction, as follows

$$\Psi = \Psi_0 + \mu_0 C + \Psi_{\text{net}} + \Psi_{\text{mix}}, \tag{2.17}$$

where Ψ_0 is a constant, μ_0 stands for the chemical potential energy of a solvent molecule in a bath, Ψ_{net} denotes the strain energy density of polymer network, and Ψ_{mix} is the mixing energy of polymer with solvent molecules. The strain energy density of polymer network is given by

$$\Psi_{\text{net}} = W_{\text{e}}(J_{\text{e1}}, J_{\text{e2}}, J_{\text{e3}}), \tag{2.18}$$

where J_{ei} (i $= 1,2,3$) denotes principal invariants of the Cauchy-Green tensor. The mixing energy between solvent molecules and polymer chains [143] reads

$$\Psi_{\text{mix}} = \frac{k_B T}{v}\Big(\frac{\varphi_{\text{sol}}}{\varphi_{\text{net}}} \ln \varphi_{\text{sol}} + \chi \varphi_{\text{sol}}\Big), \tag{2.19}$$

where χ is the Florry-Huggins parameter. Finally, after substituting Eqs. 2.18, 2.19 into Eq. 2.17, the specific free energy is obtained by

$$\Psi = \Psi_0 + \mu_0 C + W_{\text{e}}(J_{\text{e1}}, J_{\text{e2}}, J_{\text{e3}}) + \frac{k_B T}{v}\big(Q \ln \varphi_{sol} + \chi \varphi_{sol}\big). \tag{2.20}$$

Substituting φ_{net} and φ_{sol} from Eq. 2.11 into the time derivative of Eq. 2.20, reads

$$\dot{\Psi} = K\dot{C} + 2\mathbf{K}_{\text{e}} : \mathbf{D}, \tag{2.21}$$

where

$$\begin{aligned} K =& \mu_0 + k_B T \left(\frac{\ln Q}{1+Q} + \frac{1}{1+Q} + \frac{\chi}{(1+Q)^2} \right), \\ \mathbf{K}_\mathrm{e} =& \frac{\partial W_\mathrm{e}}{\partial J_{\mathrm{e}1}} \mathbf{B}_\mathrm{e} - J_{\mathrm{e}3} \frac{\partial W_\mathrm{e}}{\partial J_{\mathrm{e}2}} \mathbf{B}_\mathrm{e}^{-1} + (J_{\mathrm{e}2} \frac{\partial W_\mathrm{e}}{\partial J_{\mathrm{e}2}} + J_{\mathrm{e}3} \frac{\partial W_\mathrm{e}}{\partial J_{\mathrm{e}3}}) \mathbf{I}. \end{aligned} \tag{2.22}$$

2.1.5 Derivation of constitutive equations

The free energy inequality equation is adopted from [141] for a hydrogel in an isothermal condition:

$$\dot{\Psi} \leq \mathbf{S} : \dot{\mathbf{F}} + \mu \dot{C} - \mathbf{j}_0 \cdot \boldsymbol{\nabla}_0 \mu \ , \tag{2.23}$$

where $\dot{\Psi}$ denotes the derivative of free energy density, and $\mathbf{S}$ is the first Piola-Kirchhoff stress tensor. It is known that the free energy of any thermodynamic system may not be increasing. To meet thermodynamics restrictions, the power attributed to the external forces together with the power corresponding to the diffusion of solvent molecules, need to be greater than the internal free energy of the hydrogel per unit time.

The first term of inequality equation (Eq. 2.23) can be written in terms of the Cauchy stress tensor as follows

$$\mathbf{S} : \dot{\mathbf{F}} = (\det \mathbf{F}) \mathbf{T} : \mathbf{D}, \tag{2.24}$$

where $\mathbf{T}$ is the Cauchy stress tensor.

It depicts that functions C and $\mathbf{F}$ meet the inequality condition by taking the deriva-

tive of the equation of incompressibility condition (Eq. 2.10) as follows,

$$\dot{C}v - (\det \mathbf{F})\mathbf{I} : D = 0. \tag{2.25}$$

An arbitrary function Π is multiplied to Eq. 2.25, and summed with the inequality equation Eq. 2.23 which implies that

$$K\dot{C} + 2\mathbf{K}_e : \mathbf{D} - (\mu - \Pi v)\dot{C} - (\det \mathbf{F})(\mathbf{T} + \Pi\mathbf{I}) : \mathbf{D} + \mathbf{j}_0 \cdot \nabla_0 \mu \leq 0. \tag{2.26}$$

Since the last term of Eq. 2.26 is a non-positive term (refer to Eq. 2.14), the thermodynamic inequality condition is satisfied if

$$\mathbf{T} = -\Pi\mathbf{I} + \frac{2}{\det \mathbf{F}}\mathbf{K}_e, \quad \mu = K + \Pi v. \tag{2.27}$$

Substituting $\mathbf{K}_e$ with derivatives of the free energy into Eq. 2.27_1, provides the stress-strain relation as follows

$$\mathbf{T} = -\Pi\mathbf{I} + \frac{2}{1+Q}\Big(\frac{\partial W_e}{\partial J_{e1}}\mathbf{B}_e - J_{e3}\frac{\partial W_e}{\partial J_{e2}}\mathbf{B}_e^{-1} + (J_{e2}\frac{\partial W_e}{\partial J_{e2}} + J_{e3}\frac{\partial W_e}{\partial J_{e3}}\mathbf{I})\Big), \tag{2.28}$$

and substituting K in Eq. 2.27_2 provides the chemical potential energy

$$\mu = \mu_0 + k_B T\big(\ln\frac{Q}{1+Q} + \frac{1}{1+Q} + \frac{\chi}{(1+Q)^2} + \frac{\Pi v}{k_B T}\big). \tag{2.29}$$

2.1.6 Stress-strain relation for a specific free energy density

A neo-Hookean strain energy function is used to determine the strain energy density of the hydrogel

$$W_{\mathrm{e}} = \frac{1}{2}G\big[(J_{\mathrm{e}1}-3)-\ln J_{\mathrm{e}3}\big], \tag{2.30}$$

where G denotes shear modulus. From substitution of Eq. 2.30 into Eq. 2.28, the Cauchy stress is determined by

$$\mathbf{T} = -\Pi\mathbf{I} + \frac{G}{1+Q}(\mathbf{B}_{\mathrm{e}}-\mathbf{I}). \tag{2.31}$$

2.2 Swelling of a deformable core/shell hydrogel

Swelling of a core/shell hydrogel is the transportation of solvent molecules into a hydrogel driven by the diffusion of solvent molecules from a bath, their interaction with polymer chains and consequently, the stretch of polymer network. In this study, a spherical geometry is used to describe the structure of a core/shell hydrogel which has a deformable core with the radius of r^C , and a deformable shell with the inner radius of r_1 and the outer radius of r_2. In the initial state, the dry core occupies a domain $\{0 \le R \le R^C,\ 0 \le \Theta^C \le \pi,\ 0 \le \Phi^C \le 2\pi\}$, and the dry hollow shell occupies another domain $\{R_1 \le R \le R_2,\ 0 \le \Theta^S \le \pi,\ 0 \le \Phi^S \le 2\pi\}$ where $\{R,\ \Theta,\ \Phi\}$ are the spherical coordinates with unit vectors $e_R, e_\Theta,$ and e_Φ. After polymerization process, the

core-shell hydrogel occupies another domain $\{\bar{r},\ \bar{\theta},\ \bar{\phi}\}$.

The deformation gradient $\mathbf{f}$ for transformation of a hydrogel from the initial configuration (dry gel) to the as-prepared configuration (partially-swollen gel), reads

$$\mathbf{f} = f^{\frac{1}{3}}\mathbf{I}, \tag{2.32}$$

where $f = 1 + Q_0$ is the coefficient of volume expansion for neutral gels and $Q_0 = C_0 v$ knowing that C_0 as the concentration of solvent molecules in the reference state. The field of deformation is characterized by $\mathbf{f}$ under spherically symmetric transformation

$$\mathbf{f} = \bar{r}\,'\mathbf{e}_R\,\mathbf{e}_R + \frac{\bar{r}}{R}(\mathbf{e}_\Theta\mathbf{e}_\Theta + \mathbf{e}_\Phi\mathbf{e}_\Phi). \tag{2.33}$$

where $\bar{r}\,' = \mathrm{d}\bar{r}/\mathrm{d}R$ is the radial stretch, and $\bar{r}(R)$ describes the radial deformation in the reference configuration. Using Eqs. 2.10, 2.32 and Eq. 2.33, this radial deformation can be expressed by

$$d\bar{r} = f\big(\frac{R}{\bar{r}}\big)^2 dR. \tag{2.34}$$

For a deformable core-shell hydrogel, its volume in the dry state can be characterized by Q_0 as follows (refer to Apipendix A),

$$R_1 = \frac{\bar{r}_1}{(f^S)^{\frac{1}{3}}}, \quad R_2 = \frac{\bar{r}_2}{(f^S)^{\frac{1}{3}}}, \tag{2.35}$$

where f^S and f^C are the volume expansion coefficients for core and shell domains, respectively. The continuity of radial stretch in the reference configuration states that the radius of core $\bar{r}^C$ is equal to the inner radius of the shell $\bar{r}_1$. Thus, the inner radius of the shell in the dry state reads

$$R_1 = \left(\frac{f^C}{f^S}\right)^{1/3} R^C. \tag{2.36}$$

In case of equal coefficient of the volume expansion of the core and the shell ($f^C = f^S$), the inner radius of the shell becomes equal to the radius of the core in the dry state ($R_1 = R^C$).

2.2.1 Equilibrium swelling of a deformable core/shell hydrogel

When a hydrogel submerges into a bath, it swells due to thermodynamic comparability of polymer network and water. In the analysis of core/shell hydrogels, governing equations are solved only for the shell domain, since core is assumed to have a homogeneous deformation under swelling. This assumption has been verified in chapter three by considering one continuous domain for core/shell hydrogels with different mechanical and swelling properties for each domain. However, the distribution of swelling through the shell may not be homogeneous. In this section, an analysis for the distribution of swelling $Q(R)$ and stress $\mathbf{T}(R)$ within a hydrogel is given.

The deformation gradient which maps the deformation from initial to actual config-

uration, is given by

$$\mathbf{F} = r'\mathbf{e}_R\mathbf{e}_R + \frac{r}{R}(\mathbf{e}_\Theta\mathbf{e}_\Theta + \mathbf{e}_\Phi\mathbf{e}_\Phi). \tag{2.37}$$

The radial deformation $r(R)$ is obtained from Eqs. 2.10 and 2.37

$$r'r^2 = (1+Q)R^2. \tag{2.38}$$

Substituting Eqs. 2.38 and 2.37 into Eq. 2.1, results in the deformation gradient for elastic deformation which is expressed by

$$\mathbf{F}_\mathrm{e} = \frac{1}{f^{\frac{1}{3}}}\left((1+Q)\left(\frac{R}{r}\right)^2\mathbf{e}_R\mathbf{e}_R + \frac{r}{R}(\mathbf{e}_\Theta\mathbf{e}_\Theta + \mathbf{e}_\Phi\mathbf{e}_\Phi)\right). \tag{2.39}$$

Insertion of Eq. 2.39 into Eq. 2.31 provides the Cauchy stress in radial and tangential directions

$$\begin{aligned} T_R &= -\Pi + \frac{G}{1+Q}\left(\frac{(1+Q)^2}{f^{\frac{2}{3}}}\left(\frac{R}{r}\right)^4 - 1\right), \\ T_\Theta &= -\Pi + \frac{G}{1+Q}\left(\frac{1}{f^{\frac{2}{3}}}\left(\frac{r}{R}\right)^2 - 1\right). \end{aligned} \tag{2.40}$$

2.2.2 Mechanical equilibrium condition

Mechanical equilibrium condition for a spherical hydrogel particle in the actual state reads

$$\frac{\partial T_R}{\partial r} + \frac{2}{r}(T_R - T_\Theta) = 0. \tag{2.41}$$

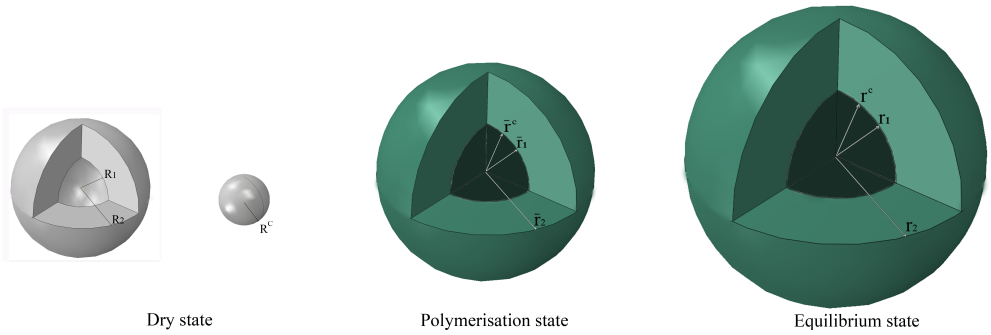

Figure 2.2: Schematic of core/shell composite hydrogels at three different states. Core and shell are shown separately in the dry state since this drying process. The polymerization state is taken as the reference state which is differentiated from the initial dry state. The equilibrium state coincides with the actual state of gels.

Eq. 2.41 is rewritten to take derivative with respect to R, and T_Θ is substituted from Eq. 2.40_2. Thus, we arrive at

$$\frac{\partial T_R}{\partial R} + \frac{2G}{r f^{\frac{2}{3}}}\left((1+Q)^2\left(\frac{R}{r}\right)^6 - 1\right) = 0. \tag{2.42}$$

Subsequently, integration from Eq. 2.42 and application of the boundary condition ($T_R|_{R=R_2} = 0$), result in the stress in the shell as follows

$$T_R = \int_R^{R_2} \frac{2G^S}{r(f^S)^{\frac{2}{3}}}\left((1+Q^S)^2\left(\frac{\hat{R}}{r}\right)^6 - 1\right) d\hat{R}, \tag{2.43}$$

where G^S is the shear modulus of the hydrogel in the shell. Then, in an analogy with Eq. 2.38, it implies that

$$\int_0^{r^C} d\tilde{r} = \int_0^{R^C} (1+Q^C)\left(\frac{R}{r}\right)^2 d\tilde{R}. \tag{2.44}$$

By knowing that swelling ratio of core is constant, Eq. 2.44 is solved for the radius of the core

$$r^C = (1+Q^C)^{\frac{1}{3}} R^C. \tag{2.45}$$

Two boundary conditions exist at the core/shell interface in the actual state:

1. Lateral stretch is continuous through the boundary ($r_1/R_1 = r^C/R^C$). Using this continuity condition and Eq. 2.45 in integration of Eq. 2.38, determines the radius of the shell as follows

$$r^3 = (1+Q^C)R_1^3 + 3\int_{R_1}^{R} (1+Q^S)\hat{R}^2 d\hat{R}, \tag{2.46}$$

where R_1 is described in Eq. 2.36.

2. Radial stress is continuous through the boundary. The internal radial stress of the shell is equal to the radial stress of the core $T_{R_1} = T_R|_{R=R_1} = T_R^C$. The radial stress of the core is constant through the core thickness ($\partial T_R^C/\partial R = 0$). This continuity condition is used to determine the radial stress in the core from Eq. 2.43. Thus,

$$T_R^C = T_{R_1} = \int_{R_1}^{R_2} \frac{2G^S}{(f^S)^{\frac{2}{3}}} \left((1+Q^S)^2 \left(\frac{\tilde{R}}{r}\right)^6 - 1 \right) \frac{d\tilde{R}}{r}. \tag{2.47}$$

Insertion of the radial stress of the shell and the core into T_R from Eq. 2.40_1 reads

$$\Pi^C = \frac{G^C}{1+Q^C} \left[\frac{(1+Q^C)^2}{(f^C)^{\frac{2}{3}}} \left(\frac{R^C}{r^C}\right)^4 - 1 \right] - T_R^C, \tag{2.48}$$

$$\Pi^S = \frac{G^S}{1+Q^S}\left[\frac{(1+Q^S)^2}{(f^S)^{\frac{2}{3}}}\left(\frac{R}{r}\right)^4 - 1\right] - T_R. \tag{2.49}$$

By using Eq. 2.48 and Eq. 2.49 and applying chemical equilibrium condition, the swelling of the core Q^C and the shell Q^S are to be found.

2.2.3 Chemical equilibrium condition

In equilibrium swelling, the exchange of water molecules from a bath to polymer network of shell ceases. Thus, the chemical potential at the outer boundary of the shell becomes equal to that of the bath ($\mu^S|_{R=R_2} = \mu_0$). Moreover, the gradient of chemical potential within the shell becomes zero. The chemical potentials of core and shell domains become constant and equal to the chemical potential of the bath,

$$\mu^S(R) = \mu^C(R) = \mu_0. \tag{2.50}$$

Insertion of Eq. 2.50 into Eq. 2.29 results in

$$\Pi = -\frac{k_B T}{v}\left(\ln\frac{Q}{1+Q} + \frac{1}{1+Q} + \frac{\chi}{(1+Q)^2}\right). \tag{2.51}$$

It follows from Eqs. 2.47, 2.48 and 2.51,

$$\frac{k_BT}{v}\left(\ln\frac{Q^C}{1+Q^C}+\frac{1}{1+Q^C}+\frac{\chi^C}{(1+Q^C)^2}\right)+\frac{G^C}{1+Q^C}\left[\frac{(1+Q^C)^2}{(f^C)^{\frac{2}{3}}}\left(\frac{R^C}{r^C}\right)^4-1\right] \tag{2.52}$$
$$-\int_{R_1}^{R_2}\frac{2G^S}{r(f^S)^{\frac{2}{3}}}\left((1+Q^S)^2\left(\frac{\tilde{R}}{r}\right)^6-1\right)d\tilde{R}=0,$$

where χ^C is the Flory-Huggins interaction parameter of the core.

$$\frac{k_BT}{v}\left(\ln\frac{Q^S}{1+Q^S}+\frac{1}{1+Q^S}+\frac{\chi^S}{(1+Q^S)^2}\right)+\frac{G^S}{1+Q^S}\left[\frac{(1+Q^S)^2}{(f^S)^{\frac{2}{3}}}\left(\frac{R}{r}\right)^4-1\right] \tag{2.53}$$
$$-\int_{R}^{R_2}\frac{2G^S}{r(f^S)^{\frac{2}{3}}}\left((1+Q^S)^2\left(\frac{\hat{R}}{r}\right)^6-1\right)d\hat{R}=0,$$

where χ^S is the Flory-Huggins interaction parameter of shell.

These nonlinear equations (Eq. 2.52 and Eq. 2.53) together with Eqs. 2.36, 2.45 and 2.46, are to be solved to find equilibrium swelling ratio of the shell $Q^S(R)$ and the core Q^C.

2.2.4 Numerical algorithm

The governing equation for the core/shell hydrogel – together with boundary conditions and constitutive relations – are solved with COMSOL Multiphysics 5.0 [144]. The one-dimensional problem are implemented using equation-based modeling feature and a

direct solver (MUMPS) with a relative convergence tolerance of 10^{-9}. Two differential equations Eq. 2.42 and Eq. 2.40 – including the governing equation for the Cauchy stress and the equation for radial deformation, respectively – together with two algebraic equations (Eq. 2.38 and Eq. 2.51) as boundary conditions, are implemented. Since the problem is fully coupled, an automatic highly nonlinear method is applied. Simulation is performed on a computer with 2.4 GHz dual processor with 4 GB RAM and 64-bit operating system.

The solution obtained from COMSOL and also an in-house MATLAB code. For the MATLAB code, an iterative method is applied to find swelling ratio of core and shell. The inner and outer radius of the shell ($R_1,\ R_2$) in the dry state are given by Eq. 2.35. The shell domain in the dry state $[R_1,\ R_2]$ is discretized into $N = 400$ divisions with $R_n = R_1 + (R_2 - R_1)/N \quad (n = 0, 1, \ldots,\ N)$. The iterative algorithm has two loops in five steps which has been explained below. The first loop includes step I and step II to find Q^C, and the second loop comprises steps III and IV to obtain Q^S.

- Step I: At the ith iteration, Eq. 2.54 is solved by the Simpson's method for an arbitrary value of Q^s. The external stress on the core from the shell, α_n^{i-1} is expressed by

$$\alpha_n^{i-1} = \int_{R_1}^{R_2} \frac{2G^S\nu}{k_BT} \times \frac{1}{r(f^S)^{\frac{2}{3}}} \left((1+Q^S)^2 \left(\frac{\tilde{R}}{r}\right)^6 - 1 \right) d\tilde{R}. \tag{2.54}$$

- Step II: α_n^{i-1} found from Eq. 2.54 is inserted into Eq. 2.55, and the value of Q^C

is determined by the Newton-Raphson method.

$$\ln\frac{Q^{C\,i}}{1+Q^{C,i}}+\frac{1}{1+Q^{C,i}}+\frac{\chi^C}{(1+Q^{C,i})^2}+\frac{G^C v}{k_B T}\left(\frac{1+Q^{C,i}}{(f^C)^{\frac{2}{3}}}\left(\frac{R_n^C}{r^C(R_n)}\right)^4-\frac{1}{1+Q^{C,i}}\right)=\alpha_n^{i-1}, \tag{2.55}$$

where $r^C(R_n)$ is determined from Eq. 2.45 using $Q^{C,(i-1)}$. A termination criterion is defined to stop the algorithm,

$$\delta_i = max \mid Q^{C,i}-Q^{C,i-1} \mid \leq 10^{-5}. \tag{2.56}$$

- Step III: At the jth iteration, the radial stress of the shell reads

$$\beta_n^{j-1}=\int_R^{R_2}\frac{2G^S v}{k_B T}\times\frac{1}{r(f^S)^{\frac{2}{3}}}\left((1+Q^S)^2\left(\frac{\hat{R}}{r}\right)^6-1\right)d\hat{R}, \tag{2.57}$$

which is solved by the Simpson's method for β_n^{j-1}.

- Step IV: For the value of $Q^S(R)$, the following equation

$$\ln\frac{Q^{S,j}(R_n)}{1+Q^{S,j}(R_n)}+\frac{1}{1+Q^{S,j}(R_n)}+\frac{\chi^S}{(1+Q^{S,j}(R_n))^2}+\frac{G^S v}{k_B T}\left(\frac{1+Q^S(R_n)}{(f^S)^{\frac{2}{3}}}\left(\frac{R_n}{r^S(R_n)}\right)^4-\frac{1}{1+Q^S}(R_n)\right)=\beta_n^{j-1}, \tag{2.58}$$

is solved by the Newton-Raphson method. A termination criterion is also deter-

mined for this loop, which reads

$$\delta_j = max \mid Q^{S,j}(R_n) - Q^{S,(j-1)}(R_n) \mid \leq 10^{-5} \tag{2.59}$$

- Step V: At the end of each iteration, the convergence of $Q^S(R_n)$ from step IV and step I is calculated by the following criterion

$$\delta_{iter} = max \mid Q^{S,(iter)}(R_n) - Q^{S,(iter-1)}(R_n) \mid \leq 10^{-5}. \tag{2.60}$$

This five-step procedure is repeated until the convergence criterion is satisfied (in Eq. 2.60: $iter \rightarrow iter + 1$).

2.2.5 Comparison between results from in-house MATLAB code and COMSOL

The internal structure of core/shell hydrogels depends on the mutual deformation of core and shell caused by swelling and mechanical forces. Core/shell gels are considered to be neutral in this chapter. Equal physical parameters are prescribed to compare the results between the in-house code and the COMSOL model.

The partial swelling of both domains (Q_0^S and Q_0^C) is equal to 0.5 which is a common value for isopropyl acrylamide (NIPA) gel above the volume phase transition temperature (VPTT) [145]. Equal partial swelling in the core and the shell, results in $R_1 = R^C$. The Flory-Huggins interaction parameter for both domains (χ^S and χ^C) is taken to be

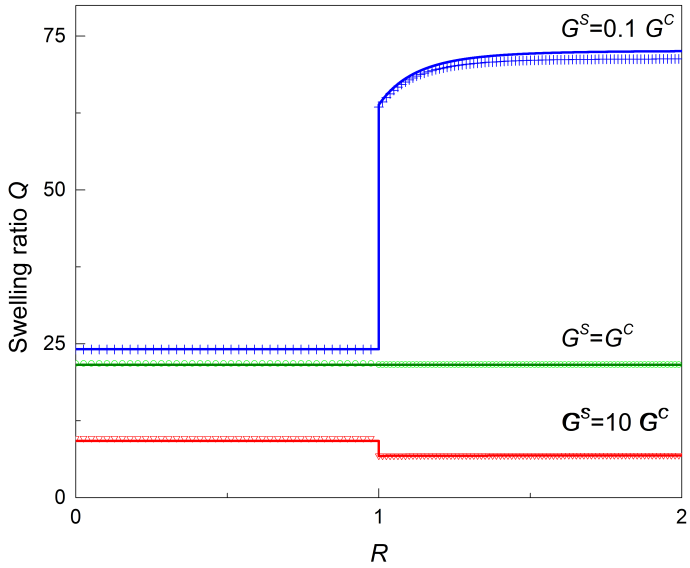

Figure 2.3: Swelling ratio in the core/shell hydrogels is calculated when $G^C = 40$ KPa for three different cases when the swelling in the shell is more, equal or less than the swelling in the core. Symbols show the results from an in-house code and lines are the results from COMSOL.

0.4 for a water bath. The shear modulus of core G^C is assumed to be 40 KPa as a common value for hydrogels [14]. Three different values for the modulus of the shell G^S is considered: ten times higher, equal, and ten times lower than G^C. Consequently, the shell will have lower, equal or higher swelling ratio than that of the core.

Fig. 2.3 shows the comparison between results obtained from the in-house code and the model built in Comsol. Calculations show that the relative error is not exceeding than 2%.

2.3 Summary

A theoretical model is applied to determine the coupled large deformation and solvent diffusion of a hydrogel under swelling. The model is developed based on three states: initial state, reference state, and actual state. The reference state is considered to be different from the initial state. Constitutive relations are extended further to model the equilibrium swelling of core/shell hydrogels in the spherical coordinate. The model is implemented in COMSOL using equation-based modeling feature, and also in MATLAB by scripting an in-house code for three special cases where different swelling ratios evolve in core and shell domains. The comparison shows an acceptable error between two models. The model which is developed in COMSOL, is preferred to be used in the next chapters for swelling analysis of stimuli-responsive hydrogels composed of multi phases.

Chapter 3

Temperature-sensitive core/shell composite gels

There are various types of hydrogels classified based on different factors including their physical and chemical structures or their stimuli-responsive behavior [22]. In this chapter, the focus is on temperature-sensitive hydrogels classified as positive or negative thermo-sensitive gels which show an increasing or a decreasing swelling as a function of temperature, respectively.

The most common negative temperature- sensitive hydrogel is poly(N-isopropyl acrylamide) (pNIPAM) with a lower critical solution temperature (LCST) of 32-35 °C for the linear polymer which is close to the volume phase transition temperature (VPTT) of pNIPAM hydrogels [32]. The phase transition of temperature-sensitive composite hydrogels depends on the interaction of water and hydrophilic groups of the polymer, formation/breakage of hydrogen bonding, and also the balance between hydrophilic and

hydrophobic groups of the polymer [33]. At lower temperature, the hydrophilic groups become dominant and soluble in water; however, at higher temperature, hydrophobic interactions dominate the swelling.

The theory of gel swelling has been developed based on the fundamental work of Flory and Rehner [97, 98]. Flory-Rehner theory has also been modified to describe the behavior of various types of hydrogels [89]. In the last decade, numerous constitutive models have been developed in the thermodynamic framework to express solvent diffusion and elastic response of three-dimensional finite deformation of neutral gels [101–108, 146, 147] and temperature-sensitive hydrogels [109–113, 127, 132]. The most common approach to model temperature-dependent swelling is to employ an effective Flory-Huggins parameter which is a function of temperature and polymer density [31, 114]. Moreover, a mechanism for phase deformation between hydrophilic and hydrophobic groups is involved in the specific strain energy of a hydrogel is also reported in [111, 112]. In this study, the common approach to use an effective Flory-Huggins parameter is applied.

Inspired by motions in plants [58], composite hydrogels are developed which display exotic behavior through their anisotropic swelling behavior. The 2D layered structure of a composite gel can deform to a 3D complex structure – cylinder, helical or even cone – during swelling [59, 60]. Geometry constraints can induce an anisotropic swelling in composite core/shell gels with separated domains. Several models are also developed to determine inhomogeneous swelling of core/shell hydrogels having a rigid or soft core [125–132, 135, 136, 139].

In particular, temperature-sensitive core/shell hydrogels are studied in this chapter. Core/shell hydrogels have gained attention in the last decade due to their multi-responsive behavior (e.g. pH- and temperature-sensitive) [37,65,66,148]. A theoretical model is developed in this chapter based on thermodynamics of gel swelling, and an experiment is used to quantitatively verify the model. The experiment is on a dual temperature-sensitive core/shell microgel – the core contains poly(N-isopropyl acrylamide) (pNIPAM), and the shell includes poly(N-isopropyl methacrylamide) (pNIPMAM) – which has been recently synthesized and studied in [66]. The volume phase transition temperature (VPTT) of the core (34°C) is different from that of the shell (44°C). Its swelling can be triggered by the human body temperature which is in between the VPTTs of the core and shell domains. This microgel exhibits a rapid swelling – due to its micron size – in response to changes in temperature. The swelling behavior of this microgel is desirable for various biomedical applications and also for mechanical modeling.

Among different techniques to characterize the structure of hydrogels [81], there are two most well-established methods: dynamic light scattering (DLS) and small angle neutron scattering (SANS) to measure the size of microgel particles and the polymer density within core and shell domains, respectively. Experiments on pNIPAM/pNIPMAM core/shell microgels revealed that the size of the particle reduces by increasing temperature [149]. The size of microgels dropped monotonically with temperature at one transition point for microgels with a thin shell. Moreover, two transition points were observed by increasing the shell thickness. Gernandt et al. [128] employed

a nonlinear field theory to model the swelling behavior of the dual thermo-sensitive core/shell microgel. The interaction of the core and shell domains at the swollen and collapsed states was well studied and qualitatively compared with experimental data from SANS. However, a shortcoming of these models is that their predictions are not verified with experimental results from DLS and SANS. Simplification of the interaction between the core and shell is considered in some studies to find approximate results [129, 140]. Accurate predictions can be achieved by accounting for the swelling in each domain and their mutual interaction, and finding the thermodynamic equilibrium between the swelling and mechanical forces.

A thermodynamic model has recently been developed to study solvent diffusion and elastic deformation of neutral core /shell hydrogels based on the free energy inequality, and to analyze the equilibrium swelling of core /shell microgels with a rigid core [131]. In this chapter, the thermodynamic model has been extended to capture the equilibrium swelling of temperature-sensitive core/shell microgels with a deformable core, and to investigate the effect of temperature and shell thickness on the swelling ratio. Our approach differs from existing constitutive models in two ways: (i) the reference state is differentiated from the initial state where hydrogels are dried and undeformed; (ii) a continuous domain is assumed for core/shell hydrogels, and individual discontinuous elastic modulus and polymer-solvent interaction parameters are assigned to physical parameters of each domain. The core/shell model is then validated with experimental data from dynamic light scattering and small angle neutron scattering experiments on pNIPAM/pNIPMAM core/shell microgels [148].

3.1 Governing equations

The governing equation for a core/shell hydrogel is derived in the spherical coordinate in the actual state

$$\frac{\partial T_R}{\partial r} + \frac{2}{r}(T_R - T_\Theta) = 0. \tag{3.1}$$

Eq. 3.1 is reformatted to be in the initial state, and the tangential stress T_Θ is substituted from Eq. 2.40_2. The simplified equation for radial stress T_R implies that

$$\frac{\partial T_R}{\partial R} + \frac{2G}{r f^{\frac{2}{3}}}\left((1+Q)^2\left(\frac{R}{r}\right)^6 - 1\right) = 0. \tag{3.2}$$

The radial deformation $r(R)$ is given (refer to Eq. 2.38) by

$$r^2\frac{\partial r}{\partial R} = (1+Q)R^2. \tag{3.3}$$

The constitutive framework developed to study the deformation of a core/shell hydrogel subjected to mechanical and swelling forces, is described in Chapter 2. Here, constitutive relations are modified for temperature-sensitive hydrogels.

The volume transition of temperature-sensitive core/shell gels is considered by an effective Flory-Huggins parameter in the mixing energy between solvent molecules and polymer chains [150, 151]. The mixing energy in Eq. 2.19 is replaced by

$$\Psi_{mix} = \frac{k_B T}{v}(Q\ln\frac{Q}{1+Q} + \chi(T,Q)\frac{Q}{1+Q}), \tag{3.4}$$

where $\chi(T,Q)$ is the effective Flory-Huggins parameter and introduced as a function of temperature and swelling ratio [114,152,153]. Following [109], the effective interaction parameter is expressed by

$$\chi(T,Q) = -\frac{\Delta s}{k_B} + \frac{\Delta h}{k_B(T-\Delta T)} + \frac{\chi_2}{1+Q}, \tag{3.5}$$

where χ_2 denotes the volume fraction dependence, ΔT is added to this formula to account for the shift in the VPTT for different hydrogels, and Δs and Δh are the entropy and enthalpy contributions to the interaction parameter, respectively. The condition of chemical equilibrium from Eqs. 2.48, 2.49 and 2.51, states that

$$\frac{k_B T}{v}\left(\ln\frac{Q}{1+Q} + \frac{1}{1+Q} + \frac{\chi(T,Q)}{(1+Q)^2}\right) + \frac{G}{1+Q}\left[\frac{(1+Q)^2}{f^{\frac{2}{3}}}\left(\frac{R}{r}\right)^4 - 1\right] - T_R = 0. \tag{3.6}$$

3.1.1 Numerics

The theoretical model needs to be solved to determine the equilibrium swelling of temperature sensitive core/shell hydrogels in the core and shell domains. The core/shell hydrogel is modeled by only one continuous domain with distinct discontinuous elastic modulus G and interaction parameter χ for the core and shell. These parameters are introduced as field variables which change from the core to shell domain with a continuous second-order transition function at the core/shell boundary.

Dependent variables T_R and $Q(R)$ are to de found from two differential equations (Eq. 3.2 and Eq. 3.3) and one algebraic equation (Eq. 3.6). The commercial software

COMSOL [144] was employed to implement the model. Two appropriate boundary conditions were applied at the inner and outer domain of the hydrogel. The inner radius of the spherical gel is zero, and the outer surface of the spherical gel is stress-free. Therefore, the boundary conditions are given by

$$\begin{aligned} r(R=0) &= 0, \\ T_R(R_{out}) &= 0. \end{aligned} \tag{3.7}$$

For this model, the maximum element size of 10^{-3} nm was chosen to ensure that the solution is mesh independent. Number of elements were ~ 170000 adding up to $\sim 1 \times 10^6$ degrees of freedom.

3.2 Results and discussion

The internal structure of core/shell hydrogels depends on the mutual interaction between core and shell domains subjected to swelling. Swelling of the core and shell can be induced by a change in environmental parameters, such as: humidity, temperature, pH, salt concentration, and specific molecules [9]. A study on a double temperature-sensitive microgel with pNIPAM/pNIPMAM core/shell structure is used as a reference experiment to verify our simulation results [149]. The hydrodynamic radius of microgels from DLS measurements, and also the polymer density within microgels from SANS measurements are compared with simulation results.

3.2.1 Parameters

The geometry of core/shell hydrogels is defined in the initial configuration by two parameters: R_{in} and R_{out}. R_{in} denotes the radius of the core and is set to 40 nm close to the experimental data. The outer radius of the microgel particle R_{out} is the only fitting parameter. Another parameter is the partial swelling of hydrogel which describes the evolution of the reference state. The partial swelling of the core and the shell are set to $Q_0 = 0.96$ according to the experiment.

The elastic modulus of the core and the shell are determined by fitting to the swelling-temperature curve of a specific size of the microgel which is $V_{shell}/V_{core} = 0.73$. The elastic modulus G is set to be the same for the core and the shell, and in the admissible range of the modulus of hydrogels as illustrated in Fig. 1.3.

The interaction parameter $\chi(T,\varphi)$ is required to capture the volume phase transition temperatures (VPTT) of the pNIPAM core and the pNIPMAM shell which are 34 °C and 44 °C, respectively. Swelling-temperature curve of isolated pNIPAM microgels are used to find χ^C from Fig. 3.1. The interaction parameter of the shell χ^S is determined by fittings to DLS measurements from the microgel with a specific volume fraction of $V_{shell}/V_{core} = 0.73$ – shown by solid yellow triangle symbols in Fig. 3.2. All required parameters for numerical simulation are listed in Table 3.1.

Table 3.1: Physical and geometry parameters of the core/shell hydrogel

General physical parameters	
V_{shell}/V_{core}	$1.74, 1.33, 0.73, 0.33$
k_B	$1.38 \times 10^{-23}\,\mathrm{J\,K^{-1}}$
φ_0	0.51
v	$10^{-28}\,\mathrm{m^3}$
Physical parameters of the core	
Δs^C	$-3.7 \times 10^{-23}\,\mathrm{J\,K^{-1}}$
Δh^C	$-9.2 \times 10^{-21}\,\mathrm{J}$
χ_2^C	0.35
G^C	$20 \times 10^3\,\mathrm{N\,m^{-2}}$
ΔT^C	20 °C
Physical parameters of the shell	
Δs^S	$-2.35 \times 10^{-23}\,\mathrm{J\,K^{-1}}$
Δh^S	$-5 \times 10^{-21}\,\mathrm{J}$
χ_2^S	0.48
G^S	$20 \times 10^3\,\mathrm{N\,m^{-2}}$
ΔT^S	0 °C

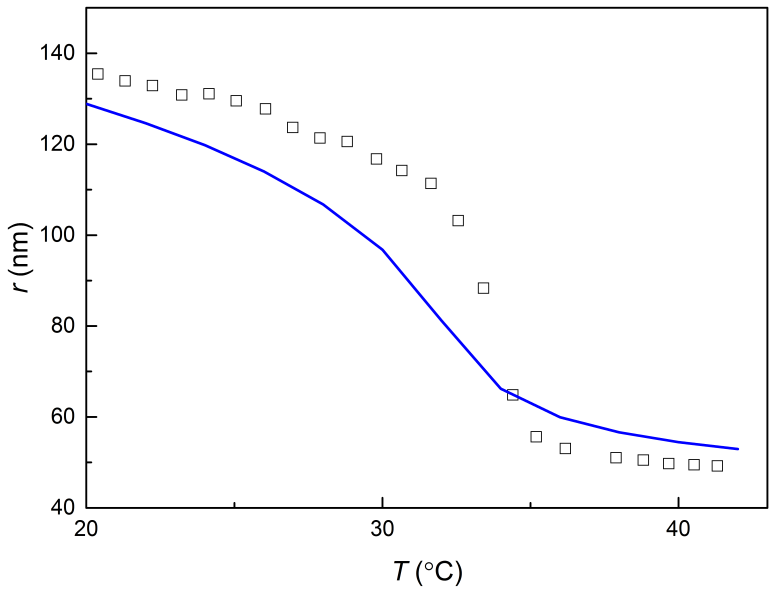

Figure 3.1: Radius of isolated core of microgels as a function of temperature; the line is from our simulation results and symbols are experimental data

3.2.2 The influence of temperature and shell thickness on the swelling behavior of core/shell particles

The radial deformation of the core/shell hydrogel has been calculated by numerical simulation as a function of temperature and shell thickness. The radius of the core/shell hydrogel is found to decrease as temperature increases, and displays a transition around the VPTTs of the core and the shell.

3.2.2.1 Size of core/shell hydrogels

When temperature is higher than the VPTTs of the core and the shell ($T > 44$ °C), increasing the shell thickness enhances the swelling degree of the hydrogel (Fig. 3.2) in accord with the experiment although both domains are at their collapsed states. When temperature reduces below the VPTT of the shell, the shell starts to expand and the radius of hydrogel increases; however, the core is still in its collapsed state. In this case, hydrogels with a thin shell show a small increase in their swelling degree with a smooth transition. Increasing the shell thickness results in a pronounced increase in the size of swollen hydrogels with relatively sharp transitions. It may be explained that the swelling of the shell is constrained by the collapsed core only to a certain shell thickness which is more effective for hydrogels with thin shells. In contrast, hydrogels with thick shell have more room for the shell to expand inhomogeneously in the radial direction and their overall volume is less affected.

Decreasing temperature below the VPTTs of both domains, results in swollen core and shell domains. In this case, the maximum degree of swelling in the shell is obtain-

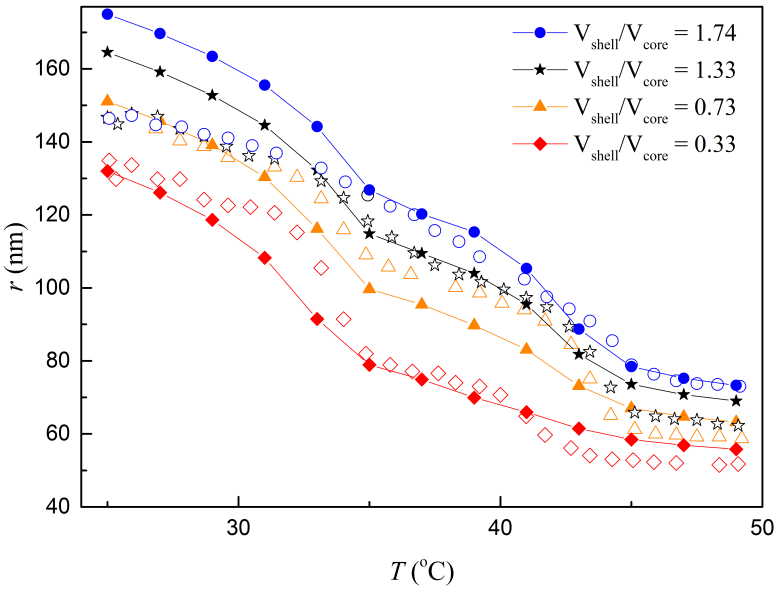

Figure 3.2: Radius of core/shell microgels as a function of temperature and shell thickness; lines with symbols are simulation results, and symbols are experimental data; the line with solid yellow triangle signs is used for parameter-adaptation and the shell thickness is the only fitting parameter

able since the core applies no constraint on the shell. It is revealed that the corresponding transition point ($T \approx 34$ °C) is not affected by changing the shell thickness. At this transition temperature point, hydrogels display an increase in the size whereas those with a thick shell demonstrate a less pronounced increase. This behavior is in agreement with the readings of SANS, since the scattering density measurements are directly proportional to the degree of swelling in hydrogels (refer to Figure 4 in [148]). However, DLS observations demonstrate that the swelling degree of microgels with thicker shells cannot increase beyond a certain value.

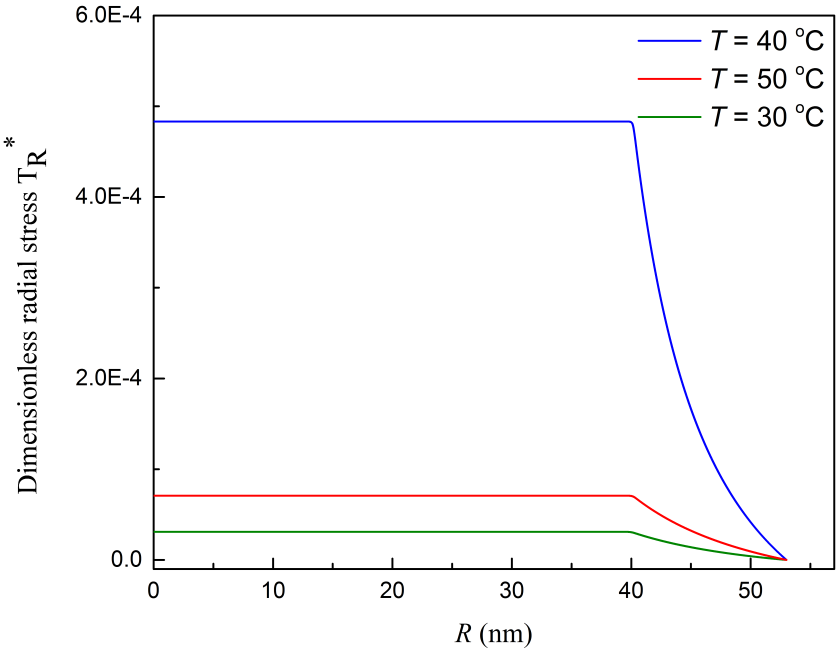

Figure 3.3: Radial stress in the pNIPAM/pNIPMAM core/shell hydrogel with $V_{shell}/V_{core} = 1.33$ at three different temperatures

3.2.2.2 Stress distribution within the core/shell structure

The radial and tangential stresses are calculated as a functional of the radius of the core/shell hydrogel with a shell volume fraction of $V_{shell}/V_{core} = 1.33$ at temperatures of $T = 30,\ 40$ and $50\ ^{\circ}$C. The dimensionless radial and tangential stresses are defined by $\mathrm{T}_{\mathrm{R}}^{*} = \mathrm{T}_{R}\nu/(k_B T)$ and $\mathrm{T}_{\theta}^{*} = \mathrm{T}_{\theta}\nu/(k_B T)$, respectively. It can be seen in Fig. 3.3 and Fig. 3.4 that the stresses are constant throughout the core domain which is due to the constant polymer density and the swelling in the core. The homogeneous swelling of the core is in agreement with the findings in [154]. However, the stresses in the shell show a radial distribution through the shell thickness.

Fig. 3.3 depicts that the radial stresses decay from its maximum value at the core/shell

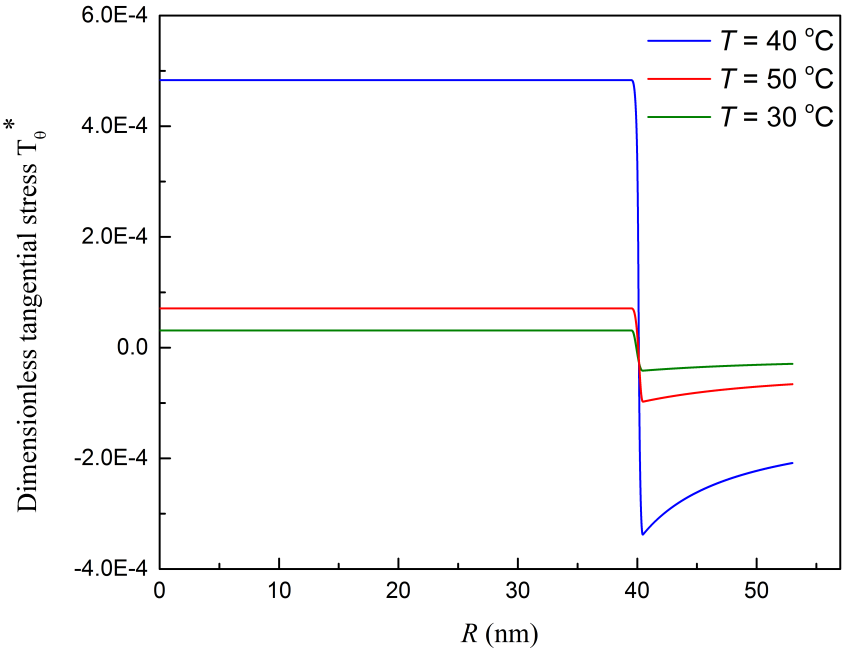

Figure 3.4: Tangential stress in the pNIPAM/pNIPMAM core/shell hydrogel with $V_{shell}/V_{core} = 1.33$ at three different temperatures

interface to zero at the outer radius of the shell. The radial stress is positive for all three temperatures due to the expansion of the shell and application of radial stress on the core. The radial stresses increase by increasing temperature until $T = 45$ °C which is the VPTT of the shell. Further increase in temperature coincides with the collapse of the shell which results in the reduction of the degree of swelling and subsequently the radial stresses.

Furthermore, the tangential stresses are displayed in Fig. 3.4. In the core domain, the tangential stresses are equal to the radial stresses in Fig. 3.3. In the shell domain, the tangential stresses are found to be negative since the core is less swollen than the shell. The core constrains the expansion of the shell circumferentially and applies a lateral

contraction on the shell. The absolute value of the circumferential stresses decreases with the radius of the hydrogel. The value of tangential stresses is increasing with temperature when $T < 45$ °C and further increase in temperature leads to the reduction of stresses and the swelling of the core/shell hydrogel.

3.2.2.3 Polymer density distribution within the core/shell structure

The core-shell model – verified with DLS observations – is used to predict the polymer density in the pNIPAM core and the pNIPMAM shell without any modification. Fig. 3.5 shows the polymer density – which is defined in Eq. 2.11 – in the core-shell particles for a shell volume fraction of $V_{shell}/V_{core} = 1.33$ at temperatures of $T = 30,\ 40$ and 50 °C. Each domain can be either at its swollen or collapsed state in response to different temperatures. Simulation results are relatively in the same range of the experimental data, although the calculated polymer density is quantitatively lower than measured density from SANS at equal temperatures.

Both domains are swollen when $T < 34$ °C, yet still the shell is less denser than the core. When temperature increase to 40 °C, the polymer density in the core increases more pronouncedly than that in the shell. The radial distribution of density within the shell can be seen in Fig. 3.5. The polymer density within the shell is radially distributed which is higher near the core/shell boundary and decreases to a constant value near the outer radius of the shell. In this situation, the collapsed core constrains the swelling of the shell specifically the volume in the shell near the core/shell boundary. Increasing temperature furthermore makes core and shell domains collapse since the temperature

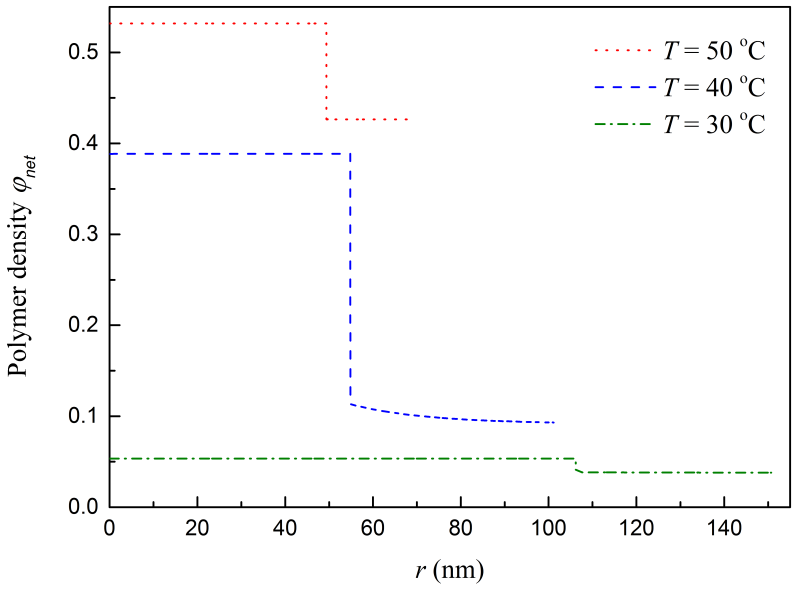

Figure 3.5: Polymer density in the pNIPAM/pNIPMAM core/shell hydrogel with $V_{shell}/V_{core} = 1.33$ at three different temperatures

becomes higher than the VPTTs of both domains. Simulation results show that the core is always denser than the shell at all temperatures which is in agreement with experimental results at $T = 30$ and 40 °C. However at $T = 50$ °C, the polymer density from SANS show that the density in the shell is slightly higher than that in the core.

Contradictions between simulation results and experimental data can be attributed to our assumption of equal elastic modulus and partial swelling of the core and shell. This assumption is made due to the lack of detailed knowledge about the polymer density and the radial distribution of cross-links in the core/shell microgels. Moreover, the relation between crosslink density and the modulus of polymer network is approximate [155].

3.3 Conclusion

The equilibrium swelling of a doubly temperature-sensitive core/shell gel has been studied in response to changes in temperature and shell thickness. A thermodynamic model which has been recently used for neutral core /shell gels with a rigid core, has been further extended to include temperature-induced swelling by incorporating an effective Flory-Huggins interaction parameter. A continuous domain is considered to represent the core/shell hydrogel with discontinuous elastic modulus and interaction parameter for the deformable core and shell domains. The equilibrium swelling of poly (N-isopropyl acrylamide)/ poly (N-isopropyl methacrylamide) core/the shell with different volume phase transition temperature (VPTT) for each domain has been determined by finding the mutual interaction between core and shell. Moreover, polymer density in the core and the shell has also been validated with experimental data from small angle neutron scattering. A homogeneous and isotropic swelling of the core, and a radial inhomogeneous swelling of the shell have been predicted at different temperatures. Predictions of the model have also been verified with the experimental data from dynamic light scattering. It is revealed that increasing the shell thickness develops a two-step transition behavior in the swelling-temperature curves which attribute to the VPTTs of the core and shell polymer network. In contrary, hydrogels with thin shells exhibit only one transition point attributed to the VPTT of the core.

Chapter 4

Dual pH- and temperature-sensitive core/shell composite gels

Hydrogels are new materials which have gained tremendous attention in the 1960s after their first appearance as contact lens, due to their swelling properties and stimuli-responsive behavior [7]. One class of hydrogels – known as smart materials – is responsive to external stimuli such as temperature, pH, pressure, solvent composition, light, sound, electric or magnetic fields, ionic strength, enzymes, alcohol, and specific solutes [23–25]. Experimental studies are mostly involved in the synthesis of hydrogels which are responsive to one stimulus at a time. Multi-responsive hydrogels respond to more than one stimulus – particularly to pH and temperature – have been synthesized and studied since 1990 [62–64]. Later, a series of dual-responsive pNIPAM-co-AAc hydrogels have been synthesized in the form of microgels [38, 67, 68] and macrogels [69–72]. These composite hydrogels were produced by adding acrylic acid (AAc)

– a popular polyelectrolyte hydrogel – to poly(N-isopropyl acrylamide) (pNIPAM) – a usual stable temperature-sensitive hydrogel – as the base material. The swelling behavior of these composite hydrogels is as a multifunction of solution pH, AAc concentration, and temperature.

This research is motivated by an experimental study on pNIPAM-co-AAc hydrogels. The swelling behavior of these copolymer hydrogels has been studied and the following main features are extracted:

1. The size of the pNIPAM-co-AAc hydrogel increases by adding ionic AAc monomers to the side chains of pNIPAM polymer, and increases even further with higher AAc fraction and higher pH values of bath.

2. The volume phase transition temperature (VPTT) of ionic hydrogels including microgels and macrogels, shifts to a higher temperature in a salt-free bath. This shift is much smaller for microgels than that for macrogels.

3. Two-step volume phase transition behavior appears when macrogels have a substantial amount of AAc monomers or microgels are subjected to swelling in the bath with a high pH value (close to seven or higher).

The most important feature of these ionic polymer gels is considered to be the shift in their VPTT compared to the VPTT of temperature-sensitive hydrogels. This shift is a function of AAc molar fraction and pH. The swelling of the dual-responsive ionic gels causes the shrinkage of their volume to happen at a higher temperature.

Swelling of ionic polymer gels – also called pH-sensitive hydrogels – basically oc-

curs when pH exceeds the dissociation of functional groups of the polymer network pK_a. The charge of functional groups determines whether a gel is anionic, cationic or ampholytic. The swelling of ionic polymer gels can be explained by two mechanisms [37–39]: (i) the increased osmotic pressure resulting from excess counter ions intake, and (ii) the pressure induced by the repulsive forces between bound charges on the backbone of the polymer network. The first mechanism is conventionally considered as the main mechanism to describe the equilibrium swelling of ionic polymer gels. The contribution of the second mechanism to the swelling of pH-sensitive hydrogels are not well addressed by a simple mathematical formulation for the analysis of experimental data [156].

The swelling of pH-sensitive hydrogels has been the focus of many theoretical models [115–122]. Most of these theoretical models account only for the contribution of ionic pressure which arises from the gradient of ion concentration inside and outside of the polymer network. There are few models which incorporate the effect of electrostatic repulsion between bound charges attached to the backbone of the network [142, 157]. Besides modeling pH-sensitive gels, a theoretical model is also needed to describe the temperature-induced swelling of pH- /temperature-responsive (dual-responsive) hydrogels. Following the approach described in Chapter 3, an equivalent Flory-Huggins parameter is incorporated into the mixing energy of solvent and network to account for the volume phase transition behavior of thermo-sensitive gels.

This chapter provides a study on the equilibrium swelling of pH-/temperature-responsive core/shell hydrogels. Core/shell hydrogels have been synthesized and studied in the last

decade due to their multi-responsive behavior [37,65,66,148]. The anisotropic swelling of neutral core/shell gels – due to its geometry constraint at the core/shell boundary – has recently been studied by a number of theoretical models [128–130, 135–139]. Despite these studies on temperature-sensitive core/shell hydrogels, the coupled influence of temperature and pH on the swelling behavior of core/shell hydrogels has not been addressed.

pH-sensitive hydrogels subjected to swelling have been studied recently by a thermodynamic model which treats an anionic hydrogel to be consisted of three phases: polymer network, solvent (water molecules), and solutes (mobile ions) [142]. The energy of transportation of solvent and solutes, the mechanical stress of the polymer network, the ionic pressure and the electrostatic repulsion between bound charges are considered in the free energy of the hydrogel. It is demonstrated that this model is consistent with the Henderson-Hasselbach equation for the calculations of pH – acidity changes by the production of mobile ions and the dissociation of functional groups – and also, the van't Hoff formula for ionic pressure. The model is then formulated for mechanical and chemical (the Donnan's equilibrium law) equilibrium conditions.

The aim of this study is to extend the thermodynamic model to express the equilibrium swelling of a pH-/temperature-responsive core/shell hydrogel with the deformable core and shell domains. This approach is grounded on the assumption that the reference state is differentiated from the initial state where hydrogels are dried and undeformed, two distinct domains are assumed for core/shell hydrogels, and individual discontinuous elastic modulus and polymer-solvent interaction parameters are assigned to physical

parameters of each domain. The simulation results are compared with the experimental data from dynamic light scattering on pNIPAM-co-AAc (core)/pNIPAM (shell) microgels [37].

4.1 Mathematical formulation

In this model, an anionic hydrogel is assumed to be consisted of three phases: polymer network, solvent (water molecules), and solutes (mobile ions). Water molecules and mobile ions are allowed to diffuse into the polymer network. Migration of water and mobile ions occurs due to the chemical reactions of mobile ions and polymer network with water molecules and furthermore, these reactions are accelerated by the electric field generated among the bound charges on the backbone of the network.

4.1.1 Chemical reactions

Pure water has a low electrical conductivity ($0.055\mu S.cm^{-1}$) due to its self-ionization reaction

$$2H_2O \leftrightarrows H_3O^+ + OH^-, \tag{4.1}$$

which produces hydroxide ions H^+ (attached to water molecules) and OH^- hydroxyl ions whose activities are controlled by their concentration. Therefore, the water dissociation constant is given by $pK_w = [H^+][OH^-]$; therefore, at room temperature $pK_w = 14$, where p denotes a co-logarithm. The bath is assumed to be acidic in this chapter. Dissolving a strong acid (e.g. HCl) in water makes an acidic environment by reducing the

pH of neutralized water below 7. The neutrality condition at room temperature states that pH = pOH = 7. This reaction produces H^+ (attached to water molecules) and Cl^- chloride ions

$$H_2O + HCl \leftrightarrows H_3O^+ + Cl^-. \tag{4.2}$$

Anionic hydrogels with functional (carboxyl) groups become ionized when submerged in water

$$H_2O + COOH \leftrightarrows H_3O^+ + COO^-. \tag{4.3}$$

A n_1 fraction of total number of COOH groups (n) becomes ionized COO^- attached to the polymer chains. Then, the degree of ionization per chain is defined as

$$\alpha = \frac{n_1}{n}. \tag{4.4}$$

The molar fraction of ions are found from the concentrations of ions in the bath as

$$[H^+] = k\frac{\bar{c}_{H^+}}{\bar{c}},\ [OH^-] = k\frac{\bar{c}_{OH^-}}{\bar{c}},\ [Cl^-] = k\frac{\bar{c}_{Cl^-}}{\bar{c}}, \tag{4.5}$$

where $\bar{c}$, $\bar{c}_{H^+}$, $\bar{c}_{OH^-}$, and $\bar{c}_{Cl^-}$ represent the concentration of water molecules, hydroxide ions, hydroxyl ions, and chloride ions in the bath, respectively, and $k = 55.\bar{5}$ is the molarity of water.

As a common assumption, the infinite amount of solvent molecules and solutes are available in the bath which maintains the concentration of mobile ions constant. The ionization of water molecules and hydrochloric acid and also, association of H^+ mobile

ions with water molecules in Eq. 4.3 are disregarded in this model.

For kinematics of a hydrogel, readers are referred to Section 2.1.1 in Chapter 2.

4.1.2 Kinetic relations

A kinetic law is used to describe transportation of solvent molecules into an isotropic network, as follows

$$\mathbf{J} = -\frac{DC}{k_B T}\mathbf{F}^{-1} \cdot \boldsymbol{\nabla}_0 \mu \cdot \mathbf{F}^{-1}, \tag{4.6}$$

where D is diffusivity, k_B is the Boltzmann constant, $C = c$ det$\mathbf{F}$ denotes the concentration of solvent molecules per unit volume in the actual state, $\mathbf{J}$ is the solvent flux in the initial state, and $\boldsymbol{\nabla}_0 \mu$ is the gradient of chemical potential energy in the initial state [131]. Eq. 4.6 is then substituted into mass conservation law for solvent molecules

$$\dot{C} + \boldsymbol{\nabla}_0 \cdot \mathbf{J} = 0, \tag{4.7}$$

when there is no external source to inject more solvent molecules. Finally, the diffusion equation implies that

$$\dot{C} = \boldsymbol{\nabla}_0 \cdot (\frac{DC}{k_B T}\mathbf{F}^{-1} \cdot \boldsymbol{\nabla}_0 \mu \cdot \mathbf{F}^{-1}). \tag{4.8}$$

The flux vector of mobile ions in the initial state can be derived analogous to Eq.

4.6, and are expressed by

$$\begin{aligned}
\mathbf{J}_{\mathrm{H}^+} &= -\frac{D_{\mathrm{H}^+}C_{\mathrm{H}^+}}{k_B T}\mathbf{F}^{-1}\cdot\boldsymbol{\nabla}_0\mu_{\mathrm{H}^+}\cdot\mathbf{F}^{-1},\\
\mathbf{J}_{\mathrm{OH}^-} &= -\frac{D_{\mathrm{OH}^-}C_{\mathrm{OH}^-}}{k_B T}\mathbf{F}^{-1}\cdot\boldsymbol{\nabla}_0\mu_{\mathrm{OH}^-}\cdot\mathbf{F}^{-1},\\
\mathbf{J}_{\mathrm{Cl}^-} &= -\frac{D_{\mathrm{Cl}^-}C_{\mathrm{Cl}^-}}{k_B T}\mathbf{F}^{-1}\cdot\boldsymbol{\nabla}_0\mu_{\mathrm{Cl}^-}\cdot\mathbf{F}^{-1},
\end{aligned} \tag{4.9}$$

where $D_{\mathrm{H}^+}, D_{\mathrm{OH}^-}$, and D_{Cl^-} are the diffusivity of mobile ions, respectively, and $\mu_{\mathrm{H}^+}, \mu_{\mathrm{OH}^-}$ and μ_{Cl^-} are the equivalent chemical potentials, respectively. The corresponding mass conservation laws are given by

$$\begin{aligned}
\dot{C}_{\mathrm{H}^+} &+\boldsymbol{\nabla}_0\cdot\mathbf{J}_{\mathrm{H}^+} &&= \Gamma_{\mathrm{H}^+},\\
\dot{C}_{\mathrm{OH}^-} &+\boldsymbol{\nabla}_0\cdot\mathbf{J}_{\mathrm{OH}^-} &&= 0,\\
\dot{C}_{\mathrm{Cl}^-} &+\boldsymbol{\nabla}_0\cdot\mathbf{J}_{\mathrm{Cl}^-} &&= 0,
\end{aligned} \tag{4.10}$$

where $\Gamma_{\mathrm{H}^+} = \alpha\dot{C}_b$ is the rate of production of H^+ ions due to the ionization of ionic polymers and the dissociation of functional groups. In addition, the concentration of total bound charges attached to chains is denoted by $C_b = Mn$ where M reads the number of chains. In the initial configuration, $C_{b^-} = \alpha C_b$ defines the concentration of bound charges per unit volume in the initial state.

The work produced to transfer solvent and mobile ions into the gel (per unit volume in the initial state and per unit time) has been described in [142, 158] by

$$u_{\mathrm{dif}} = \mu\dot{C} + \mu_{\mathrm{H}^+}(\dot{C}_{\mathrm{H}^+} - \dot{\alpha}C_b) + \mu_{\mathrm{OH}^-}\dot{C}_{\mathrm{OH}^-} + \mu_{\mathrm{Cl}^-}\dot{C}_{\mathrm{Cl}^-} + \bar{u}_{\mathrm{dif}}, \tag{4.11}$$

where the last term is given by

$$\bar{u}_{\text{dif}} = -(\mathbf{J}\cdot\boldsymbol{\nabla}_0\mu + \mathbf{J}_{\text{H}^+}\cdot\boldsymbol{\nabla}_0\mu_{\text{H}^+} + \mathbf{J}_{\text{OH}^-}\cdot\boldsymbol{\nabla}_0\mu_{\text{OH}^-} + \mathbf{J}_{\text{Cl}^-}\cdot\boldsymbol{\nabla}_0\mu_{\text{Cl}^-}). \tag{4.12}$$

$\bar{u}_{\text{dif}}$ is a non-negative term in Eq. 4.12 according to Eq. 4.9.

4.1.3 Electric field

The formation of bound charges on the chains of polyelectrolyte (PE) hydrogels and the distribution of mobile ions inside the network creates an electric field $\mathbf{e}$ which may be described by

$$\mathbf{e} = -\boldsymbol{\nabla}\Phi, \qquad \mathbf{E} = -\boldsymbol{\nabla}_0\Phi \tag{4.13}$$

where $\boldsymbol{\nabla}\Phi$ and $\boldsymbol{\nabla}_0\Phi$ are the gradient of the potential energy of the electric field in the actual and initial configuration, respectively, whose relation is described by

$$\boldsymbol{\nabla}\Phi = \boldsymbol{\nabla}_0\Phi\cdot\mathbf{F}\ . \tag{4.14}$$

Analogous to a dielectric elastomer, the electric displacement vector of a gel (in the actual state) is given by

$$\mathbf{h} = \varepsilon\mathbf{e}, \tag{4.15}$$

where ε is the permittivity of material. Using chain rule for differentiation of Eqs. 4.13,4.14, and 4.15 results in

$$\mathbf{E} = \mathbf{e} \cdot \mathbf{F}, \qquad \mathbf{h} = \varepsilon \mathbf{F}^{-\mathrm{T}} \cdot \mathbf{E} \tag{4.16}$$

The Gauss law is used to relate the electric displacement vector to the charge density as follows

$$\int_{\partial\omega} \mathbf{h} \cdot \mathbf{n} \mathrm{d}a = \int_{\omega} \mathrm{r} \mathrm{d}v, \tag{4.17}$$

where r denotes the charge density in the actual state, ω defines an arbitrary volume with boundary $\partial\omega$ in the initial state. Applying the Nanson's and Stokes formula to Eq. 4.17 results in

$$\nabla_0 \cdot \mathbf{H} = \mathrm{R}, \tag{4.18}$$

where $\mathbf{H}$ is the nominal electric displacement and $\mathrm{R} = \mathrm{r}\, J$ is the charge density in the initial state, which is given by

$$\mathrm{R} = e(C_{\mathrm{H}^+} - C_{\mathrm{OH}^-} - C_{\mathrm{Cl}^-} - \alpha C_b), \tag{4.19}$$

where e denotes the charge of an electron. The relation between the electric displacement field $\mathbf{H}$ and the electric field in the initial configuration $\mathbf{E}$ can be found from these relations and Eqs. 4.13, 4.15, and 4.17

$$\mathbf{H} = \varepsilon J \mathbf{C}^{-1} \cdot \nabla_0 \Phi \tag{4.20}$$

where $\mathbf{C}$ is the left Cauchy-Green tensor for macrodeformation. Substituting $\mathbf{H}$ from Eq. 4.20, and R from Eq. 4.19 into Eq. 4.18 gives the Poisson's equation

$$\boldsymbol{\nabla}_0 \cdot (\varepsilon J \mathbf{C}^{-1} \cdot \boldsymbol{\nabla}_0 \Phi) = e(C_{\mathrm{H}^+} - C_{\mathrm{OH}^-} - C_{\mathrm{Cl}^-} - \alpha C_b). \tag{4.21}$$

The energy of the electric field of a hydrogel occupying a volume Ω in the initial state and a volume ω in the actual state, is given by [158].

$$\int_{\omega} \frac{\mathbf{h} \cdot \mathbf{h}}{2\varepsilon} \mathrm{d}v = \int_{\Omega} \frac{1}{2\varepsilon J} \mathbf{H} \cdot \mathbf{C} \cdot \mathbf{H} \mathrm{dV}. \tag{4.22}$$

Therefore, the electric field of mobile ions and fixed charges has a free energy density which can be described in the initial state by

$$W_{\mathrm{el}} = \frac{1}{2\varepsilon J} \mathbf{H} \cdot \mathbf{C} \cdot \mathbf{H}. \tag{4.23}$$

The work of the electric field (per unit time and unit volume in the initial configuration) is determined by [158],

$$u_{\mathrm{el}} = \mathbf{E} \cdot \dot{\mathbf{H}} - \Phi \dot{R}, \tag{4.24}$$

and it follows from substituting Eq. 4.19 into Eq. 4.24 that this work reads

$$u_{\mathrm{el}} = \mathbf{E} \cdot \dot{\mathbf{H}} - e\Phi(\dot{C}_{\mathrm{H}^+} - \dot{C}_{\mathrm{OH}^-} - \dot{C}_{\mathrm{Cl}^-} - \dot{\alpha} C_b). \tag{4.25}$$

4.1.4 Free energy density of a neutral hydrogel

The free energy of a gel comprising three-phase medium is given in [142]. In this study, the specific free energy of a pH-sensitive hydrogel Ψ per unit volume in the initial configuration is described by the summation of six terms divided in four categories: 1) the strain energy of solvent and mobile ions in solutes with no mixing, 2) the strain energy of polymer network, 3) the three mixing energies including polymer-solvent interaction, mobile ions-solvent interaction, and ionized and neutral functional groups of polymer chains, 4) the energy of the electric field produced by mobile ions and fixed charges. Thus, the free energy density implies that

$$\Psi = \Psi_{\text{non-mix}} + \Psi_{\text{net}} + \Psi_{\text{mix1}} + \Psi_{\text{mix2}} + \Psi_{\text{mix3}} + \mathrm{W}_{\text{el}}. \tag{4.26}$$

The specific strain energy density $\Psi_{\text{non-mix}}$ is expressed by [122]

$$\Psi_{\text{non-mix}} = \mu^0 C + \mu^0_{\mathrm{H}^+} C_{\mathrm{H}^+} + \mu^0_{\mathrm{OH}^-} C_{\mathrm{OH}^-} + \mu^0_{\mathrm{Cl}^-} C_{\mathrm{Cl}^-}, \tag{4.27}$$

where μ^0, $\mu^0_{\mathrm{H}^+}$, $\mu^0_{\mathrm{OH}^-}$, and $\mu^0_{\mathrm{Cl}^-}$ are the chemical potential energies of water molecules and different mobile ions (excluding their mixing effect), respectively. Ψ_{net} denotes the strain energy density of polymer network

$$\Psi_{\text{net}} = W(I_{\text{e}1}, I_{\text{e}2}, I_{\text{e}3}, \alpha, f). \tag{4.28}$$

where I_{ei} $(i = 1,2,3)$ denotes principal invariants of the Cauchy-Green tensor for elastic deformation. An equivalent polymer network is used to replace the original network in order to simplify constitutive relations [142]. The equivalent network is presumed to be a non-charged network with a volume expansion coefficient equal to $f(\alpha)$. In the equivalent network, the energy of the electrostatic interaction between bound charges is explicitly taken into account. $f(\alpha)$ is assumed to be proportional to the degree of ionization and is determined by [142]

$$f = 1 + Q_0 + q_1 C_b \alpha, \tag{4.29}$$

where Q_0 is the partial swelling of a hydrogel in the reference state and q_1 is a material parameter. The simplified format of the strain energy density of polymer network is given by

$$\Psi_{net,eq} = W_{eq}(I_{e1}, I_{e2}, I_{e3}). \tag{4.30}$$

The mixing energy Ψ_{mix1} between water molecules and polymer chains [150] reads

$$\Psi_{mix1} = \frac{k_B T}{v}(Q \ln \frac{Q}{1+Q} + \chi(T,Q)\frac{Q}{1+Q}), \tag{4.31}$$

where $\chi(T,Q)$ is the equivalent Flory-Huggins parameter provided in Eq. 3.5 in Chapter three. ΔT in Eq. 3.5 accounts for the shift in the VPTT of charged hydrogels at different pH values. Traditionally, the interaction between water molecules and mobile ions, and also the mixing of mobile ions and neutral functional groups on polymer

chains are described by [118]

$$\begin{aligned}\Psi_{\text{mix2}} =& k_B T \left[C_{\text{H}^+} \ln\left(\frac{C_{\text{H}^+}}{C} - 1\right) + C_{\text{OH}^-} \ln\left(\frac{C_{\text{OH}^-}}{C} - 1\right) \right. \\ & \left. + C_{\text{Cl}^-} \ln\left(\frac{C_{\text{Cl}^-}}{C} - 1\right) \right], \\ \Psi_{\text{mix3}} =& k_B T C_b \Big(\alpha \ln \alpha + (1-\alpha)\ln(1-\alpha) \Big).\end{aligned} \tag{4.32}$$

4.1.5 Constitutive relations

The free energy inequality equation for a three-phase hydrogel with finite deformation is given by

$$\dot{\Psi} - u_{\text{mech}} - u_{\text{dif}} - u_{\text{el}} - u_{\text{dis}} \leq 0, \tag{4.33}$$

where $\dot{\Psi}$ denotes the derivative of free energy density. The mechanical work on gel reads

$$u_{\text{mech}} = J\mathbf{T} : \mathbf{D}, \tag{4.34}$$

where $\mathbf{T}$ is the Cauchy stress tensor, and $\mathbf{D}$ denotes the rate-of-strain tensor and is given by $\mathbf{D} = \frac{1}{2}(\mathbf{L} + \mathbf{L}^{\text{T}})$ as the symmetric part of the velocity gradient $\mathbf{L} = \dot{\mathbf{F}} \cdot \mathbf{F}^{-1}$.

The works created by migration of mobile ions and water molecules u_{dif}, and by the electric field u_{el} can be found from Eqs. 4.11 and 4.25, respectively. The formation of ion pairs and the dissociation of functional groups of anionic gels induce a work which

is determined by [142]

$$u_{\text{dis}} = \dot{\alpha}\ \Delta\mu\ C_b, \tag{4.35}$$

where $\Delta\mu$ denotes by the difference between the potentials of neutral and ionized functional groups.

The derivative of molecular incompressibility condition (Eq. 2.10) is added to the inequality equation (Eq. 4.33) using an arbitrary function Π to incorporate the incompressibility condition as described in [102]. Therefore,

$$\dot{\Psi} - u_{\text{mech}} - u_{\text{dif}} - u_{\text{el}} - u_{\text{dis}} + \Pi(\dot{C}v - J\mathbf{I} : \mathbf{D}) \leq 0. \tag{4.36}$$

The differentiation of Eq. 4.26 and the substitution of six Eqs. 4.23, 4.27, 4.30, 4.31 and 4.32 imply that

$$\begin{aligned}\dot{\Psi} =& 2(\mathbf{K}_{\text{mech}} + \mathbf{K}_{\text{el}}) : \mathbf{D} + \mathbf{E}\cdot\dot{\mathbf{H}} + \\ & \Theta_C\dot{C} + \Theta_{\text{H}^+}\dot{C}_{\text{H}^+} + \Theta_{\text{OH}^-}\dot{C}_{\text{OH}^-} + \Theta_{\text{Cl}^-}\dot{C}_{\text{Cl}^-} + \Theta_\alpha\dot{\alpha}C_b,\end{aligned} \tag{4.37}$$

where the terms are given by Eqs. B.8, B.16 and B.17. Using Eq. 4.37, the inequality

condition Eq. 2.26 is obtained as

$$\begin{aligned}&[2(\mathbf{K}_{\text{mech}}+\mathbf{K}_{\text{el}})-J(\mathbf{T}+\Pi\mathbf{I})]:\mathbf{D}+(\Theta_C+\Pi v-\mu)\dot{C}+\\&(\Theta_{\text{H}^+}+e\Phi-\mu_{\text{H}^+})\dot{C}_{\text{H}^+}+(\Theta_{\text{OH}^-}-e\Phi-\mu_{\text{OH}^-})\dot{C}_{\text{OH}^-}\\&+(\Theta_{\text{Cl}^-}-e\Phi-\mu_{\text{Cl}^-})\dot{C}_{\text{Cl}^-}+(\Theta_\alpha-e\Phi+\mu_{\text{H}^+}-\Delta\mu)\dot{\alpha}C_b\leq 0.\end{aligned}\tag{4.38}$$

This relation meets the inequality condition in case of describing the Cauchy stress by

$$\mathbf{T}=-\Pi\mathbf{I}+\frac{2}{J}(\mathbf{K}_{\text{mech}}+\mathbf{K}_{\text{el}}),\tag{4.39}$$

and the potentials of water and mobile ions reads

$$\begin{aligned}&\mu=\Theta_C+\Pi v,\qquad \mu_{\text{H}^+}=\Theta_{\text{H}^+}+e\Phi,\\&\mu_{\text{OH}^-}=\Theta_{\text{OH}^-}-e\Phi,\qquad \mu_{\text{Cl}^-}=\Theta_{\text{Cl}^-}-e\Phi,\end{aligned}\tag{4.40}$$

and the equation for the degree of ionization is given by

$$\Theta_\alpha-e\Phi+\mu_{\text{H}^+}-\Delta\mu=0.\tag{4.41}$$

The Cauchy stress can be found by replacing $J,\mathbf{K}_{\text{mech}}$, and $\mathbf{K}_{\text{el}}$ in Eq. 4.39. Thus,

$$\mathbf{T}=-\Pi\mathbf{I}+\frac{2}{1+Q}\left[\frac{\partial W}{\partial J_{\text{e}1}}\mathbf{B}_{\text{e}}-J_{\text{e}3}\frac{\partial W}{\partial J_{\text{e}2}}\mathbf{B}_{\text{e}}{}^{-1}+(J_{\text{e}2}\frac{\partial W}{\partial J_{\text{e}2}}+J_{\text{e}3}\frac{\partial W}{\partial J_{\text{e}3}})\mathbf{I}\right]+\mathbf{T}_{\text{M}},\tag{4.42}$$

where $\mathbf{T}_{\mathrm{M}}$ denoting the Maxwell stress is given by

$$\mathbf{T}_{\mathrm{M}} = \frac{1}{\varepsilon}[\mathbf{h}\otimes\mathbf{h} - \frac{1}{2}(\mathbf{h}\cdot\mathbf{h})\mathbf{I}]. \tag{4.43}$$

To simplify the implementation of the governing equations, the Maxwell stress is shown to be lower than the mechanical stress by a few orders of magnitude [142]. The chemical potentials – using Eqs. 4.40 and B.17 – are explicitly expressed by

$$\begin{aligned}
&\mu = \mu^0 + k_B T\left[\ln\frac{Cv}{1+Cv} + \frac{1}{1+Cv} + \frac{\chi}{(1+Cv)^2} + \frac{\Pi v}{k_B T} - \frac{C_{\mathrm{H}^+} + C_{\mathrm{OH}^-} + C_{\mathrm{Cl}^-}}{C}\right],\\
&\mu_{\mathrm{H}^+} = \mu^0_{\mathrm{H}^+} + k_B T\ln\frac{C_{\mathrm{H}^+}}{C} + e\Phi, \qquad \mu_{\mathrm{OH}^-} = \mu^0_{\mathrm{OH}^-} + k_B T\ln\frac{C_{\mathrm{OH}^-}}{C} - e\Phi,\\
&\mu_{\mathrm{Cl}^-} = \mu^0_{\mathrm{Cl}^-} + k_B T\ln\frac{C_{\mathrm{Cl}^-}}{C} - e\Phi.
\end{aligned} \tag{4.44}$$

These formulations show the interconnected relations between the chemical potentials and the electrochemical potentials which are clearly distinguished due to the incorporation of the energy of the electric field in the inequality Eq. 4.33.

Finally, Eqs. 4.41, 4.44 and B.17, are used to obtain the degree of ionization by

$$\ln\frac{1-\alpha}{\alpha} = \ln\frac{C_{\mathrm{H}^+}}{C} - \ln \mathrm{K}'_a, \tag{4.45}$$

where K'_a denotes the acid association constant is defined by [142]

$$\mathrm{K}'_a = \exp\left(\frac{\Delta\mu - \mu^0_{\mathrm{H}^+}}{k_B T}\right). \tag{4.46}$$

The degree of ionization is found by solving Eq. 4.45 and expressed by

$$\alpha = \mathrm{K}'_a \left(\mathrm{K}'_a + \frac{C_{\mathrm{H}^+}}{C} \right)^{-1}, \tag{4.47}$$

which is equivalent to the Henderson-Hasselbach equation which desribes the derivation of acidity in biological and chemical systems.

4.2 Equilibrium swelling of a dual-responsive core/shell hydrogel

When a hydrogel submerges into a bath, it swells due to thermodynamic comparability between polymer network, solvent and solutes. This equilibrium swelling is uniform for hydrogels with homogeneous structure. In a core-shell hydrogel, simulation results from Chapter three confirm that the swelling in core is homogeneous and isotropic; but the distribution of swelling in shell is inhomogeneous. Assuming a homogeneous swollen core, an analysis is provided in this chapter to discover the distribution of swelling degree $Q(R)$ and stress values $\mathbf{T}(R)$ only in shell as a function of temperature and pH.

4.2.1 Chemical equilibrium condition

In the event of equilibrium swelling, solvent and solutes are distributed independent of spatial coordinates. Thus according to the Donnan's law, the chemical potentials of

solvent and solutes in the gel and the bath (shown with bar sign) equalize,

$$\mu = \overline{\mu}, \quad \mu_{H^+} = \overline{\mu}_{H^+}, \quad \mu_{OH^-} = \overline{\mu}_{OH^-}, \quad \mu_{Cl^-} = \overline{\mu}_{Cl^-}. \tag{4.48}$$

The chemical potentials in the bath can be easily found by an analogy to Eq. 4.44; for instance, the chemical potential of water bath is given by $\overline{\mu} = \mu^0 - k_B T/\bar{c}(\bar{c}_{H^+} + \bar{c}_{OH^-} + \bar{c}_{Cl^-})$. It follows from Eq. 4.44 and Eq. 4.48 that

$$\ln\frac{Q}{1+Q} + \frac{1}{1+Q} + \frac{\chi}{(1+Q)^2} + \frac{v}{k_B T}(\Pi - \Pi_{ion}) = 0, \tag{4.49}$$

where the ionic pressure Π_{ion} is given by

$$\Pi_{ion} = \frac{k_B T}{v}\left(\frac{C_{H^+} + C_{OH^-} + C_{Cl^-}}{C} - \frac{\bar{c}_{H^+} + \bar{c}_{OH^-} + \bar{c}_{Cl^-}}{\bar{c}}\right). \tag{4.50}$$

Moreover, the concentration of solvent and solutes in the bath in the actual configuration from Eq. 4.44 and Eq. 4.48 are determined by

$$\begin{aligned}
\ln\frac{C_{H^+}}{C} &= \ln\frac{\bar{c}_{H^+}}{\bar{c}} - \frac{e}{k_B T}(\Phi - \bar{\Phi}),\\
\ln\frac{C_{OH^-}}{C} &= \ln\frac{\bar{c}_{OH^-}}{\bar{c}} + \frac{e}{k_B T}(\Phi - \bar{\Phi}),\\
\ln\frac{C_{Cl^-}}{C} &= \frac{\bar{c}_{Cl^-}}{\bar{c}} + \frac{e}{k_B T}(\Phi - \bar{\Phi}).
\end{aligned} \tag{4.51}$$

Resolving Eq. 4.51 states that

$$\frac{C_{H^+}}{C}\frac{C_{OH^-} + C_{Cl^-}}{C} = \frac{\bar{c}_{H^+}}{\bar{c}}\frac{\bar{c}_{OH^-} + \bar{c}_{Cl^-}}{\bar{c}}. \tag{4.52}$$

Applying the electroneutrality condition results in

$$C_{OH^-} + C_{Cl^-} = C_{H^+} - \alpha\, C_b, \qquad \bar{c}_{OH^-} + \bar{c}_{Cl^-} = \bar{c}_{H^+}, \tag{4.53}$$

and substituting Eq. 4.53 into Eq. 4.52 implies that

$$X\left(X - \alpha\,\frac{C_b}{C}\right) = \frac{1}{k^2}10^{-2p\mathrm{H}}, \tag{4.54}$$

where $X = \frac{C_{H^+}}{C}$ describes the concentration of counter ions in the gel. This expression can be modified to

$$\left(X - \frac{1}{k}10^{-\mathrm{pH}}\right) = \frac{\alpha\, C_b}{C} X\left(X + \frac{1}{k}10^{-\mathrm{pH}}\right)^{-1}. \tag{4.55}$$

The concentration of positive ions is characterized by

$$[H^+] = 10^{-\mathrm{pH}}. \tag{4.56}$$

Substitution of Eq. 4.5 and Eq. 4.56 into Eq. 4.53 implies that

$$\begin{aligned} \frac{C_{H^+} + C_{OH^-} + C_{Cl^-}}{C} &= 2X - \frac{\alpha\, C_b}{C}, \\ \frac{\bar{c}_{H^+} + \bar{c}_{OH^-} + \bar{c}_{Cl^-}}{\bar{c}} &= \frac{2}{k}10^{-\mathrm{pH}}. \end{aligned} \tag{4.57}$$

Moreover, by insertion of Eqs. 4.55, 4.57 into Eq. 4.50, the ionic pressure is reformu-

lated and expressed by

$$\Pi_{\text{ion}} = \frac{k_B T\, X}{v}\left(\frac{\alpha\, C_b}{C}\right)^2\left(X+\frac{1}{k}10^{-\text{pH}}\right)^{-2}. \tag{4.58}$$

Introducing these notations $Q = C\ v$ and $Q_b = C_b\ v$, the governing equations are summarized as follows

$$X^2 - \frac{\alpha\, Q_b}{Q}X = \frac{1}{k^2}10^{-2\text{pH}}, \qquad \alpha = \frac{\text{K}'_a}{\text{K}'_a + X}, \tag{4.59}$$

$$\ln\frac{Q}{1+Q} + \frac{1}{1+Q} + \frac{\chi}{(1+Q)^2} + \frac{v\,\Pi}{k_B T} + X\left(\frac{\alpha\, Q_b}{Q}\right)^2\left(X+\frac{1}{k}10^{-pH}\right)^{-2} = 0. \tag{4.60}$$

4.2.2 Constitutive relations of a hydrogel at equilibrium

The hydrogel has a core with the radius of r^C, and a shell with the radius of r^S in the actual state. The occupied domain by a gel in the initial configuration is denoted by the spherical coordinate $\{R, \Theta, \Phi\}$ with unit vectors e_R, e_Θ, and e_Φ, and in the reference coordinate, $\{r_0, \theta_0, \phi_0\}$ describes the spherical coordinate.

The deformation gradient which maps the deformation from the initial configuration to the actual configuration, is given by

$$\mathbf{F} = r'\mathbf{e}_R\,\mathbf{e}_R + \frac{r}{R}(\mathbf{e}_\Theta\mathbf{e}_\Theta + \mathbf{e}_\Phi\mathbf{e}_\Phi). \tag{4.61}$$

The radial deformation $r(R)$ is obtained from Eqs. 2.10 and 4.61

$$r'r^2 = (1+Q)R^2. \tag{4.62}$$

Substituting Eqs. 4.29, 4.61 and 4.62 into Eq. 2.1, provides the deformation gradient for elastic deformation as follows

$$\mathbf{F}_{\mathrm{e}} = \Big(\frac{1}{1+Q_0+\bar{q}Q_b\ \alpha}\Big)^{\frac{1}{3}}\left((1+Q)\frac{R^2}{r^2}\mathbf{e}_R\,\mathbf{e}_R + \frac{r}{R}(\mathbf{e}_\Theta\mathbf{e}_\Theta + \mathbf{e}_\Phi\mathbf{e}_\Phi)\right), \tag{4.63}$$

where $\bar{q}$ is denoted by q_1/v. The neo-Hookean material model is specified for the strain energy of network ($\Psi_{\mathrm{net,eq}}$ in Eq. 4.30). Therefore, the Cauchy stress tensor is given by

$$\mathbf{T} = -\Pi\mathbf{I} + \frac{G}{1+Q}(\mathbf{B}_{\mathrm{e}} - \mathbf{I}), \tag{4.64}$$

where G is the shear modulus of polymer network, and $\mathbf{B}_{\mathrm{e}} = \mathbf{F}_{\mathrm{e}}\cdot\mathbf{F}_{\mathrm{e}}^{\mathrm{T}}$ is the right Cauchy-Green tensor for elastic deformation.

Insertion of Eq. 4.63 into Eq. 4.64 implies that

$$\begin{aligned} T_R &= -\Pi + \frac{G}{1+Q}\left(\frac{(1+Q)^2}{(1+Q_0+\bar{q}Q_b\ \alpha)^{\frac{2}{3}}}\left(\frac{R}{r}\right)^4 - 1\right), \\ T_\Theta &= -\Pi + \frac{G}{1+Q}\left(\frac{1}{(1+Q_0+\bar{q}Q_b\ \alpha)^{\frac{2}{3}}}\left(\frac{r}{R}\right)^2 - 1\right), \end{aligned} \tag{4.65}$$

where T_R and T_Θ denote the Cauchy stress in the radial and tangential directions, respectively. According to Eq. 4.61. The mechanical equilibrium condition for a spherical

hydrogel in the actual state reads

$$\frac{\partial T_R}{\partial r}+\frac{2}{r}(T_R-T_\Theta)=0. \tag{4.66}$$

Eq. 4.66 is rewritten to take derivative with respect to R, and to substitute T_Θ from Eq. 4.65_2, as follows

$$\frac{\partial T_R}{\partial R}+\frac{2G}{r(1+Q_0+\bar{q}Q_b\ \alpha)^{\frac{2}{3}}}\left((1+Q)^2\frac{R^6}{r^6}-1\right)=0. \tag{4.67}$$

For the case of unconstrained swelling, the induced pressure by the electrostatic forces among negative bound charges is determined by [142]

$$\Pi_{\text{rep}}=\frac{G}{1+Q}\left[\left(\frac{1+Q}{1+Q_0}\right)^{\frac{2}{3}}-\left(\frac{1+Q}{1+Q_0+\bar{q}Q_b\ \alpha}\right)^{\frac{2}{3}}\right]. \tag{4.68}$$

It is required to recalculate this induced pressure for core/shell hydrogels. According to Eq. 4.65, it can be shown that

$$\Pi=-T_R+\frac{G}{1+Q}\left(\frac{(1+Q)^2}{(1+Q_0+\bar{q}Q_b\ \alpha)^{\frac{2}{3}}}\left(\frac{R}{r}\right)^4-1\right), \tag{4.69}$$

this relation can be expressed by $\Pi=\Pi^*-\Pi_{\text{rep}}$ where

$$\Pi^*=-T_R|_{\alpha=0}+\frac{G}{1+Q}\left(\frac{(1+Q)^2}{(1+Q_0)^{\frac{2}{3}}}\left(\frac{R}{r}\right)^4-1\right) \tag{4.70}$$

denotes the osmotic pressure in the non-ionic core/shell gel, and

$$\Pi_{\text{rep}} = T_R - T_R|_{\alpha=0} + \frac{G}{1+Q}\left(\frac{(1+Q)^2}{(1+Q_0)^{\frac{2}{3}}} - \frac{(1+Q)^2}{(1+Q_0+\bar{q}Q_b\ \alpha)^{\frac{2}{3}}}\right)\left(\frac{R}{r}\right)^4 \tag{4.71}$$

stands for the induced pressure by the electrostatic forces among negative bound charges.

4.2.3 Numerics

The core-shell hydrogel is solved only for the shell domain, since the core domain is demonstrated to be homogeneous and isotropic in Chapter 3. The shear modulus of the core and shell domains are assumed to be the same. Dependent variables (Q, T_R, Π, X, α and r) are found from two differential equations (Eq. 4.62 and Eq. 4.67) and four algebraic equations (Eqs. $4.59_{1,2}$, 4.60 and 4.65_1). The commercial software, COMSOL [144], is used to solve differential equations. Appropriate boundary conditions are applied at the inner and outer boundary of the shell. At the inner boundary of the shell, two boundary conditions are applied:

- the radial stress is continuous at the boundary, as if the core applies a force (compression or tension) upon the shell, an equal and opposite force applies on the core or the other way around $T_R(R^C) = T_R(R_1)$;
- the lateral stretch is continuous at the boundary which is due to the connectivity of the domains; therefore, the inner radius of the shell is determined by $r_1/R_1 = r_C/R_C = (1+Q^C)^{\frac{1}{3}}$.

Table 4.1: Physical and geometry parameters of the dual responsive core/shell hydrogel

Physical parameters of the shell	
R_1, R^C	48 nm
R_2	72 nm
G^S, G^C	18×10^3 N m^{-2}
Δs^S, Δs^C	-3.7×10^{-23} J K^{-1}
Δh^S, Δh^C	-9.2×10^{-21} J
χ_2^S, χ_2^C	0.45
ΔT^C	1.5, 4 and 8.5 °C*
Q_0^C	0
Q_b^C	10^{-5}
$\bar{q}^C$	5×10^{-5}
ΔT^S	1.5 °C
Q_0^S	Found from Eq. 2.36

∗ At pH values of 3.5, 4.5 and 6, respectively.

At the outer boundary of the shell, the shell experiences no external force at equilibrium and therefore, the condition of traction-free for the outer surface of the shell implies that

$$T_R(R_2) = 0. \tag{4.72}$$

Initial values are assigned to physical parameters to reduce the number of parameters. The initial swelling of the core is set to $Q_0^C = 0$ which means that the evolution of the reference state is not due to partial swelling but only due to the ionization of bound charges. The initial swelling of the shell is found from Eq. 2.36 assuming $R_1 = R^C$. The constant term of the effective interaction parameter in Eq. 3.5 is determined by $\chi_2 = 0.45$ for both domains. The dissociation constant of functional groups is denoted by $\mathrm{K}'_a = \mathrm{K}_a/k$. The dissociation constant of AAc comonomers is found to be $\mathrm{pK}_a = 4.7$ close to the theoretical value of 4.3 in [159].

The maximum element size of 10^{-3} nm is selected for this model to ensure that the solution is mesh independent. Number of elements are 4800 for the shell – whose thickness is half of the core – adding up to 38405 degrees of freedom. The computation is performed on a 2.4 GHz PC with 4 GB RAM.

4.3 Results and discussion

The core-shell model is developed to analyze the response of dual-stimuli responsive core-shell hydrogels subjected to swelling. This model is reformulated to describe the swelling experimental data from a core-shell hydrogel comprising a charged core (pNIPAM-co-AAc) and a neutral shell (pNIPAM) reported in [37]. The core is assumed to be a pH-/thermo-sensitive hydrogel whose swelling depends on pH and temperature, while the swelling of the shell is only temperature dependence. The equilibrium swelling has been determined through the shell thickness for the temperature range of $25-45\ ^{o}$C at three pH values (pH $= 3.5, 4.5$ and 6.5). Thereafter, the calculated radius of the core-shell hydrogel is compared with dynamic light scattering (DLS) from the pNIPAM-co-AAc/pNIPAM core/shell microgel.

4.3.1 pNIPAM-AAc/pNIPAM core/shell microgel

The reference experiment is the swelling measurements of a core/shell microgel synthesized in a multi-step reaction process. The core-shell structure of this microgel was confirmed by transmission electron microscopy (TEM) images [37]. The core was pro-

duced by free radial polymerization of co-monomers which are pNIPAM, AAc and N,N'-Methylenebisacrylamide (BIS) (with a ratio of 9:1:0.5). These constituents were dissolved in water (150 mL) at 70 °C, and ammonium persulfate (APS) (0.069 g) and sodium dodecyl sulfate (SDS) (0.069 g) were used as an initiator and a surfactant, respectively. The shell was made of pure pNIPAM (1.4 g) with the same amount of cross-linker, initiator and surfactant and similar preparation conditions were used for the core. The internal radius of the core is estimated from the experiment at high temperature when it is in the collapsed state and set to $R_1 = 48$ nm; the shell thickness is assumed to be half of R_1.

The elastic modulus of the core and the shell is assumed to be the same since they have almost the same amount of crosslinks and polymer in both domains. The parameters for temperature-induced swelling are estimated from the model developed for the pNIPAM microgel in Chapter three and assigned to be equal for the core and shell; however, the fitted parameters of χ^C and χ^S have different ΔT (Eq. 3.5) accounting for the delay of the volume transition of the core at different pH values. The list of parameters are shown in Table 4.1.

4.3.2 Coupled effect of temperature and pH on equilibrium swelling

The size of microgel particles is calculated as a functional of temperature and pH at equilibrium swelling. The calculations are fitted to the experimental data as shown in Fig. 4.1. Microgel particles shrink when temperature increases from 25 °C to 45 °C. At pH = 3.5, one transition point is calculated at $T \approx 32$ °C which is close the VPTT

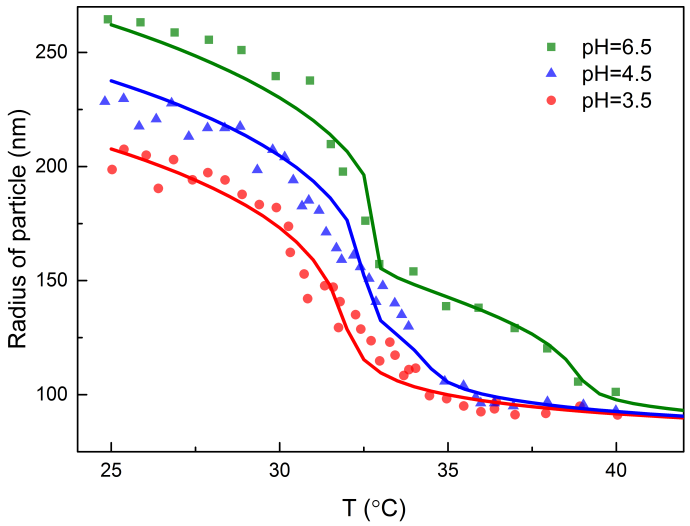

Figure 4.1: Radius of the core-shell hydrogel at three pH values. Simulation results are shown by lines considering dual effect of temperature and pH, and symbols are the experimental data from Fig. 4 in [37]

of pNIPAM microgels [31, 37]. At higher pH (pH = 4.5 and 6.5), the second transition point is appeared at a higher temperature corresponding to the VPTT of the pNIPAM-co-AAc core. After the first transition point, the density of the shell becomes nearly constant until the core collapses at the second transition point.

The shift in the VPTT of the core is determined by ΔT in the formula for χ^C which is found by parameter-fitting to observations at different pH values. Swelling versus temperature curves illustrate a two-step shrinking behavior with two transition points which attribute to the VPTT of the core and shell. The second transition point corresponding to a shift in the VPTT of the ionic core, is found to be $\Delta T = 1.5,\ 4$ and 8.5 °C at pH = 3.5, 4.5 and 6.5, respectively.

The transition from swollen to collapsed state is demonstrated in Fig. 4.2 in which the interaction parameter of the core is found from fittings. This transition occurs at

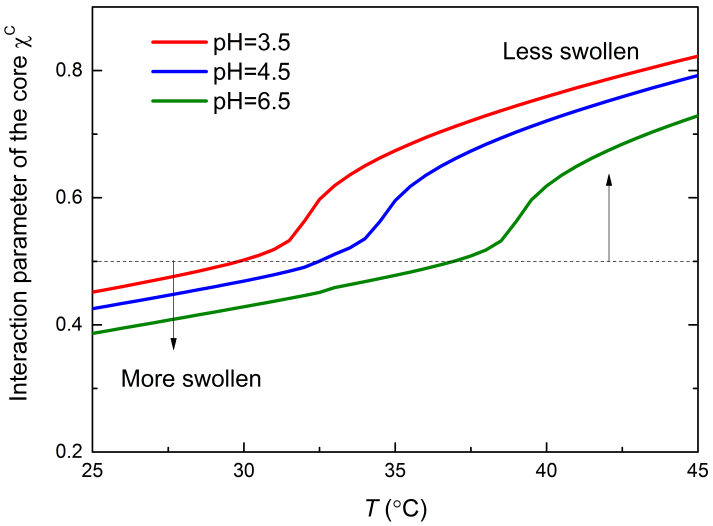

Figure 4.2: Interaction parameter of the core is found from fittings to observations considering the effect of a shift in VPTT of the core at three pH values.

$\chi = 0.5$ and the VPTT of the domain. When the value of χ is greater than 0.5, the domain is collapsed and vice versa. It is demonstrated that increasing pH shifts this transition to a higher temperature. The interaction parameter of the shell is assumed to be the same as the core at the lowest pH (pH $= 3.5$).

The ionization of functional groups of ionic polymer gels are determined by the degree of ionization. At low pH, functional groups are protonated by H^+ mobile ions. Therefore, the degree of ionization of microgel particles is very small ($\alpha^C \approx 0.06$) at pH $= 3.5$ according to Fig. 4.3. When pH exceeds $pK_a = 4.7$ of the functional groups of AAc, the degree of ionization increases to ≈ 0.7. Moreover, it is discovered that the degree of ionization of the charged core α^C decreases as temperature increases. At high temperature, a number of carboxylic groups is non-ionized ($\alpha^C < 0.2$) at pH $= 4.5$ and 6.5. These findings are in agreement with swelling experiment on ionic copolymer gels

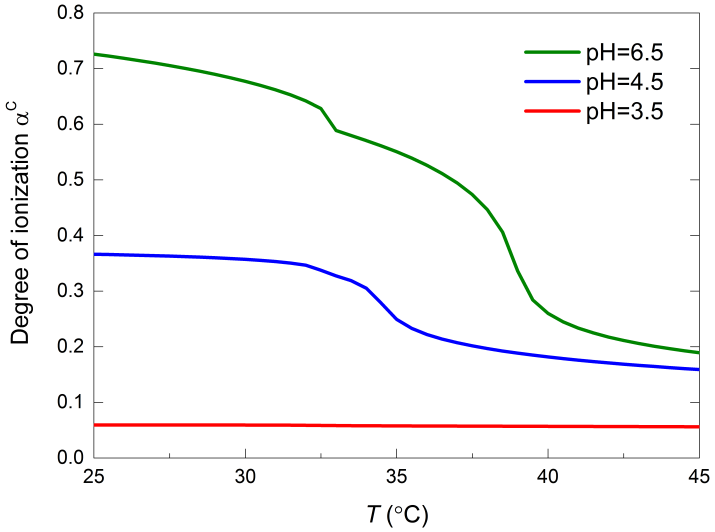

Figure 4.3: Degree of ionization of the core calculated of the core/shell microgel with pNIPAM-co-AAc in the core and pNIPAM in the shell. The interaction parameter of the pNIPAM shell is assumed to be the same as the one for the lowest pH (pH = 3).

of N-isopropylacrylamide (NIPA) and sodium acrylate which shows that α decreases with temperature for pH < 6.3 [70] and a significant fraction of the functional groups is not ionized at temperatures above the VPTT of NIPA. In addition, simulation results demonstrate that at high pH values, the decrease of α^C occurs at two points corresponding to the VPTT of the core and shell. Fig. 4.3 illustrates that α^C drops more significantly at the second transition point.

Fig. 4.4 depicts the dimensionless pressure induced from repulsive forces $\overline{\Pi}_{\text{rep}} = \Pi_{\text{rep}} v/(k_B T)$ and the ionic pressure $\overline{\Pi}_{\text{ion}} = \Pi_{\text{ion}} v/(k_B T)$ versus temperature for three pH values. $\overline{\Pi}_{\text{rep}}$ and $\overline{\Pi}_{\text{ion}}$ increase with temperature when pH is kept constant. The increase in pressure is more pronounced for $\overline{\Pi}_{\text{ion}}$. Since the number of mobile ions are fixed at a constant pH, the increase in ionic pressure may arise from the reduction of volume of the core by increasing temperature – from the swollen state at T= 25 °C

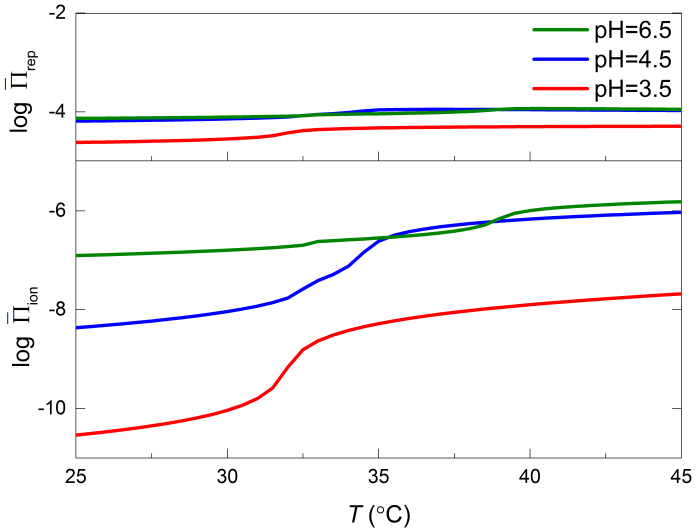

Figure 4.4: Simulation results for induced pressure by electrostatic forces $\overline{\Pi}_{rep}$ and ionic pressure $\overline{\Pi}_{ion}$ of pNIPAM-co-AAc/pNIPAM core/shell microgels.

to the collapsed state at T= 45 °C. These graphs have transition points corresponding to the VPTTs of the core and shell. Increasing pH value demonstrates an increase in $\overline{\Pi}_{ion}$ and $\overline{\Pi}_{rep}$ at a constant temperature, which may be explained by the increase in the number of mobile ions. Simulations results depict that $\overline{\Pi}_{rep}$ outweighs $\overline{\Pi}_{ion}$ by a few order of magnitude; therefore, the influence of the electrostatic forces is the dominant mechanism for swelling as pointed out in [142].

4.3.3 Radial stress in the shell

Radial and tangential stress vary through the thickness of the shell in response to changes in pH and temperature.

4.3.3.1 Effect of pH and temperature on radial stress in the shell

At low pH, the core is swollen slightly more than the shell and the radial stress at the core-shell interface is very low (in the order of 10^{-2}), so a homogeneous deformation can be assumed within the core and shell. The radial stress in the shell is illustrated in Fig. 4.5 at pH values of 4.5 and 6.5 and two temperatures of 25 °C and 45 °C. Increasing pH results in deprotonation of the core and further swelling in the core and thereafter, the shell laterally stretches to accommodate the swollen core. Thus, the shell applies a compressing radial stress on the core to constrain its swelling.

The influence of temperature on the radial stress in the shell is also depicted in Fig. 4.5. At $T = 25$ °C, the temperature is below the VPTT of the shell and both domains can expand freely without experiencing any constraint from the other domain. As temperature increases, the shell collapses sooner than the core since the VPTT of the shell is lower than that of the core. In this situation, the shell applies a compressing radial stress on the core. This stress basically decays exponentially from its maximum value at the inner boundary of the shell to zero at the outer boundary of the shell.

The maximum radial stress occurring at the core/shell boundary, is called the interface stress and shown in Fig. 4.5. The maximum interface stress is not occurring at the highest temperature ($T = 45$ °C), but at a temperature when both domains start to collapse. The first peak in Fig. 4.6 represents the collapse of the shell while the core is still swollen, and the second peak appears at the collapse of the core indicating the maximum interface stress. The magnitude of the maximum interface stress is relatively higher at higher pH value of 6.5. In between these two peaks, the evolution of the inter-

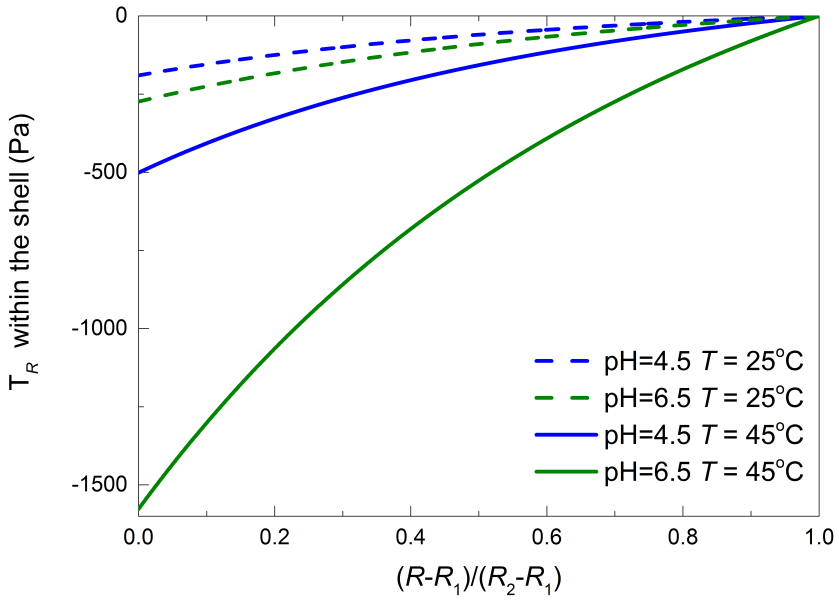

Figure 4.5: Radial stress in the shell versus normalized radius of the shell in the initial state

face stress is faster for lower pH value of 4.5 since the VPTT of the core is closer to the VPTT of the shell at this pH compared to pH value of 6.5. At pH= 6.5, the VPTT of the core is shifted to a higher temperature while the VPTT of the shell is remained the same at $T \approx 32$ °C, and in this case, our calculations show a slower rate of evolution for the interface stress, from the first peak to its maximum value.

4.3.4 Discussion

The swelling-temperature curves of isolated pNIPAM-co-AAc microgels show a two-step transition behavior (provided that substantial content of AAc is used), although these microgels do not possess a core-shell structure. For instance, Kratz et al. [38] synthesized an ionic pNIPAM-co-AAc microgel with a molar fraction of 12.5% of AAc which is required to observe the second transition point in the swelling-temperature

curves. Hoare and Pelton [160] proposed an inhomogeneous structure for ionic PNIPAM-AAc microgels based on TEM images of the stained functional groups. It was concluded that the amount of these groups are lower at the highly cross-linked center and they are located near or at the surface of the microgel.

This similarity between the inhomogeneous structure of isolated pNIPAM-co-AAc microgels and the core/shell structure of pNIPAM-co-AAc/pNIPAM core/shell microgels which were prepared in multistage reaction [37], has been pointed out in [160]. This inhomogeneous structure may influence the VPTT in the core and shell due to the higher content of AAc in the shell. Substantial fraction of AAc may be occupied in the shell and make the VPTT of the shell shift to a higher temperature than the VPTT of the core. Subsequently, this structure might lead to a two-step transition behavior in the swelling-temperature curves of isolated ionic microgels provided that they have substantial amount of the functional groups.

4.4 Conclusion

The equilibrium swelling of a dual-responsive core/shell hydrogel are studied in response to change in temperature and pH. A theoretical model recently developed for pH-sensitive hydrogels is extended to model temperature-sensitive core/ shell hydrogels accounting for temperature sensitivity and inhomogeneous swelling. The model is used to predict the equilibrium swelling of the pNIPAM-co-AAc/ pNIPAM core/shell gel as a function of temperature and pH. The volume phase transition temperature of the core which shifts to a higher temperature by increasing pH, is parameter-adapted

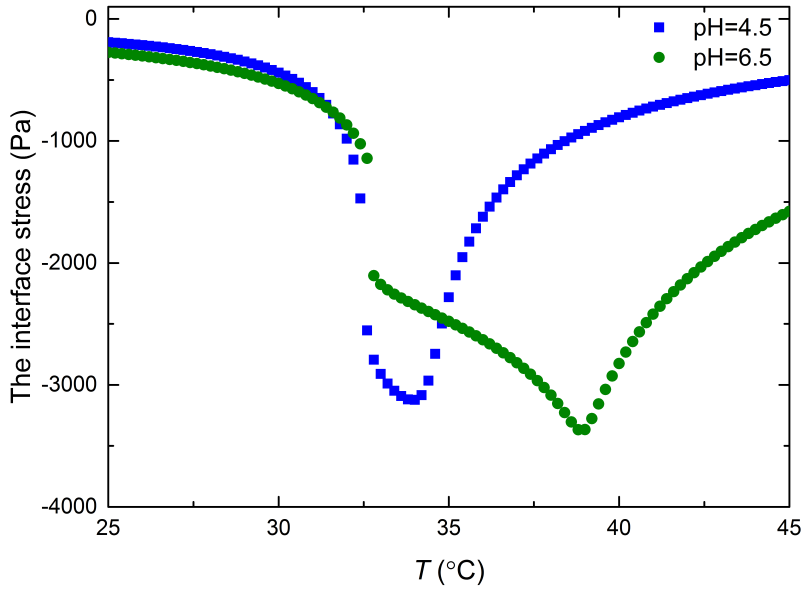

Figure 4.6: The interface stress at the core/shell boundary as a function of temperature

at different pH values. In agreement with observations, swelling ratio decreases with temperature and shows two transition points akin to the VPTT of the core and shell at higher pH values. The model predicts the decrease of the degree of ionization in the core with temperature, and this decrease occurs at two steps at higher pH. As pH increases, the shell collapses first and apply a compressing radial stress on the swollen core which collapses at a higher temperature. The maximum radial stress appears at the inner boundary of the shell and decays to zero at the outer boundary of the shell. The maximum radial stress is also a function of temperature, and has two local maximum values; the first one corresponds to the collapse of the shell and the second one relates to the collapse of the core occurring at a higher temperature.

Chapter 5

A pH-sensitive natural/synthetic composite hydrogel: Swelling experiments on Agarose-Carbopol

Polymer gels – known as hydrogels – have promising applications in tissue engineering and regenerative medicine [161]. Functionalized and biocompatible hydrogels are favorable biomaterials particularly in drug delivery systems. The desired release control of drugs may be achieved by using functionalized hydrogels (e.g. pH-responsive hydrogels) with adjustable degree of swelling and degradation rate in response to environment. Another parameter is compatibility which has been addressed by some type of hydrogels. Natural-derived hydrogels constitutionally show compatibility with hydrophilic macromolecular drugs (e.g. protein). Furthermore, injectable hydrogels which are capable of in-situ gelation, demonstrate high drug release efficiency, cell

support and low toxicity [162]. Compared to rigid scaffolds used in conventional drug delivery systems, in-situ forming gels adapt its structure to any shape, and consequently, improves biocompatibility which is a critical issue in case of neural tissue such as brain or spinal cord [163, 164].

In this chapter, a composite hydrogel is synthesized by the combination of two FDA approved polymer gels – a natural polysaccharide (agarose), and a synthetic branched polyacrylic acid (carbopol® 981P) – in order to introduce a new polymer gel which is functionalized, biocompatibile and therefore, suitable for applications in tissue engineering. The combination of natural and synthetic polymer gels may provide a composite gel with better properties than the properties of its constituents [165].

Agarose is a natural polysaccharide from the family of physical hydrogels which have transient polymeric cross-links. Heating/cooling is the most convenient method to produce physical hydrogels [166]. Agarose polymer chains are dissolved in a hot solution when temperature is higher than its T_{melt} and form random coils. Fig. 5.1 shows a schematic of the transition of agarose solution to gel by reducing temperature. Random coils are transformed into helices and through a nucleation and growth mechanism, loose fiber bundles form [167, 168]. Then, aggregation of these loose fiber bundles develop supercoiled fibers with a radius of $20-30$ nm [169] resulting in three-dimensional porous structure with pore size ζ in the range of $50-{>}300$ nm based on the agarose concentration [170]. Three-dimensional mesh of pores has been verified by atomic force microscopy performed on 2% w/V agarose with $\zeta = 364 \pm 8$ nm as shown in Fig. 5.1(d). Agarose has tunable concentration-dependent properties which

can provide desirable mechanical stiffness [168]. For the electrophoresis of large particles (e.g. DNA), agarose is preferred over most of polyacrylamide gels due to its higher stiffness and larger pore size at an equal concentration [171]. Increasing the density of agarose gels, reduces the pore size and subsequently, the permeability of molecules through agarose network [172].

The second component is carbopol (generic name: carbomer) which is a microgel including highly chemically cross-linked domains surrounded by sparse polymer chains. A conceptual schematic of carbopol hydrogels is shown in Fig. 5.2 validated experimentally by dynamic light scattering and particle tracking techniques [173, 174]. Carbopol comprises homopolymers and copolymers of acrylic acid (AAc) cross-linked with a polyalkenyl polyether. Carbopol shows pH sensitivity, temperature stability and thickening properties with its very high molecular weight even at low concentration ($0.1-0.3\%$ w/V) [175]. Carbopol in dry state has a coiled structure made of AAc chains as shown in Fig. 1.1. These chains start to swell when carbopol powder is dissolved in water to an extent allowed by cross-links. These cross-links make bridges between polymer chains by chemical bonds, and prevent carbopol polymer from dissolving in solution. Carboxyl groups existing in the backbone of AAc become fully dissociated when solution pH is higher than the dissociation constant of carbopol $pK_a = 6 \pm 0.5$ [176]. This value is higher than the dissociation constant of AAc monomers (the main compartment of carbopol) $pK_a = 4.3$, due to a change in the electronegativity of carboxyl groups forming after polymerization of AAc monomers of carbopol [177].

The maximum viscosity can be achieved by neutralizing carbopol. Viscosity mea-

surements of carbopol show a wide range of relative viscosity (RV) and also, a high yield stress even at low concentration [178]. Viscosity-pH curves demonstrate that viscosity increases with pH until it reaches a maximum value at a pH of $6-7$. The viscosity is then constant until pH $= 9$ followed by a decrease at higher pH values [179]. Moreover, the viscosity and elastic modulus of carbopol increase as its polymer concentration increases [180].

Agarose-carbopol-based hydrogels are injectable copolymer gels with proven biocompatibility and designing capabilities after using them in various applications such as 3D scaffolds for neural cell housing [181], and as drug carriers [182]. However, the functionality of these hydrogels – specifically their swelling behavior to changes in pH – has been studied very limited [183].

If the swelling of agarose-carbopol (AC) composite hydrogels shows pH dependence, it confirms that the combination of neutral agarose chains with ionic carbopol microgel results in an anionic composite hydrogel. It has been pointed out in [184] that an interpenetrating network forms in the agarose-carbopol (AC) composite hydrogels – based on the readings from Fourier transform infrared spectroscopy (FTIR) experiments – due to the interaction between hydroxyl groups from agarose and carboxyl groups from carbopol, and chemical bond formation by esterification and hydrogen bonding.

Freeze-dried samples of AC hydrogels are usually used for swelling experiments and morphological studies [184]. The challenge in the freeze-drying process is to preserve the morphology of these hydrogels. Another approach (which is used in this

study) is to use swollen samples for swelling experiments and to calculate their swelling ratio with respect to their weight in the dry powder form. The morphological study is also performed on swollen hydrogels by a special type of AFM suitable for imaging soft materials with wet surfaces. Other methods for morghological characterization such as scanning electron microscopy (SEM) or transmissible electron microscopy (TEM) on dried hydrogels has been reported in literature. It is preferred to use hydrated hydrogels in our experiments rather than freeze-dried samples which involves more complexities in preparation techniques.

This chapter is an experimental study to examine the swelling behavior of agarose-carbopol (AC) composite hydrogels in response to a wide range of pH values of the bath. The procedure to produce consistent hydrogel samples and the methods of characterization and swelling measurements are described in details. This study aims to elaborate on the swelling of AC composite gels in response to a wide range of pH, from highly acidic to highly basic. The influence of agarose and carbopol is investigated on the degree of swelling and mechanical strength of AC hydrogels by testing different compositions of these hydrogels. The results of this chapter – particularly the equilibrium swelling of AC composite gels induced by pH, and AFM imaging and force spectroscopy – will be used to guide theoretical models and estimate their physical parameters in Chapter 6.

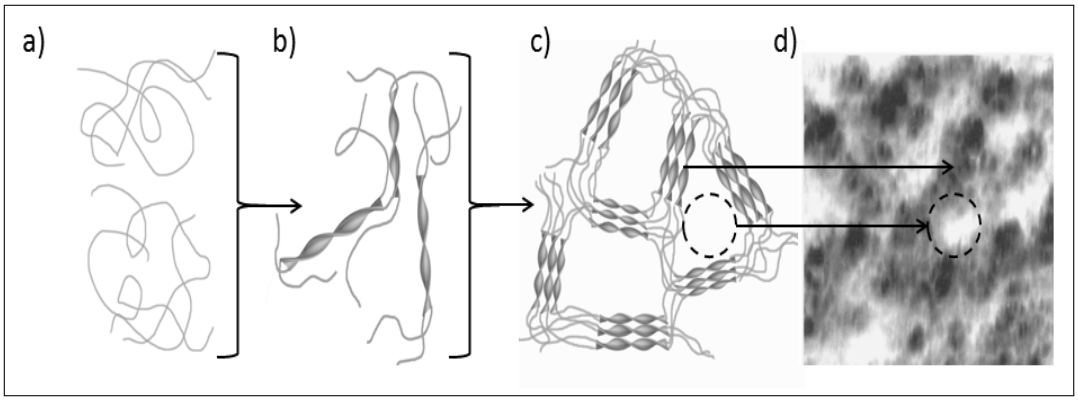

Figure 5.1: Schematic of the formation of three-dimensional network of agarose from solution by decreasing temperature a) Random coils b) Double-helix structures and evolution of loose fiber bundles c) Aggregation of fiber bundles and formation of 3D network d) Porous surface of 2% w/V agarose hydrogel by AFM [83]

5.1 Materials and methods

5.1.1 Materials

Agarose A0169 was purchased from Sigma Aldrich with low impurities ($< 7\%$ water), low electroendosmosis (EEO $= 0.09 - 0.13$), and good gel strength (≥ 1200 g cm^{-2} for 1% w/V gel). Agarose is in powder form, soluble in hot water with a temperature higher than $T_{\text{melt}} \simeq 87 \pm 1.5$ °C, and can solidify below the sol-gel transition temperature which is $T_{\text{gelation}} = 36 \pm 1.5$ °C. The chemical structure of agarose is depicted in Fig. 5.3.

The second component is carbopol® 981P provided from Lubrizol, a microgel available in fluffy and white powder which is slightly acetic. Carbopol is made of AAc cross-linked polymer network whose chemical structure is demonstrated in Fig. 5.4. The relative viscosity RV of 0.5% w/V concentration of carbopol® 981P is in the range of $4 - 11$ Pa.s under the conditions of 20 rpm at 25 °C in a neutralized solution. Sodium hydroxide (NaOH) and hydrogen chloride (HCl) were purchased from Fluka, and Mili-

Q water was used as the solvent to synthesize the composite gel.

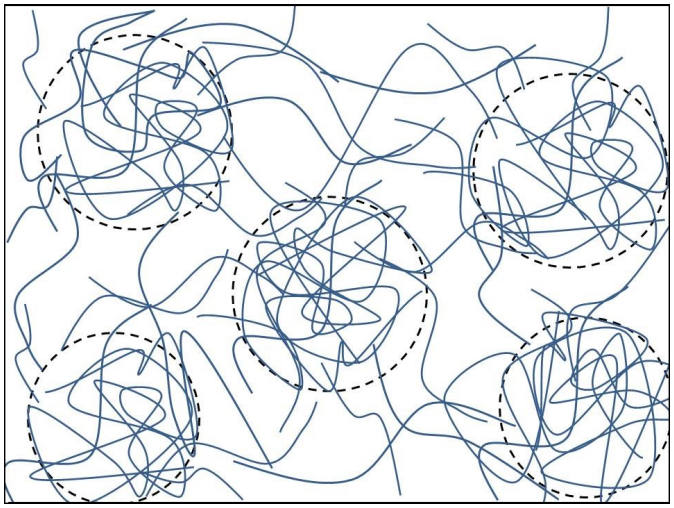

Figure 5.2: Conceptual schematic of the structure of carbopol hydrogel

5.1.2 Hydrogel synthesis

To synthesize the composite hydrogel consisting of agarose and carbopol, it is practical to begin the experiment with gradual dispersion of the carbopol powder in mili-Q water cautiously, to avoid formation of particle clumps which delays the diffusion of solvent into the interior domains, and in subsequence, increase the required time to complete mixing significantly. An amount of carbopol powder weighted accurately – by Sartorius Cubics® microbalance with a readability of 0.1 mg – was gradually added to the solvent, while stirring the solution continuously at $700 - 1000$ rpm. For each composition of AC hydrogels, a specific concentration is assigned according to Table 5.1. Then, IKA® stirrer was used to stir the solution for an hour at 1000 rpm until a clear solution was obtained with no visible floating particle.

The second part of the synthesis was the addition of agarose powder. Agarose pow-

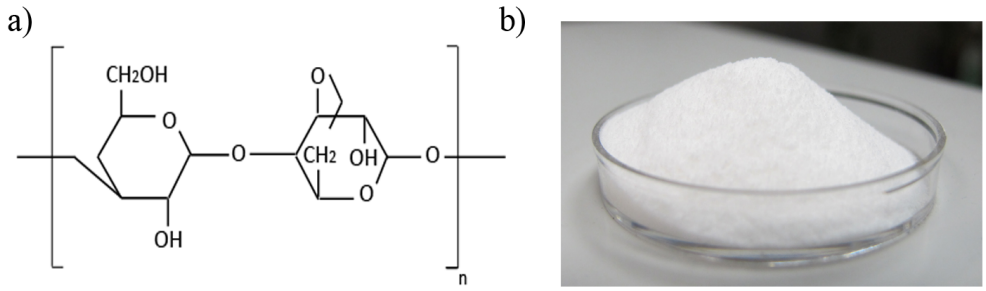

Figure 5.3: Chemical formula and physical structure of agarose: a) Molecular formula of agarose monomer b) Agarose polymer A0169 in powder form

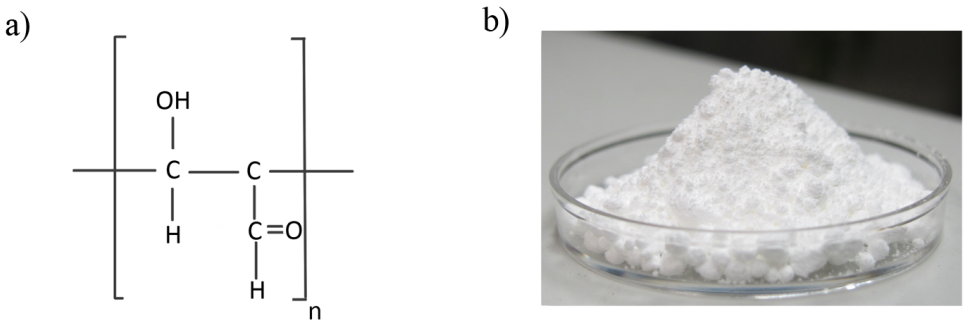

Figure 5.4: Chemical structure of acrylicacid polymer and carbopol in powder form: a) Acrylicacid monomer AAc b) Carbopol® 981P polymer in powder form

der was added to the solution to make different compositions of AC hydrogels according to Table 5.1. Microwave heating was used for effective gelation [184]. For two minutes, the polymer solution was heated with a microwave oven of 800 Watt irradiated power. Some intervals were needed to avoid overheating (according to the technical data sheet of agarose). During the interval, the solution was stirred and its temperature was maintained at 90 °C to obtain a clear solution. During synthesis, stirring the solution vigorously created air bubbles in the gel as shown in Fig. 5.5(a). In Fig. 5.5(b), it

Table 5.1: List of different compositions of agarose-carbopol hydrogels

Composite hydrogels	AC1	AC2	AC3	AC4
$C_{agarose}(\%\ g\ mL^{-1})$	1	0.75	0.5	0.5
$C_{carbopol}(\%\ g\ mL^{-1})$	0.5	0.375	0.25	0.5

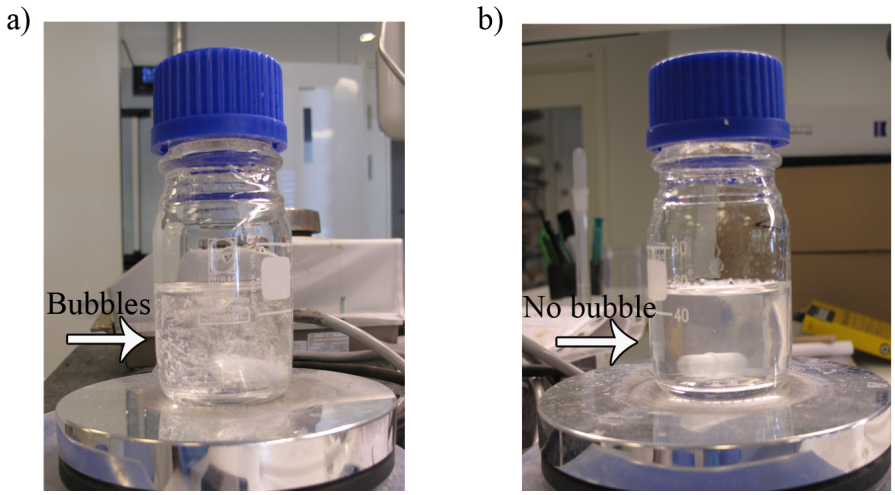

Figure 5.5: Agarose-carbopol polymer in solution and in gel form: Solving carbopol and agarose in water creates trapped air bubbles b) Slow stirring is continued for a longer time to remove all air bubbles

can be seen that air bubbles are removed from the solution by continuing stirring at a slower speed (about 200 rpm). The solution was kept in a glass container with a closed cap until its temperature reached 55 °C. This helped to minimize the evaporation of solution before transferring it to a petri dish. The gelation of solution completed when its temperature arrived at room temperature (25 °C). At this time, the composite hydrogels were ready be cut to make cylindrical specimens for swelling experiments. Fig. 5.6 depicts a schematic of this process which results in a clear cylindrical disc of composite hydrogel.

5.1.3 Spectrophotometry and temperature reading for gelation kinetics of agarose

The gelation kinetics of agarose is manipulated by temperature. In this section, agarose gelation was characterized to determine when the gelation completes. First, 0.5% w/V

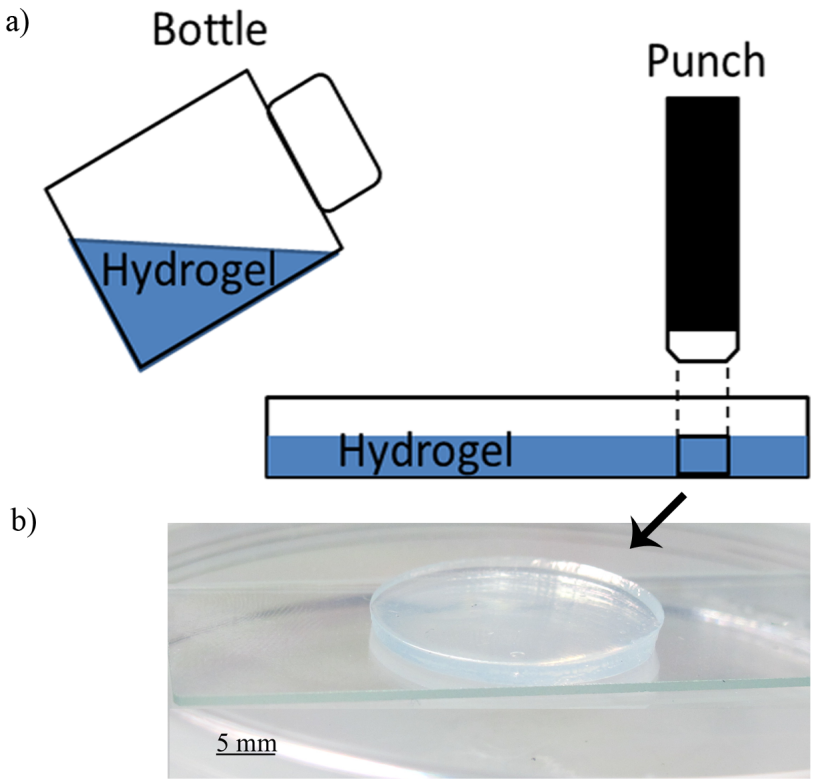

Figure 5.6: Preparation process of translucent speciments of agarose-carbopol: (a) shows transformation of clear solution to a petri dish. After hydrogel solution solidifies and reaches room temperature, samples were cut by a punch b) A cylindrical disc is obtained from translucent AC gels

agarose gel was prepared with the same method as described in Section 5.1.2. When the temperature of agarose solution reached T = 55 °C, it was transferred to wells of a cell culture plate. Each well with a diameter of D = 1.24 cm, could hold 5 ml of agarose. Spectrophometer Tecan Infinite® 200 Pro was used to determine the gelation point by measuring the intensity of light passing through the center of well vertically. After a while, the intensity reached a saturation which defines the gelation point. To select a proper wave length of light for spectrophotometry experiments, specimens were exposed to a wide range of lights with different wave lengths ranging from 230 nm to 1000 nm. Since this hydrogel showed more sensitivity to the light in the UV range, a

wave length of 350 nm was found to be suitable for this experiment.

The polymer solution was transferred to molds at $T = 55$ °C, and its temperature decreased at ambient condition until it reached the room temperature. Fig. 5.7 illustrates how a thermo-couple (Fluke 561) was used to read temperature from the center of agarose samples.

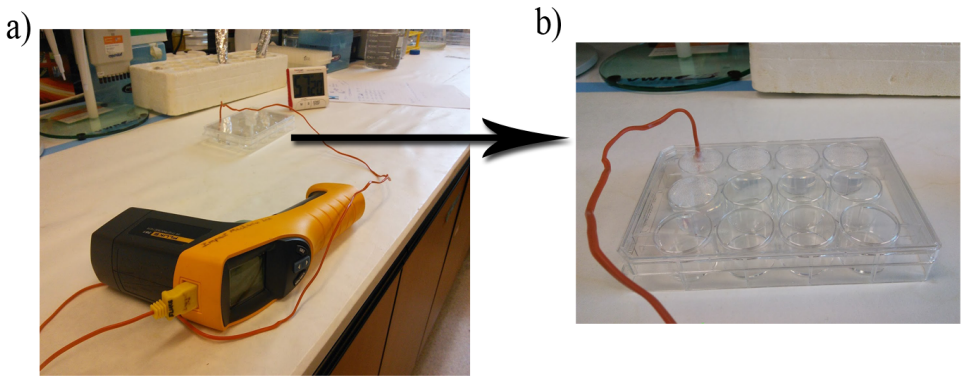

Figure 5.7: Temperature readings from agarose cylindrical samples: a) Thermocouple Fluke 561 b) Fixing wire of thermocouple in the center of an agarose specimen located in a well of a cell culture plate

5.1.4 Swelling behavior of AC hydrogels

AC composite hydrogels were punched in cylindrical shapes with a length of 0.7 mm and a diameter of 0.6 mm (with a tolerance of ± 0.05 mm). Specimens were punched in small sizes with an average weight of 0.6 mg, and then submerged in the bath to uptake the maximum amount of water and reach the equilibrium swelling. The characteristic time required to reach the equilibrium swelling can be expressed by $\tau \propto L^2/D$ demonstrating a direct relation to the square of the characteristic length L, and indirect relation to diffusivity of solvent D. Different AC hydrogels were subjected to swelling in the bath with acidic and basic solutions. Sodium hydroxide and hydrogen chloride

7.0 M were diluted to obtain a wide range of pH values, from highly acidic (pH = 2) to highly basic (pH = 14).

Cylindrical specimens were weighted prior to swelling. After swelling, the specimens were taken out of the bath and their surfaces were wiped off by an absorbent tissue to remove the excess water. Weight measurements were conducted frequently over time in order to extract more data points at the beginning of the experiment and less number of points as time evolves until a saturation point reached. It is assumed that specimens were subjected to free swelling, since a relatively large volume of bath (eight times of the sample size) was provided. From the amount of water uptake, degree of swelling Q is expressed by

$$Q = \frac{m(\mathrm{t}) - m_0}{m_0}, \tag{5.1}$$

where t is the swelling time, $m(\mathrm{t})$ is the mass of the specimen at each time and m_0 is the mass of the pure polymer in dry format.

5.1.5 Atomic force microscopy: imaging and force spectroscopy

Atomic force microscopy (AFM) was used in imaging mode to obtain micrographs of highly swollen AC hydrogels and also in force spectroscopy mode to obtain elastic modulus. AFM measurements were conducted on hydrogels when they were in their wet condition. Alternatively, gel specimens can be freeze-dried under special circumstances to make them prepared for morphological studies [185]. Since preservation of the actual morphology of hydrogels during lyophilization process might be challenging, the morphology of AC hydrogels were studied when they are in their swollen state.

For AFM imaging, microlever AFM probes were used which have soft silicon nitride cantilevers with silicon nitride tips. Two common type of tips are pyramidal and spherical tips. Pyramidal tips in contact mode are suitable for imaging extremely soft materials. The sharp tips used in this experiment had nominal spring constant of 0.03 N/m, nominal length of 225 μm, and nominal width of 20 μm. Conversely, spherical beads were preferred to measure the elastic modulus of soft materials, since the assumption of small deformation required for the Hertz model is simply violated in case of using sharp tips [85]. A silica spherical bead (with a diameter of 4.5 μm) attached to the silicon nitride cantilever (with a nominal spring constant of 0.03 N/m) was used to apply a force (the maximum applied force is 4 nN). The frequency of 1 Hz was prescribed for scanning the wet surface of hydrogels for both AFM modes. The photodiode sensitivity (m/V) and spring constant (N/m) of the cantilever were calibrated by laser before the experiment.

The elasticity measurements were carried out using force-distance $F-\delta$ curves in the contact mode. From the force curves, the Young's modulus was calculated using the Sneddon's equation [186] – a modified version of the Hertz's model [187] suitable for samples showing no adhesion – for a spherical tip

$$F = \frac{4\sqrt{R}}{3}\frac{E}{1-\nu^2}\delta^{\frac{3}{2}}, \tag{5.2}$$

where R is the bead radius, ν is the Poisson's ratio (assumed to be 0.5 for soft biological materials), δ is the indentation depth, F is the force (4 nN applied on our samples), and

E is the Young's modulus. Few locations were chosen for each sample and 64 points were mapped at each location covering an area of 8×8 μm^2 with the frequency of 1 Hz. The elastic modulus of the hydrogel was found from the mean value of these 64 indentation points.

5.2 Results and discussion

5.2.1 Spectrophotometry study of agarose gelation process

The experiment of spectrophotometry on agarose polymer solution demonstrates that the light absorption increases as a function of time due to the transition of the solution to gel by the formation of double-helix structure of agarose hydrogels. The light absorption reaches a maximum value which is a sign for the completion of the formation of three-dimensional network of agarose hydrogels. Fig. 5.8 exhibits the evolution of light absorption with temperature. Concurrently, the temperature was read from the center of agarose specimens as shown in Fig. 5.9. When the temperature of agarose specimens decrease to ambient temperature, physical crosslinks between polymer chains may not develop any further and the gelation process is presumably completed according to Fig. 5.8. Moreover, it was observed that addition of carbopol to agarose delays this gelation process and the temperature decreases to room temperature in a longer period of time. Thus, it was confirmed that after two hours the temperature of the solution of agarose-carbopol hydrogels arrives at room temperature.

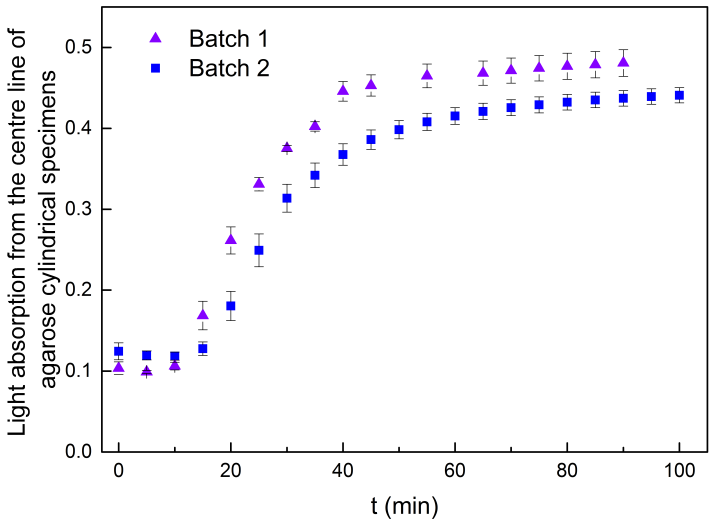

Figure 5.8: Evolution of light absorption with time during the transition of agarose polymer solution to polymer gels at ambient condition. Light absorption is read from the center of specimens. Average value of five specimens in each batch is shown with standard deviation bars.

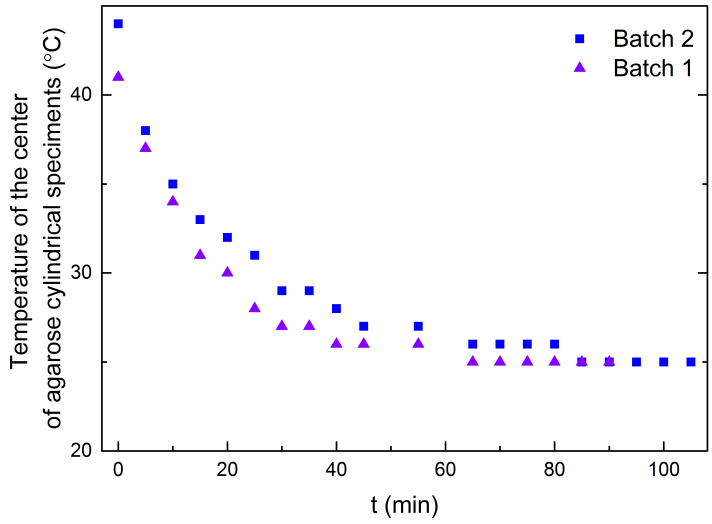

Figure 5.9: Evolution of temperature with time during the transition of agarose polymer solution to polymer gels at ambient condition. Temperature readings are from the center of agarose specimens using a thermocouple.

5.2.2 Microstructure of agarose-carbopol

Fig. 5.10 depicts AFM micrographs which were obtained from the surface of one composition of AC hydrogels (AC1). The porous structure of AC1 gels are shown when they are highly swollen at deionized water (at a pH of 7). A distribution of pores whose shapes are close to a circle, can be seen in Fig. 5.10(a). The surface roughness is demonstrated by bright and dark domains in Fig. 5.10(b). The microstructure of AC composite gels varies by agarose concentration C_{agarose}, carbopol concentration C_{carbopol}, solution pH and many more. One composition of AC gels is only used for AFM imaging due to complexities and numerous parameters affecting the structure of these hydrated gels.

AFM images demonstrate that agarose and carbopol make an entangled network where the constituents may not be differentiated at this scale. Polarized light microscopy and phase-contrast microscopy were also used to observe the microstructure of carbopol particles in our composite hydrogel. Unfortunately, the diffraction and absorbency of light passing through the translucent medium of AC hydrogels, cannot reveal their microstructure. In [185], the microstructure of a composite hydrogel made of similar components (agarose, carbomer 974P and chondroitinase chABC) was observed by environmental scanning electrode microscopy (ESEM) and a highly interpenetrated nanostructure was also noticed.

The AFM images of AC1 hydrogels are very similar to AFM images of pure agarose reported in [83]. Since the major component of AC hydrogels is agarose, agarose polymer network is dominant and supposed to determine the porous structure of AC hy-

drogels. The microstructure of AC composite hydrogels is suspected to have highly crosslinked domains of carbopol microgels separated by a loose network of agarose. This structure could have been modeled by a core/shell structure whose core and shell were carbopol and agarose, respectively. Despite our expectations, the highly crosslinked domains of carbopol cannot be differentiated from agarose in AC hydrogels by imaging at the micro level. Hence, agarose-based AC hydrogels are considered to have a homogeneous structure at the continuum level.

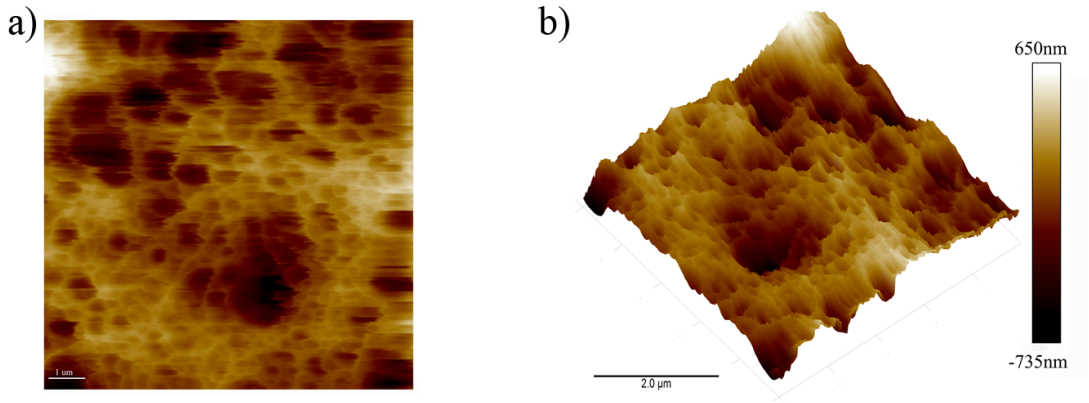

Figure 5.10: AFM imaging shows the morphology of the surface of an agarose-caropol (AC1) hydrogel at highly swollen state a) Porous structure of the hydrogel b) 3D image of the surface of the hydrogel

5.2.3 Elastic modulus by AFM force spectroscopy

AFM force spectroscopy experiments were conducted on two specimens of AC1 hydrogels at a number of different locations (between 40-60 random positions) using microspheres of 4.5 μm as the probe tip. The average value and standard deviation of the estimate of the Young's modulus E are found from force-displacement curves. The measured Young's modulus (E) is 1367.2 KPa $\pm$ 222.4. This value is in agreement

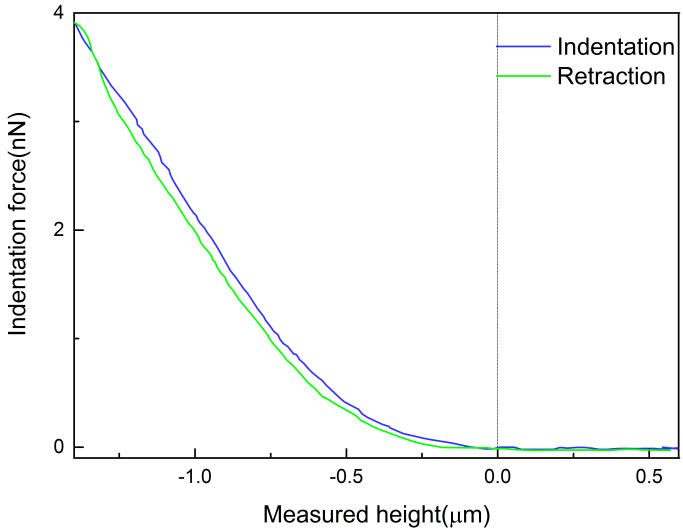

Figure 5.11: Force-displacement curves obtained from AFM force spectroscopy experiment for indentation on AC1 hydrogels when they are highly swollen. The retraction curve is also shown in this graph.

with reports from a rheology experiment on a similar composite gel [184]. Since highly swollen specimens have wet surfaces, they can easily slip off the grips of the machines for rheology, compression or tensile tests. Therefore, AFM has some advantages over mechanical machines to work with these soft hydrogels with wet surfaces. Fig. 5.11 depicts the indentation and the retraction curves from one indentation point. There are variations in reading forces from different locations across the specimen surface arising from inhomogeneities in the microstructure of the composite gels. The fact that the retraction force is very close to the indentation force, indicates that the viscoelastic properties of AC1 composite hydrogels can be neglected when they are in their highly swollen state.

5.2.4 Swelling behavior of AC hydrogels

Pure agarose hydrogels and agarose-carbopol composite gels are subjected to swelling in acidic and basic solutions in order to discover the transient and equilibrium swelling in response to various pH values. The as-prepared cylindrical specimens were swollen approximately for 18 hours to reach their equilibrium.

5.2.4.1 Swelling behavior of pure agarose gels

Swelling of pure agarose gels was studied at different pH values of $= 2,\ 3,\ 6,\ 8$ and 14. Fig. 5.12 shows that nearly no change ($< 5\%$) is noticeable between the equilibrium and initial swelling of agarose. Agarose hydrogels have no ionizable groups which result in no swelling in pure water [188]. Therefore, agarose has no contribution to the swelling of composite hydrogels.

5.2.4.2 Swelling behavior of AC composite hydrogels

Addition of carbopol to agarose creates an ionic polymer gel provided that agarose-carbopol composite gels make a hybrid network. Time-dependent swelling of AC composite gels was studied as a function of pH. Fig. 5.13, Fig. 5.14, Fig. 5.15 and Fig. 5.16 illustrate the evolution of swelling ratio of four different composite hydrogels (AC1, AC2, AC3 and AC4) versus the swelling time at different pH values of the bath. After about 200 min, the swelling ratio became close to its saturation line which was confirmed by another reading at t $\approx$ 1100 min (18 hrs.). For definiteness, the swelling ratio after 18 hours is used as the equilibrium swelling ratio. Although the volume of bath

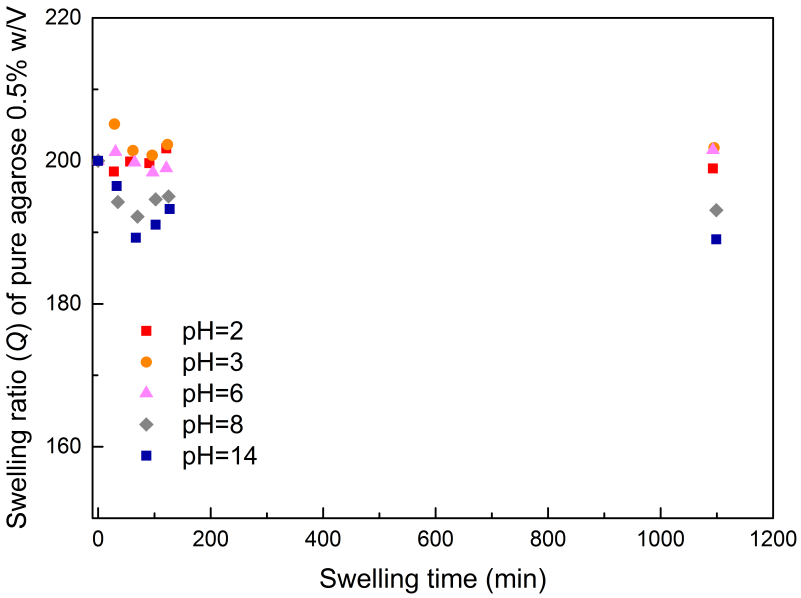

Figure 5.12: Swelling behavior of 0.5% g mL^{-1} pure agarose hydrogel as a function of time at different pH values of the bath

is assumed to be eight times larger than the volume of specimens, the solution pH may not be kept constant over 18 hrs of swelling and this might be a source of error which results in a difference between the equilibrium swelling at t $\approx$ 200 and 1100 min.

The initial swelling ratio $Q(t = 0)$ is higher when the amount of agarose and carbopol is lower. The maximum initial swelling is found for AC3 composite hydrogels with the minimum polymer density of 0.5% w/V of agarose and 0.25% w/V of carbopol. When specimens are subjected to swelling, different swelling curves are obtained based on pH values of the bath. For pH values in the range of $5.5 \leq pH \leq 9$ – which is higher than the typical dissociation constant for carbopols $pK_a = 6 \pm 0.5$ – the swelling ratio increases monotonically with time. This can be explained by deprotonation of carboxyl groups attached to the backbone of polymer network (refer to Eq. 4.3). At high pH val-

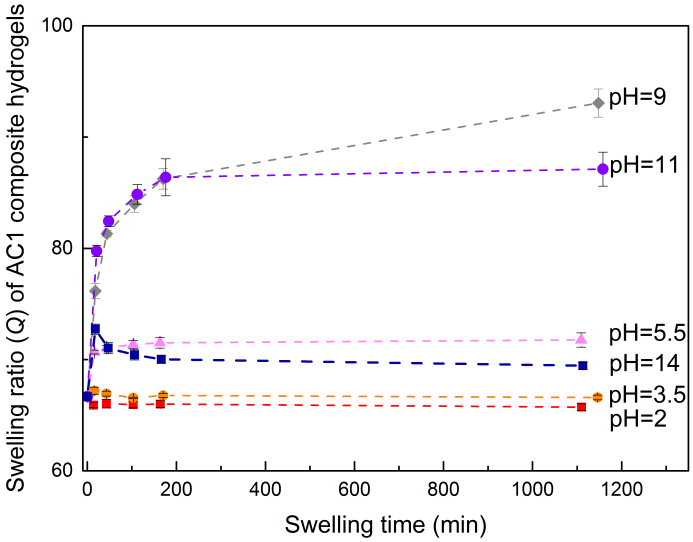

Figure 5.13: Swelling ratio of as-prepared AC1 composite hydrogels as a function of swelling time; the average value of five specimens is shown at different pH values with standard deviation bars.

ues ($11 \leq \text{pH} \leq 14$), swelling-temperature graphs show an increase in swelling shortly after submerging samples, followed by a slight shrinkage. At low pH values ($\text{pH} \leq 3.5$), composite hydrogels show either a non-monotonic or monotonic shrinkage.

Three composite hydrogels (AC1, AC2 and AC3) have a constant ratio of C_{agarose} / $C_{\text{carbopol}} = 2$ which provides relatively stiff specimens even at their highly swollen states. When C_{carbopol} increases and becomes equal to C_{agarose} as is the case for AC4 gels, the swelling degree of composite gels increases more as shown in Fig. 5.16. For a better comparison, the equilibrium swelling ratio of AC3 and AC4 gels are depicted in Fig. 5.17. It can be seen that increasing C_{carbopol} results in an increase in the equilibrium swelling ratio specially when pH value is close to 7. Increasing C_{carbopol} further, increases the swelling of composite hydrogels, reduces the stiffness of polymer network, and provides softer hydrogels when they are highly swollen. Specimens of AC4

composite hydrogels break easily at pH = 7.6, and their swelling-temperature curve can not be completed at higher temperatures by referring to Fig. 5.16.

Equilibrium swelling ratio Q(t = 18 hrs.) of AC1, AC2 and AC3 composite hydrogels and 0.5% w/V pure agarose are all extracted and exhibited in Fig. 5.18. Compared to agarose hydrogels, composite hydrogels show a pH-dependent swelling behavior indicating the formation of connection between neutral agarose and pH-sensitive carbopol. Equilibrium swelling of composite gels increases with pH and reaches its maximum at about pH = 9; as pH increases further, it starts to decrease.

The maximum equilibrium swelling is obtained for AC3 composite hydrogels (relative to the equilibrium swelling at the lowest pH value), although it has the minimum concentration of carbopol. A higher concentration of carbopol results in a higher swelling ratio as shown in Fig. 5.17 due to an increase in the number of functional groups attached to the polymer network. However, AC1 and AC2 gels show a smaller swelling ratio compared to AC3 hydrogels, although they have a higher concentration of carbopol. It can be concluded that the smaller swelling ratio of AC1 and AC2 hydrogels is due to the fact that the concentration of agarose is relatively high which results in formation a stiffer polymer network which restrains the swelling of the carbopol network from achieving its maximum swelling ratio. Thus, agarose polymer which has no direct contribution to the swelling, has a considerable influence on the overall swelling of the composite hydrogels by forming a stronger network.

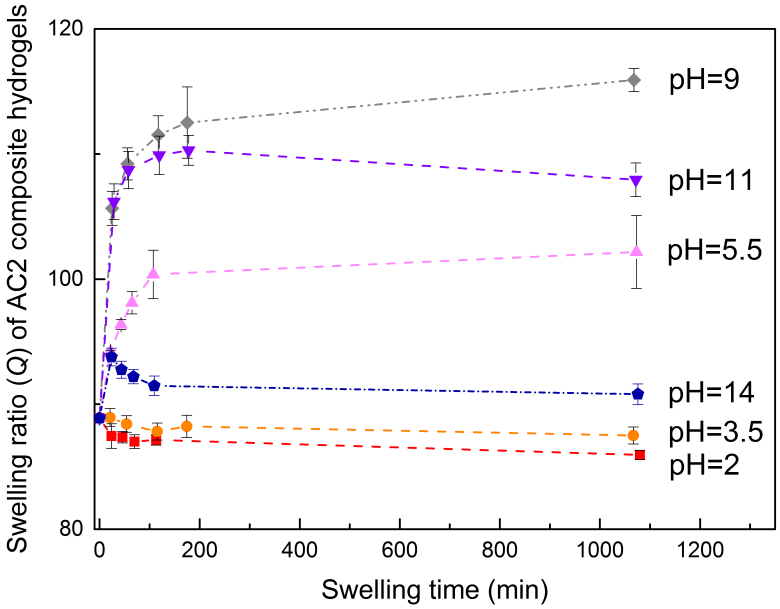

Figure 5.14: Swelling ratio of as-prepared AC2 composite hydrogels as a function of swelling time; the average value of five specimens is shown with standard deviation bars for different pH values.

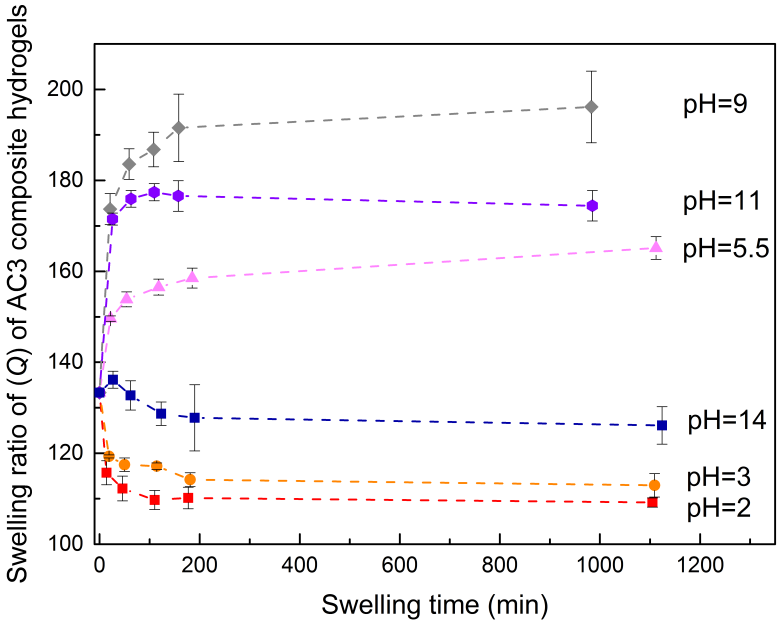

Figure 5.15: Swelling behavior of as-prepared AC3 composite hydrogels as a function of swelling time; the average value of five specimens is shown with standard deviation bars for different pH values.

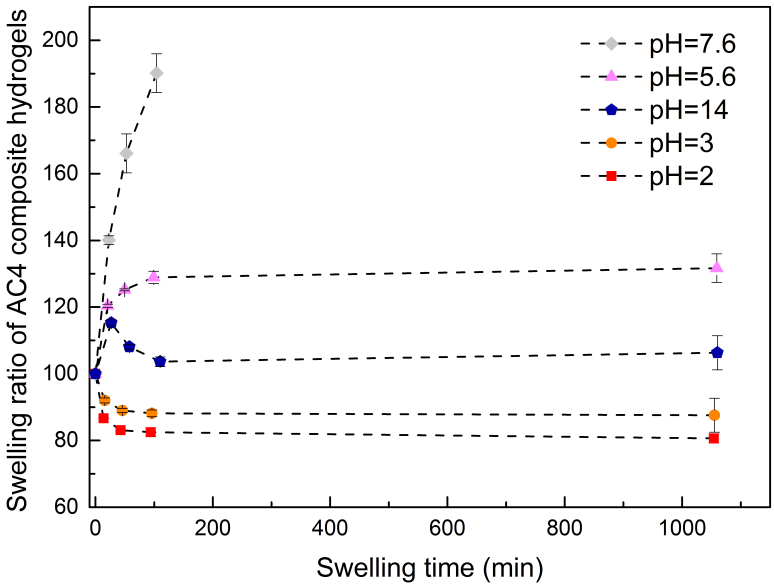

Figure 5.16: Swelling ratio of as-prepared AC4 composite hydrogels as a function of swelling time; the average value of five specimens is shown with standard deviation bars for different pH values.

5.3 Conclusion

In this experimental study, composite hydrogels were prepared by co-polymerization of agarose and carbopol, and their swelling behavior were studied in response to a wide range of pH values of the bath. This co-polymerization results in a pH-sensitive hydrogel with non-monotonic swelling versus pH. Moreover, AFM imaging confirms that the composite hydrogels form one integrated network whose constituent networks can not be differentiated. AFM force microscopy was also used to determine the elastic modulus of the composite hydrogels. In addition, the swelling behavior of different compositions of agarose-carbopol composite gels was investigated in order to decouple the influence of increase in agarose and carbopol concentration.

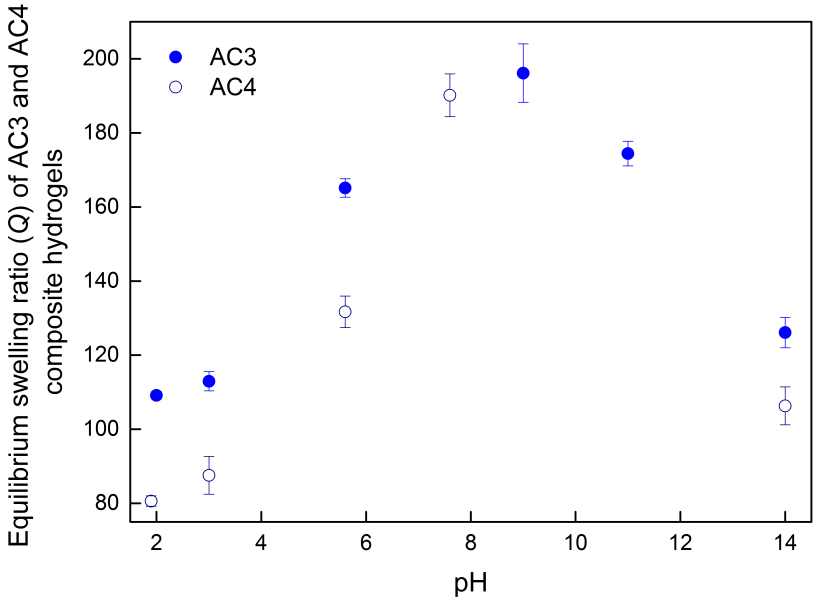

Figure 5.17: Equilibrium swelling ratio of AC3 and AC4 composite gels as a function of time and pH; the average value of five specimens for AC3 gels and three specimens for AC4 gels are shown with standard deviation bars

It is suggested that agarose polymer has a significant effect on swelling ratio of the composite hydrogels by forming a strong network and constraining the swelling of carbopol polymer. This composite hydrogel with modular properties (concentration-based mechanical and swelling properties) is favorable to engineer smart hydrogels for applications in tissue engineering and drug delivery. In chapter six, a theoretical model will be presented grounded on these findings in order to elaborate more on the equilibrium swelling of AC composite hydrogels in response to very low to very high pH.

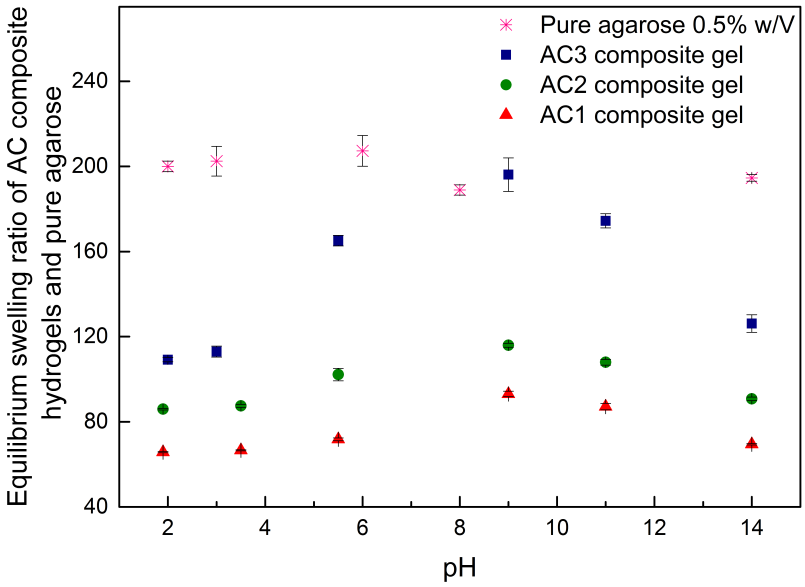

Figure 5.18: Equilibrium swelling ratio as a function of pH levels of swelling solvent for the composite hydrogels (three compositions) and agarose hydrogel

Chapter 6

Modeling equilibrium swelling of agarose-carbopol composite gels

Observations on polyelectrolyte (PE) hydrogels reveals that their swelling increases as pH increases until the swelling ration reaches a saturation. The evolution of swelling ratio of PE gels may be explained by two mechanisms (as described in Chapter 4). The first mechanism is the increase in the ionic pressure (the osmotic pressure)by free ions entrapped inside the gel. The ionic pressure is determined by the gradient of ion concentration from inside the gel to outside in the water bath. The second mechanism is the increase in the induced pressure from the electrostatic forces between bound charges [5]. In present literature, swelling of PE gels is mainly described by the first mechanism [189]. However, the influence of electrostatic forces is sometimes considered as a secondary mechanism to explain the difference between simulation results and observations [156]. It can be due to the fact that simple expressions for the energy of

electrostatic forces are not available [190–193].

In anionic gels (which are PE gels with acidic functional groups), functional groups are fully associated at low pH values and become fully dissociated when the solution pH exceeds their pK_a. Therefore, the swelling of anionic gels increases as pH increases, their maximum swelling ratio is obtained at a pH which is higher than the pK_a of functional groups, and maintains constant between pH values of 7 and 9 [36, 194]. In Chapter 5, swelling experiments on agarose-carbopol (AC) hydrogels are studied for a wide range of pH values. Its swelling behavior is similar to other PE gels when pH$<$ 9. At higher pH values, swelling decreases possibly due to the presence of cations (e.g. Na^+) dissociated from the basic solution (e.g. NaOH), and the induced ionic pressure from these cation ions. This induced ionic pressure may qualitatively describe the shrinkage of a PE gel with the Donnan's equilibrium law [195]; however, this shrinkage cannot quantitatively be explained by this approach [43]. There are three additional mechanisms suggested to accurately verify observations of the shrinkage of a PE gel due to the influence of ionic strength, as follows:

1. Counter-ion condensation around functional groups which causes screening or shielding of Coulomb forces [44, 45, 196];

2. Ion-pair formation between free mobile ions and bound charges which produces neutral combinations leading to a reduction in the number of functional groups [45–47];

3. Development of the chemical potential of solvent caused by excess free ions,

which makes an increase in the Flory-Huggins parameter of mixing energy of solvent and polymer network [48, 49].

Numerous theoretical models are developed to model swelling behavior of pH sensitive hydrogels [115–122] and also, ampholytic gels – which is a PE gel which has acidic and basic functional groups – [121, 197] by considering coupled diffusion and large deformation. The influence of ionic strength has also been studied to explain swelling behavior of PE hydrogels in the presence of salt [198, 199]. There is a need for a theoretical model to explain swelling-shrinking behavior of the PE gels (such as AC hydrogels) in response to pH ranging from very low to high values.

Recently, a theoretical model is developed to simulate anionic hydrogels subjected to swelling considering the influence of pH and ionic strength [189]. Both ionic pressure, and induced pressure from electrostatic repulsion of bound charges are involved in swelling of ionic polymer gels at any arbitrary pH value. When the bath is basic (pH$>$ 7), the formation of neutral ion pairs is additionally considered as the main mechanism for shrinkage of PE gels. In this chapter, the aim is to describe swelling-shrinking behavior of the agarose-carbopol (AC) hydrogels from pH$=$ 2 to pH$=$ 14. Furthermore, the properties of different compositions of AC hydrogels are extracted – by fitting observations to the theoretical model – in order to investigate the influence of constituents on the mechanical stiffness and the swelling behavior of AC hydrogels.

6.1 Theoretical model

To study the swelling behavior of AC hydrogels, a model developed for swelling of polyelectrolyte hydrogels is adapted from [142]. In this model, a gel is assumed to be a three-phase medium where water (solvent phase) and mobile ions (solutes phase) are allowed to diffuse into the polymer network (solid phase). Migration of water and mobile ions occurs due to the chemical reactions of solutes and polymer network with water bath and furthermore, accelerated by the electric field generated among the bound charges on the backbone of the network. Moreover, the influence of ionic strength on swelling of PE gels is described by the combination of free counter ions with fixed charges, and the formation of neutral ion pairs. Increasing ionic strength causes the swelling ratio of PE gels to shrink by two to three orders of magnitude.

This model is applied to calculate the macro-deformation of AC composite hydrogels and to explain their non-monotonic swelling in the bath with pH values ranging from highly acidic to highly basic. It has been discussed in [189] that the influence of salt and high pH on swelling of PE gels is similar. Therefore, the evolution of ion-pairs between counter mobile ions with bound charges is considered as the main mechanism for shrinking of AC hydrogels subjected to swelling at pH values higher than 7.

6.1.1 Chemical reactions

Ionization of solvent and solutes produces mobile ions via chemical reactions. It is assumed that solvent and solutes are infinitely available in the bath and therefore, the

concentration of mobile ions remains constant. Ionization of water (the solvent)

$$2H_2O \leftrightarrows H_3O^+ + OH^-, \tag{6.1}$$

is confirmed by a low electrical conductivity ($0.055\,\mu S cm^{-1}$) of pure water. This ionization produces hydroxide ions H^+ (attached to water molecules) and OH^- hydroxyl ions. The molar concentration of hydroxide and hydroxyl ions denoted by $[H^+]$ and $[OH^-]$, are measured by

$$pH = -\log[H^+], \qquad pOH = -\log[OH^-]. \tag{6.2}$$

The water dissociation constant is expressed by $K_w = [H^+][OH^-]$ and the electrical neutrality condition states that $pH = pOH = 7$; thus, $pK_w = 14$ (where p denotes a co-logarithm).

HCl, as a strong acid, is added to water to reduce the solution pH below 7. This reaction produces H^+ (attached to water) and Cl^- chloride ions.

$$H_2O + HCl \leftrightarrows H_3O^+ + Cl^-. \tag{6.3}$$

Sodium hydroxide is added to the bath to increase the solution pH above 7 and due to the dissociation of NaOH

$$H_2O + NaOH \leftrightarrows Na^+H_2O + OH^-. \tag{6.4}$$

The dissociation reaction of HCl and NaOH (Eqs. 6.3 and 6.4) are neglected in this model assuming that in this fast reaction, hydrogen chloride and sodium hydroxide are fully dissociated.

When an anionic polyelectrolyte gel – having carboxyl groups COOH – is submerged in a water bath, its functional groups become ionized

$$H_2O + COOH \leftrightarrows H_3O^+ + COO^-. \tag{6.5}$$

This reaction produces positive mobile ions and negative bound ions COO^- attached to the polymer chains. Entire functional groups subdivide into ionized and non-ionized carboxyl groups. At pH values higher than 7, the ionized functional groups make a reaction with sodium cations

$$Na^+H_2O + COO^- \leftrightarrows Na^+COO^- + H_2O. \tag{6.6}$$

This reaction results in neutral ion pairs Na^+COO^-. Dissociation of these ion pairs produces sodium cations whose concentration $[Na^+]$ is defined by θ as follows

$$\theta = \begin{cases} 0 & \text{pH} \leq 7 \\ 10^{\text{pH}-\text{pK}_\text{w}} - 10^{\text{pH}} & \text{pH} > 7. \end{cases} \tag{6.7}$$

When pH is below 7, no sodium cations exist in the bath. As the bath becomes basic, Na^+ cations increases. The second relation is found from Eq. 6.2 and the electrical neutrality condition $[Na^+] + [H^+] = [OH^-]$.

Functional groups are divided into three categories and denoted by n_1, n_2 and n_3 the number of ionized carboxyl groups COO^-, non-ionized groups COOH, ion-pai groups Na^+COO^-. Therefore, the degree of ionization is as described in Eq. 4.4. The fraction of neutral groups COOH and Na^+COO^- are given by

$$\beta_{\mathrm{H}} = \frac{n_2}{n}, \qquad \beta_{\mathrm{Na}} = \frac{n_3}{n}, \tag{6.8}$$

and consequently,

$$\alpha = 1 - \beta_{\mathrm{H}} - \beta_{\mathrm{Na}}. \tag{6.9}$$

Beside molar fraction of ions given in Eq. 4.5, the molar fraction of sodium cations is determined by

$$[\mathrm{Na}^+] = \theta = k\frac{\bar{c}_{\mathrm{Na}^+}}{\bar{c}}. \tag{6.10}$$

6.1.2 Macrodeformation and free energy imbalance relations

The deformation of a hydrogel is similar to the formulation given for pH-sensitive hydrogels in Chapter 4. Concentration of sodium cations are added to the relations. Electric field is formulated as described in Section 4.1.3 in Chapter 4. However, the charge density is changed in this chapter which results in a new relation for the work of the electric field per unit volume in the initial state per unit time as follows

$$u_{\mathrm{el}} = \mathbf{E}\cdot\dot{\mathbf{H}} - e\Phi(\dot{C}_{\mathrm{H}^+} + \dot{C}_{\mathrm{Na}^+} - \dot{C}_{\mathrm{OH}^-} - \dot{C}_{\mathrm{Cl}^-} - \dot{\alpha}C_b). \tag{6.11}$$

Kinetic relations developed in Section 4.1.2 in Chapter 4, are extended to account for Na^+ ions. $\mathbf{J}_{Na^+}$ denotes the flux vector for sodium cations in the initial configuration and is given by (in analogy with Eq. 4.9)

$$\mathbf{J}_{Na^+} = -\frac{D_{Na^+} C_{Na^+}}{k_B T} \mathbf{F}^{-1} \cdot \boldsymbol{\nabla}_0 \mu_{Na^+} \cdot \mathbf{F}^{-1}, \tag{6.12}$$

where μ_{Na^+} is the chemical potential of mobile Na^+ ions. Moreover, mass conservation equation (Eq. 4.10) are expressed by

$$\begin{aligned} \dot{C}_{H^+} + \boldsymbol{\nabla}_0 \cdot \mathbf{J}_{H^+} &= \Gamma_{H^+}, \\ \dot{C}_{Na^+} + \boldsymbol{\nabla}_0 \cdot \mathbf{J}_{Na^+} &= \Gamma_{Na^+}, \\ \dot{C}_{OH^-} + \boldsymbol{\nabla}_0 \cdot \mathbf{J}_{OH^-} &= \Gamma_{OH^-}, \\ \dot{C}_{Cl^-} + \boldsymbol{\nabla}_0 \cdot \mathbf{J}_{Cl^-} &= 0, \end{aligned} \tag{6.13}$$

where Γ_{OH^-} is the rate of production of OH^- ions due to ionization of water, Γ_{H^+} is the rate of production of H^+ ions generated by ionization of water and dissociation of functional groups, and Γ_{Na^+} is the rate of production of Na^+ ions due to dissociation of ion pairs. Combination of Eqs. 6.1, 6.5 and 6.6 results in

$$\begin{aligned} \Gamma_{OH^-} &= -\Gamma_0, \\ \Gamma_{H^+} &= -\Gamma_0 - \dot{\beta}_H C_b, \\ \Gamma_{Na^+} &= -\dot{\beta}_{Na} C_b, \end{aligned} \tag{6.14}$$

where Γ_0 is the rate of association OH^- and H^+ in the self-ionization of water, $-\dot{\beta}_H C_b$

is the rate of creation of H^+ by self-ionization of water, and $-\dot{\beta}_{Na}C_b$ is the rate of production of sodium cations by dissociation of ion pairs. C_b is the concentration of functional groups in the initial state. In analogy with Eq. 4.11, the work produced by the diffusion of solvent and solute is determined by

$$\begin{aligned} u_{dif} =& \mu(\dot{C} - 2\Gamma_0) + \mu_{H^+}(\dot{C}_{H^+} - \Gamma_{H^+}) + \mu_{Na^+}(\dot{C}_{Na^+} - \Gamma_{Na^+}) \\ &+ \mu_{OH^-}(\dot{C}_{OH^-} - \Gamma_{OH^-}) + \mu_{Cl^-}\dot{C}_{Cl^-} + \bar{u}_{dif}, \end{aligned} \tag{6.15}$$

where

$$\bar{u}_{dif} \geq 0. \tag{6.16}$$

Kinematic relations are the same as described in Section 2.1.1 in Chapter 2.

The free energy relation is derived similar to Section 4.1.4 in Chapter 4 with a small modification regarding addition of sodium cations to mobile ions. The specific free energy density is the summation of the non-interacting energy of solvent and solutes $\Psi_{non\text{-}mix}$, the strain energy of polymer network Ψ_{net}, and the mixing energy of polymer-water Ψ_{mix1}, water-mobile ions Ψ_{mix2} and non-charge and charged functional Ψ_{mix3}. Eq. 4.26 is used to describe the free energy density of a PE gel and three terms in this equation $\Psi_{non\text{-}mix}$, Ψ_{mix2}, and Ψ_{mix3} are modified to account for the presence of sodium cations. The specific energy density $\Psi_{non\text{-}mix}$ reads

$$\Psi_{non\text{-}mix} = \mu^0 C + \mu^0_{H^+} C_{H^+} + \mu^0_{Na^+} C_{Na^+} + \mu^0_{OH^-} C_{OH^-} + \mu^0_{Cl^-} C_{Cl^-}, \tag{6.17}$$

where μ^0, $\mu^0_{H^+}$, $\mu^0_{Na^+}$, $\mu^0_{OH^-}$, and $\mu^0_{Cl^-}$ stand for the chemical potential energies of non-

mixing water molecules and free ions, respectively. The specific mixing energy Ψ_{mix2} and Ψ_{mix3} are given by

$$\begin{aligned}\Psi_{\text{mix2}} =& k_B T \left[C_{\text{H}^+} \ln\left(\frac{C_{\text{H}^+}}{C} - 1\right) + C_{\text{Na}^+} \ln\left(\frac{C_{\text{Na}^+}}{C} - 1\right) + C_{\text{OH}^-} \ln\left(\frac{C_{\text{OH}^-}}{C} - 1\right) \right. \\ & \left. + C_{\text{Cl}^-} \ln\left(\frac{C_{\text{Cl}^-}}{C} - 1\right) \right], \\ \Psi_{\text{mix3}} =& k_B T C_b \left(\beta_{\text{H}} \ln \beta_{\text{H}} + \beta_{\text{Na}} \ln \beta_{\text{Na}} + (1 - \beta_{\text{H}} - \beta_{\text{Na}}) \ln(1 - \beta_{\text{H}} - \beta_{\text{Na}}) \right).\end{aligned} \tag{6.18}$$

Governing equations for modeling mechanical responses of a hydrogel with finite strain are derived using the free energy inequality equation

$$\dot{\Psi} - u_{\text{mech}} - u_{\text{dif}} - u_{\text{el}} - u_{\text{dis}} + \Pi(\dot{C}v - J\mathbf{I} : \mathbf{D}) \leq 0. \tag{6.19}$$

Works produced by the mechanical force, the electric field, and the transport of solvent and solutes are given in Eq. 4.34, Eq. 6.11 and Eq. 6.15, respectively. The work produced by the dissociation of functional groups and formation of ion pairs, is described by

$$u_{\text{dis}} = -(\dot{\beta}_{\text{H}} \, \Delta\mu_{\text{H}} + \dot{\beta}_{\text{Na}} \, \Delta\mu_{\text{Na}}) C_b, \tag{6.20}$$

where $\Delta\mu_{\text{H}}$ and $\Delta\mu_{\text{Na}}$ denote the differences between chemical potentials of ionized functional groups and neutral ions pairs of H^+COO^- and Na^+COO^-.

The inequality relation is satisfied provided that the Cauchy stress is determined by

$$\begin{aligned}\mathbf{T} = -\Pi\mathbf{I} + \frac{2}{1+Q}\Bigg[\frac{\partial W}{\partial J_{e1}}\mathbf{B}_e - J_{e3}\frac{\partial W}{\partial J_{e2}}\mathbf{B}_e{}^{-1} + (J_{e2}\frac{\partial W}{\partial J_{e2}} + J_{e3}\frac{\partial W}{\partial J_{e3}})\mathbf{I} \\ + \frac{1+Q}{2\varepsilon}\left(\mathbf{h}\otimes\mathbf{h} - \frac{1}{2}(\mathbf{h}\cdot\mathbf{h})\mathbf{I}\right)\Bigg],\end{aligned} \tag{6.21}$$

the chemical potentials of water and mobile ions are expressed by

$$\begin{aligned}&\mu = \Theta_C + \Pi v, \qquad \mu_{H^+} = \Theta_{H^+} + e\Phi, \qquad \mu_{Na^+} = \Theta_{Na^+} + e\Phi, \\ &\mu_{OH^-} = \Theta_{OH^-} - e\Phi, \qquad \mu_{Cl^-} = \Theta_{Cl^-} - e\Phi,\end{aligned} \tag{6.22}$$

and the equations for the concentration of non-ionized functional groups are given by

$$\begin{aligned}\frac{\Theta_{\beta_H}}{C_b} + e\Phi + \Delta\mu_H - \mu_{H^+} = 0, \\ \frac{\Theta_{\beta_{Na}}}{C_b} + e\Phi + \Delta\mu_{Na} - \mu_{Na^+} = 0,\end{aligned} \tag{6.23}$$

where Θ_C, Θ_{H^+}, Θ_{Na^+}, Θ_{OH^-}, Θ_{Cl^-}, Θ_{β_H}, and $\Theta_{\beta_{Na}}$ are provided in Eq. C.1. Moreover, the rate of association of H^+ and OH^- is given by

$$\Gamma_0 = -\overline{\Gamma}(2\mu - \mu_{H^+} - \mu_{OH^-}), \tag{6.24}$$

where $\overline{\Gamma}$ is an arbitrary positive function. The governing equation are then derived as explicitly described in [189].

6.1.3 Equilibrium swelling of a PE hydrogel in a bath at a wide range of pH

When a hydrogel submerges into a bath, it swells due to thermodynamic comparability between polymer network, solvent and solutes. Swelling ratio Q is found based on the state of stress in a boundary-value problem under the thermodynamic equilibrium. The macro-deformation of a gel specimen subjected to unconstrained swelling has been derived based on the free energy inequality equation considering the incompressibility condition. Moreover, the Donnan's law states that the chemical potentials inside the gel equalize with those outside in the bath; therefore,

$$\mu = \bar{\mu}, \quad \mu_{\mathrm{H}^+} = \overline{\mu}_{\mathrm{H}^+}, \quad \mu_{\mathrm{Na}^+} = \overline{\mu}_{\mathrm{Na}^+}, \quad \mu_{\mathrm{OH}^-} = \overline{\mu}_{\mathrm{OH}^-}, \quad \mu_{\mathrm{Cl}^-} = \overline{\mu}_{\mathrm{Cl}^-}. \tag{6.25}$$

The Cauchy stress tensor $\mathbf{T}$ for a specimen which has traction-free surfaces is given by

$$\mathbf{T} = 0. \tag{6.26}$$

The theoretical model can be simplified to these equations as described in [189]:

$$\begin{aligned} X^2 - \frac{\alpha Q_b}{Q} X &= \frac{1}{k^2}(10^{-\mathrm{pH}} + \theta)^2, \\ \alpha &= \frac{\mathrm{K}'_a}{\mathrm{K}'_a + X(10^{-\mathrm{pH}} + \kappa\theta)(10^{-\mathrm{pH}} + \theta)^{-1}}, \end{aligned} \tag{6.27}$$

$$\ln\frac{Q}{1+Q} + \frac{1}{1+Q} + \frac{\chi}{(1+Q)^2} + \frac{g}{1+Q}\left[\left(\frac{1+Q}{1+Q_0+\bar{q}Q_b\alpha}\right)^{\frac{2}{3}} - 1\right] - \overline{\Pi}_{ion} = 0, \tag{6.28}$$

where

$$X = \frac{C_{H^+} + C_{Na^+}}{C}, \quad \kappa = \frac{K'_a}{K'_{Na}}. \tag{6.29}$$

Q_b, and Q_0 are respectively swelling ratio of functional groups and initial swelling ratio of the hydrogel; χ is the Flory-Huggins parameter; $\bar{q} = q_1/v$ and q_1 is a material constant used in Eq. 4.29; $X = (C_{H^+} + C_{H^+})/C$ describes concentration of counter ions with respect to solvent concentration in the actual state; and, κ denotes the ratio of dissociation constants for carboxyl groups (K_a) and ion pairs (K'_{Na}). Moreover, $K'_a = K_a/k$, where $k = 55.\bar{5}$ is the molarity of water. α stands for degree of ionization and is given by the extended form of the Henderson-Hasselbach equation (Eq. 4.45) to incorporate the effect of formation of Na^+COO^- ion pairs at high pH values. Furthermore, the neo-Hookean material model is specified for the strain energy of polymer network Φ_{net} with G as the shear modulus. The dimensionless shear modulus g is also introduced by $g = Gv/k_BT$ where k_B is the Boltzmann constant, T is room temperature, and v stands for the volume of a water molecule.

The dimensionless ionic pressure is expressed by

$$\overline{\Pi}_{ion} = X\left(\frac{\alpha Q_b}{Q}\right)^2\left(X + \frac{1}{k}(10^{-pH} + \theta)\right)^{-2}, \tag{6.30}$$

and the dimensionless pressure induced by the electrostatic forces between bound charges

is expressed by

$$\overline{\Pi}_{\text{rep}} = \frac{g}{1+Q}\left[\left(\frac{1+Q}{1+Q_0}\right)^{\frac{2}{3}} - \left(\frac{1+Q}{1+Q_0+\bar{q}Q_b\alpha}\right)^{\frac{2}{3}}\right]. \tag{6.31}$$

6.1.4 Numerics

Dependent variables (Q, X, α) are to de found from three algebraic equations Eqs. 6.27 and 6.28. The commercial software COMSOL [144], is used to solve this implicit equations with a relative tolerance of 10^{-9}.

6.2 Results and discussion

The model developed in this chapter is used to analyze the swelling behavior of agarose-carbopol (AC) composite hydrogels presented in Chapter 5. The experimental data of AC composite hydrogels demonstrates a non-monotonic relation between swelling ratio and solution pH. Generally, swelling of anionic hydrogels increases as pH increases until it reaches a plateau around pH $= 7-9$, and followed by a decrease at higher pH values. The previously described theoretical model is used to predict this non-monotonic behavior. The effect of increasing the concentration of constituents on swelling of the composite gels is also investigated.

In this section, the model is used to predict the equilibrium swelling of AC hydrogels for a wide range of pH spectrum (pH = $2-14$). Three batches of AC composite gels are selected (AC1, AC2, and AC3) to fit to the model. The parameters of the model are

Table 6.1: Parameter fittings for three batches of agarose-carbopol (AC) hydrogels

Physical parameters	AC1	AC2	AC3	AC4
G ($\times 10^3$ N m^{-2})	4.1	2.6	1.7	2.9
Q_b ($\times 10^{-9}$)	19.5	19.5	30	47
$\bar{q}$ ($\times 10^7$ m^{-3})	5.5	5.5	9.5	15
κ ($\times 10^{-5}$)	5.0	6.0	9.0	2.0

reduced by assuming $Q_0 = 0$ and $\chi = 0.4$. When Q_0 is zero, the initial state matches with the reference state in which functional groups are not charged. The interaction parameter χ is assigned to be slightly less than 0.5 according to solubility of polymer in water which is not a very good solvent.

Simulations are performed to find parameters individually from the best fit to experiments at different pH ranges. The shear modulus of polymeric network G has a direct influence on degree of swelling at low pH. Therefore, this parameter is exclusively obtained from different simulation runs fitted to swelling-pH curves at low pH values (pH < 3). In addition, AFM measurements on swollen AC1 hydrogels at pH≈ 7 are used as a rough estimation for G at low pH. Two other parameters of the model Q_b and $\bar{q}$ are found by parameter fittings to the experimental data of equilibrium swelling at intermediate pH ($3 <$ pH < 7). Finally, parameter κ is determined to predict the shrinking decay at high pH (pH > 9) observed in experiments.

6.2.1 Non-monotonic dependence of swelling on pH

Fig. 6.1 shows the swelling ratio of an AC composite hydrogel comprising 1% w/V of agarose and 0.5% w/V of carbopol. This composite hydrogel shows an increase in swelling as solution pH increases from 2 to 7. This is a common behavior of anionic

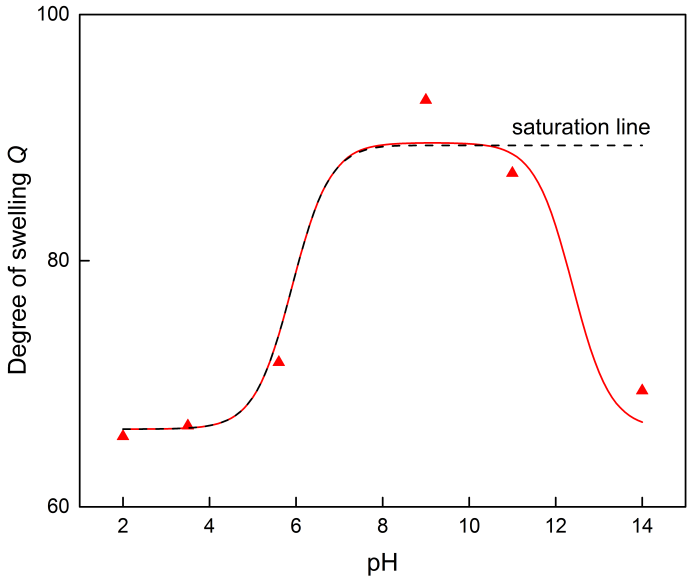

Figure 6.1: Degree of swelling Q of the AC1 composite hydrogel versus solution pH spectrum

hydrogels to reach its maximum swelling when pH exceeds the dissociation constant pK_a. The maximum swelling ratio is obtained around pH $= 7$ which is represented by a saturation line in Fig. 6.1. The dissociation constant of carbopol microgels is $pK_a = 6 \pm 0.5$ according to technical data sheet of carbopol [200]; thus, we set $pK_a = 6$ for all composite gels. These parameters found from the best-fits to experimental data of AC composite hydrogels are listed in Table 6.1.

The model can predict the non-monotonic swelling ratio as a function of solution pH. In agreement with observations, Fig. 6.1 and Fig. 6.2 illustrate simulation results with a solid line which shows the volume expansion of AC1 hydrogels under swelling at low to intermediate pH values. The volume of this AC composite hydrogel ($\overline{V}$) expands more than 30% compared to the volume at the lowest pH (pH $= 2$). The dimensionless

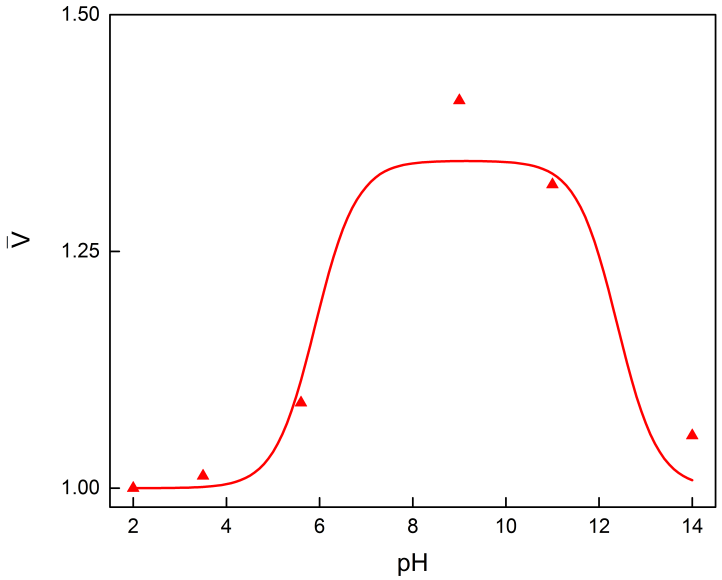

Figure 6.2: Dimensionless volume of the AC1 composite hydrogel as a function of pH

volume is defined by

$$\overline{V} = \frac{1+Q}{1+Q|_{\mathrm{pH}=2}}. \tag{6.32}$$

Furthermore, the model predicts a constant swelling ratio between pH values of 7 and 9. In addition, when NaOH is added to the bath, its pH decreases and consequently, the model demonstrates the shrinkage of swelling ratio instead of having a constant saturation line at pH higher than 9.

6.2.2 Swelling behavior of different compositions of AC hydrogels

Three batches of composite hydrogels were prepared with prescribed compositions as shown in Table 5.1. Agarose is the main component in AC1, AC2, and AC3 gels and their concentrations are kept twice the concentration of carbopol. These hydrogels have

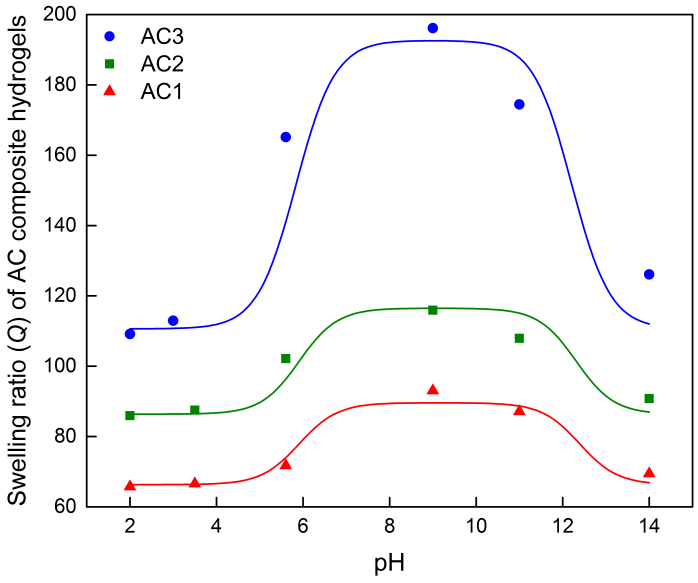

Figure 6.3: Swelling behavior of three compositions of AC composite hydrogels.

a desirable mechanical integrity (even at their highly swollen state) for experiments. Simulation results show that all hydrogels swell by increasing pH until reach their maximum swelling at pH ≈ 7, remain constant until pH ≈ 9 followed by a shrinkage as shown in Fig. 6.3. Among theses three composite gels, AC3 has a higher equilibrium swelling ratio although it contains the minimum amount of agarose and carbopol. Equilibrium swelling ratio of AC1 and AC2 gels are lower than that of AC3 gels, although the concentration of carbopol in AC1 and AC2 gels is more. Swelling of AC1 and AC2 are nearly the same, although AC2 may be expected to swell more due to its higher content of carbopol and carboxyl groups. It has been shown in Chapter 5 that agarose has no contribution to swelling, and therefore only carbopol – as an anionic polymer gel – is responsible for swelling of the hydrogels.

The dimensionless volume of these gels is determined by Eq. 6.32 to provide a

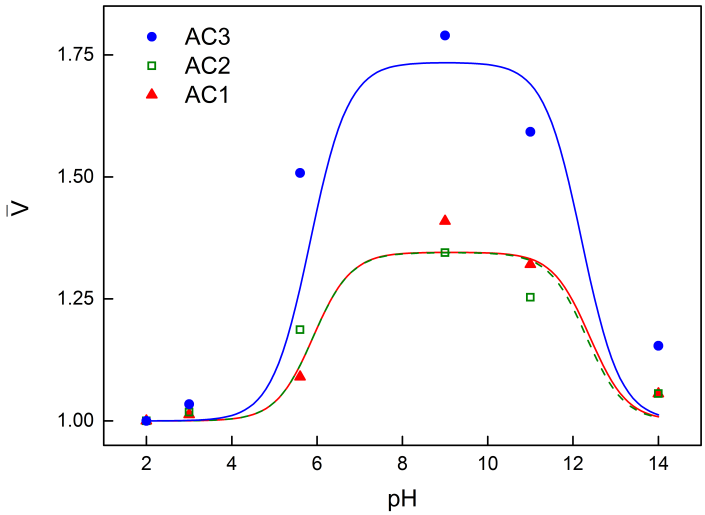

Figure 6.4: Dimensionless volume of AC composite hydrogels $\bar{V}$ as a function of pH; experimental data extracted from Fig. 6.3 and recalculated with Eq. 6.32; lines: results of simulation.

basis for comparison between the swelling ratio of AC1, AC2 and AC3 gels. Fig. 6.4 demonstrates that AC1 and AC2 have exactly the same swelling-pH curves. It can be seen that a higher concentration of carbopol in AC2 (compared to that in AC1) is not leading to a higher swelling ratio. Parameter-fitting of the model to the experimental data implies that Q_b and $\bar{q}$ are almost equal for AC1 and AC2 gels. The contribution of agarose and carbopol can be differentiated by comparison between swelling ration of AC3 and AC4 hydrogels.

6.2.3 Effect of carbopol concentration on swelling ratio

In order to individually study the effect of carbopol concentration on swelling ratio of AC composite hydrogels, another batch of gels (AC4) were prepared by doubling carbopol concentration ($C_{\text{agarose}} = C_{\text{carbopol}} = 0.5\%$ w/V) while agarose concentration

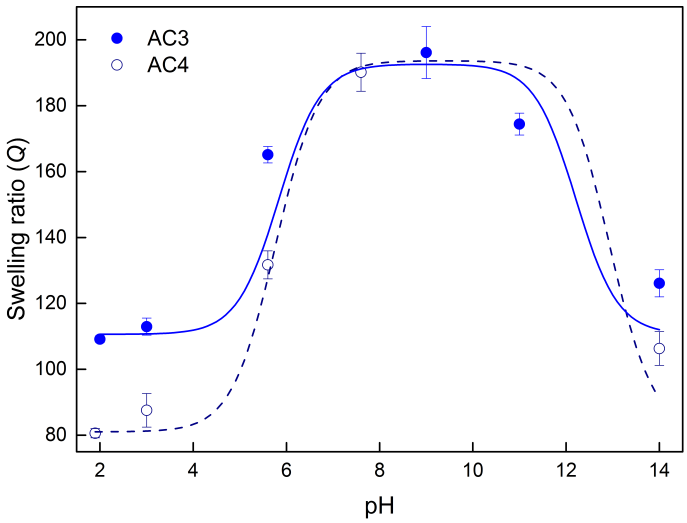

Figure 6.5: Degree of swelling Q versus pH for AC3 and AC4 gels to study the effect of doubling the concentration of carbopol. Symbols show experimental results, and lines represent simulation results.

is kept constant. Fig. 6.5 exhibits the equilibrium swelling ratio of AC3 and AC4 gels with symbols indicating experimental data and lines as simulation results. To provide a reference for comparison, the dimensionless volume is calculated for gels using Eq. 6.32. Because AC4 specimens subjected to swelling in the bath with pH values higher than 9 were very fragile, their swelling measurements could not be completed until equilibrium. Fig. 6.6 demonstrates that increasing the fraction of carbopol improves the swelling of composite hydrogels noticeably. By increasing the fraction of carbopol, the number of functional (carboxyl) groups increase and it is expected to have a higher swelling. This is consistent with observations on poly(N-isopropyl acrylamide-co-methacrylic acid) (NIPA-MAc) gels where a higher swelling ratio is obtained with a higher molar fraction of MAc [195]. A linear correlation between acid polymer fraction and swelling parameters of the theoretical model has been also proposed in [189].

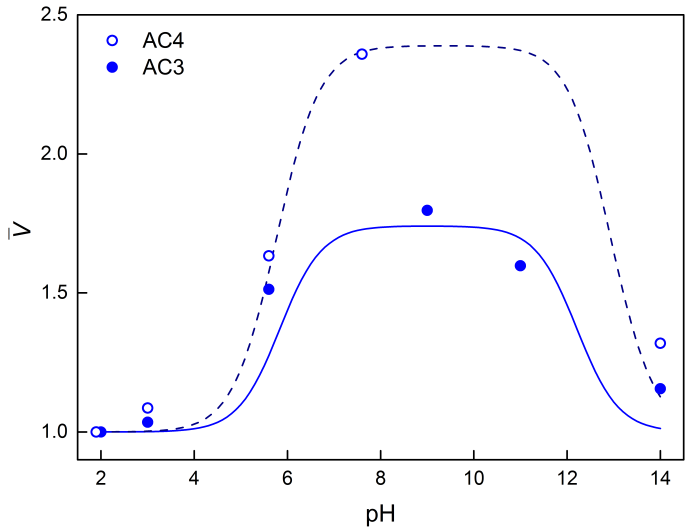

Figure 6.6: Dimensionless volume $\bar{V}$ versus pH for AC3 and AC4 gels to compare the effect of increasing the amount of carbopol, with respect to a common reference. Symbols show experimental results, and lines represent simulation results.

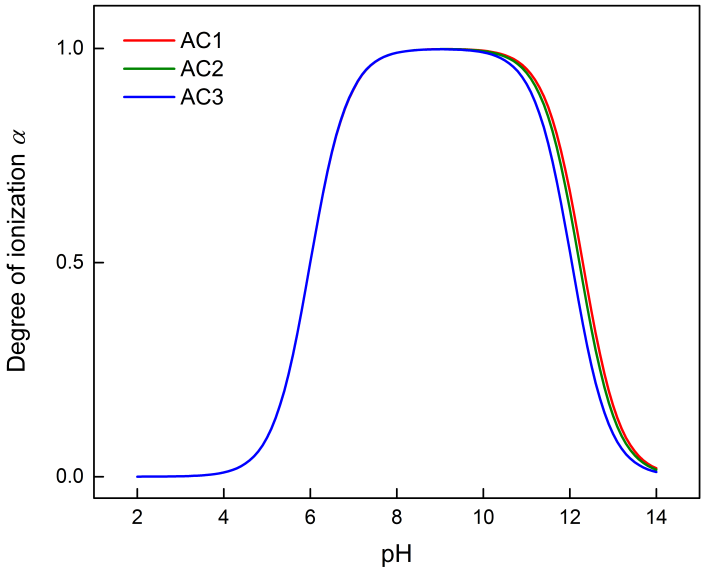

Figure 6.7: Degree of ionization α versus pH for three batches of AC gels.

6.2.4 Degree of ionization, ionic pressure and pressure induced by electrostatic forces between bound charges

Degree of ionization is found from simulation results to have a non-monotonic relation with pH of the bath (in the absence of salt) for all three batches of AC gels as shown in fig. 6.7. α is close to zero when functional groups of acid polymer are at fully associated state (pH $<<$ pK_a). As pH increases, degree of ionization increase accordingly. At pH values higher than pK_a, carboxyl groups become fully dissociated and α reaches its maximum value. Furthermore, dissociation of NaOH – added to obtain a basic bath – causes the formation of neutral pairs between Na^+ and COO^- ions and consequently, the number of carboxyl groups and free counter ions decrease. Degree of ionization α is similar for all hydrogel compositions in the acidic bath, although α of AC3 and AC2 gels are slightly lower than α of AC1 gels in the basic bath.

The model determines ionic pressure and induced pressure by electrostatic forces between bound charges for three composite hydrogels: AC1, AC2, and AC3. Since their values for these hydrogels are quite similar (the reason will be provided in Section 6.3), the results are only presented for AC1 hydrogels. Fig. 6.8 illustrates that dimensionless ionic pressure $\overline{\Pi}_{\text{ion}}$ increases until pH ≈ 7 and then, immediately decreases. Ionic pressure depends on the gradient of ion concentrations inside the gel and outside in the bath. For pH levels below 7, ionic pressure increases with pH since number of H^+ ions reduces when pH increases. Furthermore, ionic pressure decreases after pH $= 7$ due to the presence of Na^+ counter ions.

Dimensionless pressure $\overline{\Pi}_{\text{rep}}$ driven by the repulsive interaction between bound

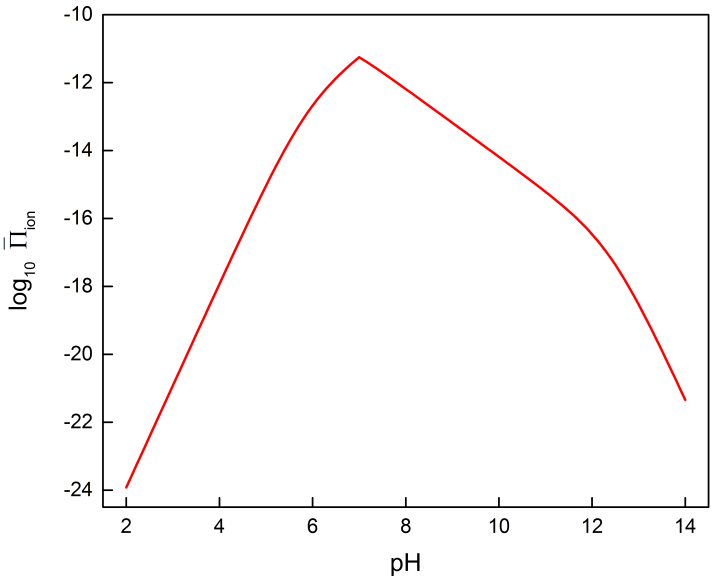

Figure 6.8: Calculated ionic pressure $\overline{\Pi}_{ion}$ of AC1 gels as a function of pH

charges is depicted in Fig. 6.9. This induced pressure in composite hydrogels increases with pH, reaches its saturation at pH ≈ 6, remains constant around pH $= 7-9$, and decreases at higher pH (similar to α-pH curves). This induced pressure depends on degree of ionization α and parameter κ which is the ratio of dissociation constants for carboxyl groups and ion pairs. Furthermore, simulation results in Fig. 6.9 demonstrate that $\overline{\Pi}_{rep}$ is orders of magnitude larger than $\overline{\Pi}_{ion}$. Therefore, the electrostatic repulsion between bound charges is determined as the main mechanism for swelling of these composite hydrogels.

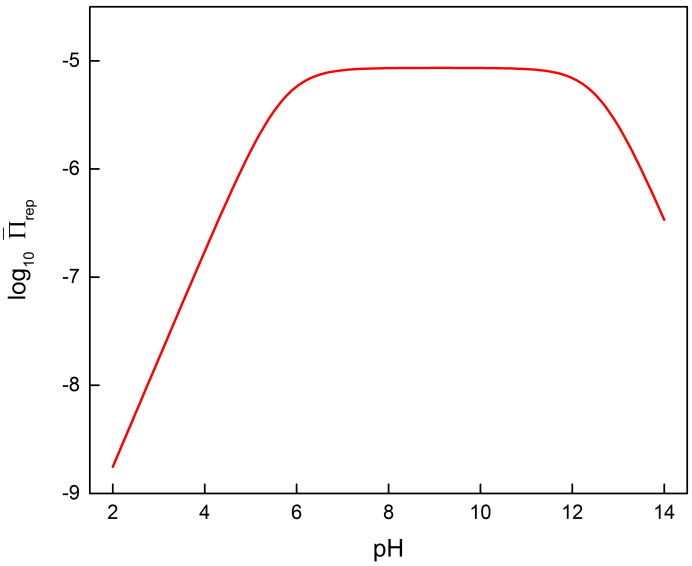

Figure 6.9: Calculated the induced pressure $\overline{\Pi}_{rep}$ by electrostatic repulsion between bound charges of AC1 gels as a function of pH

6.3 Discussion

Formation of ion pairs between fixed charges COO^- and free ions may provide an explanation for non-monotonic swelling of composite hydrogels in response to various pH values. Probability of ion pair formation increases when concentration of mobile ions increases: the number of H^+ and Na^+ ions are high at low and high pH, respectively. Neutral ion pairs are developed between COO^-, and Na^+ and H^+ ions at high and low pH, respectively. This results in neutralization of carboxyl groups, reduction of electrostatic forces, and subsequently, swelling ratio. The above mentioned mechanism can also be used to explain pH-dependent mechanical behavior of carbopol, such as viscosity and yield stress of carbopol which develops with pH [201], similar to swelling-pH curves of the composite gels.

Agarose-carbopol composite hydrogels have swelling properties arising from the carbopol component, and mechanical properties mostly to originate from the agarose component (which is higher in concentration than carbopol). The parameters of the model related to swelling ($Q_b, \bar{q}$ and α) are found to be close to each other for different AC hydrogels. This results in finding similar values for $\overline{\Pi}_{\text{ion}}$ and $\overline{\Pi}_{\text{rep}}$, and consequently, similar pH-induced swelling for different composite hydrogels.

The physical parameters of the model – obtained from parameter fittings to experimental data of AC composite hydrogels – determines that the stiffness of these hydrogels increases with the concentration of agarose, which causes the hydrogels to shrink. The concentration of agarose increases together with the concentration of carbopol. However, increasing the concentration of carbopol has a counter effect and increases the swelling of these gels. Thus, it is concluded that the influence of increasing C_{agarose} dominate the effect of C_{carbopol} on swelling of AC composite hydrogels. It is suggested that the swelling of carbopol may be hindered by the stiffness of agarose.

6.4 Conclusion

The equilibrium swelling of agarose-carbopol composite hydrogels has been analyzed by a theoretical thermodynamic model. Equilibrium swelling-pH curves follow a non-monotonic behavior in an acidic and a basic bath. The model can predict this non-monotonic behavior: swelling increases first with pH, reaches a plateau for $7 < \text{pH} < 9$ and finally decreases at high pH. The electrostatic repulsion between bound charges induces a pressure which is mainly responsible for swelling of these composite hydro-

gels in the acidic bath. Formation of ion pairs between bound ions and mobile ions can predict the shrinkage of the hydrogels in the basic bath. Moreover, investigating the influence of different compositions of the composite hydrogels suggests that the swelling of carbopol is suppressed by the mechanical stiffness of the agarose network. The swelling and the mechanical stiffness of AC composite hydrogels can be adjusted by the concentration of carbopol and agarose, for biomedical design purposes for example when used as 3D scaffolds for cell housing and also, as drug carriers.

Chapter 7

Conclusions and future works

7.1 Conclusions

This study deals with constitutive modeling, numerical simulation and experiment for equilibrium analysis of swelling deformation of composite hydrogels; particularly made of two distinct polymer gels. The governing equations for a thermodynamic equilibrium between mechanical and swelling forces are derived considering the boundary conditions. Specific material models for stimuli-responsive hydrogels are employed based on a free energy density function for a polymer gel. A continuum volume of a hydrogel is assumed as a multi-phase medium which includes a polymer network, solvent and solutes (in case of swelling in either an acidic or a basic bath). The constitutive equations which involve the stress-strain relation and the nonlinear diffusion equation for transport of solvent and solutes, are obtained, examined and validated with experimental results of equilibrium swelling. The influence of various stimuli on different

composite hydrogels – comprising temperature, pH, coupled pH/temperature and ionic strength – are investigated.

The formulations for large deformation and solvent diffusion of hydrogels subjected to swelling together with constitutive relations for neutral core/shell hydrogels under equilibrium swelling are described in Chapter 2. The first study presented in Chapter 3, is on the equilibrium swelling of a doubly temperature-sensitive core/shell composite hydrogel. The thermodynamic model developed for neutral core /shell gels are further extended to include temperature-induced swelling and to validate with experimental data from a core/shell microgel which has different volume phase transition temperature for each domain. A continuous domain is considered to represent the core/shell hydrogel with discontinuous elastic modulus and polymer-solvent interaction parameter for the deformable core and shell domains. The model determines the mutual interaction between the core and the shell, predicts the size of the core/shell hydrogel; also, its polymer density is demonstrated to be in a good agreement with experimental data from small angle neutron scattering. An isotropic swollen state of the core, and a radial anisotropic swollen state of the shell are found for various shell thickness and temperatures. Predictions of the model are furthermore verified with the experimental data from dynamic light scattering. Increasing the shell thickness develops a two-step transition behavior in the swelling-temperature curves which attribute to the volume phase transition temperatures of the core and the shell polymer network. In contrary, hydrogels with thin shells exhibit only one transition point attributed to the VPTT of the core.

In Chapter 4, the coupled effect of pH and temperature on the equilibrium swelling

of a dual-responsive core/shell composite hydrogel is studied. A theoretical model recently developed for pH-sensitive hydrogels is extended to model temperature sensitive core/shell hydrogels with a geometry constraint. The model is used to predict the equilibrium swelling of a core/shell gel whose core is pH- and thermo-responsive and whose shell is only thermo-sensitive. The volume phase transition temperature of the core which shifts to a higher temperature by increasing pH, is parameter-fitted at different pH values. In accord with observations, swelling ratio decreases with temperature and at higher pH values, shows two transition points akin to the volume phase transition temperature of the core and the shell. The model predicts the decrease of the degree of ionization in the core with temperature, and this decrease occurs at two steps for high pH values in an acidic bath. As pH increases, the shell collapses earlier than the core and applies a compressing radial stress on the swollen core. The maximum radial stress (interface stress) appears at the inner boundary of the shell, and decays to zero at the outer boundary of the shell. The interface stress is found as a function of temperature and this function has two local maximum values; the first corresponds to the collapse of the shell, and the second relates to the collapse of the core occurring at a higher temperature. The model determines that contribution of repulsion forces between bound charges to equilibrium swelling is higher than ionic pressure.

In Chapter 5, an experimental study is conducted on a composite hydrogel prepared by co-polymerization of agarose and carbopol. This co-polymerization results in a pH-responsive hydrogel by copolymerization of carbopol (ionic hydrogel) into agarose network (neutral hydrogel). Moreover, AFM imaging supports that the composite hydro-

gels form a network whose polymer structure of agarose and carbopol cannot be differentiated. The elastic modulus of this hydrogel (determined by AFM force microscopy) in the swollen state, shows a relatively soft hydrogel at neutral pH. Swelling behavior of agarose-carbopol hydrogels are studied in response to various pH values ranging from highly acidic to highly basic, and a non-monotonic dependence of swelling ratio on pH is revealed.

In chapter six, experimental results obtained in Chapter 5 for the equilibrium swelling of agarose-carbopol composite hydrogels are analyzed by a theoretical thermodynamic model. Equilibrium swelling-pH curves demonstrate a non-monotonic behavior which is determined by the model: swelling increases first with pH, reaches a plateau at $7 < \text{pH} < 9$ and finally reduces at high pH. The induced pressure by the electrostatic repulsion between bound charges – compared to ionic pressure – is discovered to be the main mechanism for swelling of these composite hydrogels in the acidic bath.

In addition, formation of ion pairs between bound ions and mobile ions well predicts the shrinkage of the hydrogels in the basic bath. In agreement with observations, the model predicts the equilibrium swelling of different compositions of agarose-carbopol hydrogels and overall, it is suggested that agarose polymer network has a significant effect on swelling ratio indirectly by forming a relatively strong network and constraining the swelling of carbopol polymer network. This composite hydrogel with modular properties (concentration-based mechanical and swelling properties) is favorable as an engineering smart hydrogel for biomedical applications in tissue engineering and drug delivery.

7.2 Recommendations for future works

Numerical simulations are used as a tool to estimate swelling behavior of composite hydrogels. Simulation results might be approximate due to the limitations of phenomenological relations, assumptions, and physical parameters utilized. The main intention of applying theoretical models is to predict main features observed in experiments instead of exact reproducibility of experimental data. The results of this study may be developed further in future studies if new understandings of observations or new approaches for mathematical modeling are discovered.

Although equilibrium swelling of composite hydrogels is analyzed in this thesis, their transient swelling behavior is another prominent feature which promotes further investigations. Transient analysis of swelling deformation of composite hydrogels which are stimuli-responsive may be addressed in future studies by considering the time-dependent diffusion relation of molecular transport within the same thermodynamic framework. For instance, swelling experiments on agarose-carbopol composite hydrogels which are provided in Chapter 5, demonstrate an exotic non-monotonic dependence of swelling on time. Transient swelling of these composite hydrogels at different pH values may be further studied to provide an explanation for this kind of behavior.

Three-dimensional matrix including embedded particles may also be studied with governing equations and constitutive relations developed for large deformation and solvent (solutes) diffusion of stimuli-responsive hydrogels. Each of the embedded particles may be responsive to various external stimuli. In this study, composite hydrogels are

only composed of two distinct domains. However, composite hydrogels basically include numerous particles (e.g. microgels or nanogels) which are randomly distributed in a three-dimensional matrix [20]. These composite hydrogels will have a multi-responsive three dimensional structure whose swelling can be controlled in multiple ways. A three-dimensional theoretical model should be implemented to give an insight into the swelling behavior of composite hydrogels. Multi-scale modeling approach can be further utilized to describe the properties of particles and their interface layer with their surrounding matrix.

Appendix A

Derivation of radius of hollow shell in the dry state

Transformation from the initial state to the reference state is denoted by deformation gradient $\mathbf{F}_0$ as follows

$$\mathbf{F}_0 = \mathbf{F}_\mathrm{e} \cdot \mathbf{f}. \tag{A.1}$$

The reference configuration is assumed to be a stress-free state, thus $\mathbf{F}_\mathrm{e} = \mathbf{I}$. Deformation gradient $\mathbf{f}$ for partial swelling in the as-prepared state is given by

$$\mathbf{F}_0 = \frac{\mathrm{d}\bar{r}}{\mathrm{d}R}\mathbf{e}_R\mathbf{e}_R + \frac{\bar{r}}{R}(\mathbf{e}_\Theta\mathbf{e}_\Theta + \mathbf{e}_\Phi\mathbf{e}_\Phi), \tag{A.2}$$

$$\mathbf{f} = f\big(\frac{R}{\bar{r}}\big)^2\mathbf{e}_R\mathbf{e}_R + \frac{\bar{r}}{R}(\mathbf{e}_\Theta\mathbf{e}_\Theta + \mathbf{e}_\Phi\mathbf{e}_\Phi). \tag{A.3}$$

where $\bar{r}$ is found by integration of Eq. 2.34 and expressed by

$$\bar{r}^3 = \bar{r}_1^3 + f(R^3 - R_1^3), \tag{A.4}$$

assuming that the volume expansion coefficient f is constant for core and shell domains.

Here, it is desired to determine stresses appear in the dry state. Eq. 2.1 is used where $\mathbf{F} = \mathbf{I}$ when the deformation gradient mapping the reference state to itself. Insertion of $\mathbf{f}$ from Eq. A.3 into Eq. 2.1, implies that

$$\mathbf{F}_\mathrm{e} = \frac{1}{f}\left(\frac{\bar{r}}{R}\right)^2 \mathbf{e}_R\mathbf{e}_R + \frac{R}{\bar{r}}(\mathbf{e}_\Theta\mathbf{e}_\Theta + \mathbf{e}_\Phi\mathbf{e}_\Phi), \tag{A.5}$$

where $\mathbf{F}_\mathrm{e}$ is the deformation gradient for the elastic deformation in the initial state.

With the application of stress-strain relation (Eq. 2.31) and the condition of the dry gel ($C = 0$), the radial and tangential components of stress is determined by

$$\begin{aligned} T_R &= -\Pi + G\left[\frac{1}{f^2}\left(\frac{\bar{r}}{R}\right)^4 - 1\right], \\ T_\Theta &= -\Pi + G\left[\left(\frac{R}{\bar{r}}\right)^2 - 1\right]. \end{aligned} \tag{A.6}$$

The mechanical equilibrium equation in the reference state is expressed by

$$\frac{\partial T_R}{\partial R} + \frac{2}{R}(T_R - T_\Theta) = 0. \tag{A.7}$$

The boundary conditions of Eq. A.7 are traction-free surfaces of the hollow shell ($T_{R_2} =$

$T_{R_1} = 0$). Therefore, the equilibrium condition reduces to

$$\int_{R_1}^{R_2} G^S \left[\frac{1}{(f^S)^2} \left(\frac{\bar{r}_1^3 + f^S(\hat{R}^3 - R_1^3)}{\hat{R}^3} \right)^2 - 1 \right] \left(\frac{\hat{R}^3}{\bar{r}_1^3 + f^S(\hat{R}^3 - R_1^3)} \right)^{\frac{2}{3}} \frac{d\hat{R}}{\hat{R}} = 0. \tag{A.8}$$

To find the solution of this integral (Eq. A.8), variable u is used to substitute $\hat{R}^3 - R_1^3$. The upper bound of this integral is determined by substituting R_2^3 in Eq. A.4, as follows

$$\bar{r}_2^3 - \bar{r}_1^3 = f^S(R_2^3 - R_1^3), \tag{A.9}$$

where f^S is the coefficient of volume expansion of the shell. Then, Eq. A.8 is described in terms of variable u:

$$\int_0^{(\bar{r}_2^3 - \bar{r}_1^3)/f^S} G^S \left[\frac{1}{(f^S)^2} \left(\frac{\bar{r}_1^3 + f^S u}{u + R_1^3} \right)^2 - 1 \right] \frac{(u + R_1^3)^{\frac{1}{3}}}{(u + R_1^3)^{\frac{1}{3}} (\bar{r}_1^3 + f^S u)^{\frac{2}{3}}} du = 0. \tag{A.10}$$

Then, the variable v is used to substitute u/R_1^3. Substituting variable v in Eq. A.10 implies that

$$\int_0^{(\gamma_2 - \gamma_1)/f^S} G^S \left[\left(\frac{\gamma_1 + f^S v}{f^S(1+v)} \right)^2 - 1 \right] \frac{\big(R_1(1+v)\big)^{\frac{1}{3}}}{(1+v)^{\frac{1}{3}} (\gamma_1 + (1+Q_0)v)^{\frac{2}{3}}} dv = 0, \tag{A.11}$$

where $\gamma_1 = \left(\frac{\bar{r}_1}{R_1}\right)^3$ and $\gamma_2 = \left(\frac{\bar{r}_2}{R_1}\right)^3$. Eq. A.11 is satisfied for an arbitrary G^S parameter

of function, provided that

$$\gamma_1 = f^S. \tag{A.12}$$

Using Eq. A.9 and Eq. A.12, the relation for the inner and the outer radius of the shell in the dry state is derived as given in Eq. 2.35. Similar method is used to derive the radius of core in the dry state shown in Eq. 2.36.

Appendix B

Derivative of free energy density of a polyelectrolyte hydrogel

Substituting Eqs. 4.27, 4.30, 4.31, 4.32 into Eq. 4.26 results in,

$$\begin{aligned}\Psi = {} & \mu^0 C + \mu^0_{H^+} C_{H^+} + \mu^0_{OH^-} C_{OH^-} + \mu^0_{Cl^-} C_{Cl^-} + k_B T \left[C(\ln \frac{Q}{1+Q} + \frac{\chi}{1+Q}) \right. \\ & \left. + C_{H^+} \ln\left(\frac{C_{H^+}}{C} - 1\right) + C_{OH^-} \ln\left(\frac{C_{OH^-}}{C} - 1\right) + C_{Cl^-} \ln\left(\frac{C_{Cl^-}}{C} - 1\right) \right] + \\ & k_B T C_b \big(\alpha \ln \alpha + (1-\alpha)\ln(1-\alpha)\big) + W_{eq} + W_{el}.\end{aligned} \tag{B.1}$$

Now, the derivatives of W_{eq} is given by

$$\dot{W}_{eq} = \frac{\partial W_{eq}}{\partial J_{e1}} \dot{J}_{e1} + \frac{\partial W_{eq}}{\partial J_{e2}} \dot{J}_{e2} + \frac{\partial W_{eq}}{\partial J_{e3}} \dot{J}_{e3}. \tag{B.2}$$

Differential equations for principal invariants of the Cauchy-Green tensors (J_{e1}, J_{e2} , J_{e3}) are obtained:

$$\dot{J}_{e1} = 2\mathbf{B}_e : \mathbf{D}_e, \quad \dot{J}_{e2} = 2(J_{e2}\mathbf{I} - J_{e3}\mathbf{B}_e^{-1}) : \mathbf{D}_e, \quad \dot{J}_{e3} = 2J_{e3}\mathbf{I} : \mathbf{D}_e, \tag{B.3}$$

where

$$\mathbf{D}_e = \mathbf{D} - \frac{\dot{f}}{3f}\mathbf{I}. \tag{B.4}$$

Substituting Eq. B.4 in B.3 implies that

$$\begin{aligned}
\dot{J}_{e1} &= 2\mathbf{B}_e : \mathbf{D} - \frac{2\dot{f}}{3f}J_{e1}, \\
\dot{J}_{e2} &= -2\mathbf{B}_e^{-1} : \mathbf{D}J_{e3} + 2\left(\mathbf{I} : \mathbf{D} - \frac{2\dot{f}}{3f}\right)J_{e2}, \\
\dot{J}_{e3} &= 2\left(\mathbf{I} : \mathbf{D} - \frac{\dot{f}}{f}J_{e3}\right).
\end{aligned} \tag{B.5}$$

As a reminder, the following relations are listed,

$$\begin{aligned}
&\mathbf{B}_e = \mathbf{F}_e \cdot \mathbf{F}_e^{\mathrm{T}}, \quad \mathbf{C}_e = \mathbf{F}_e^{\mathrm{T}} \cdot \mathbf{F}_e, \\
&\mathbf{L} = \dot{\mathbf{F}} \cdot \mathbf{F}^{-1}, \quad \mathbf{L}_e = \dot{\mathbf{F}}_e \cdot \mathbf{F}_e^{-1}, \\
&\mathbf{D} = \frac{1}{2}(\mathbf{L} + \mathbf{L}^T), \quad \mathbf{D}_e = \frac{1}{2}(\mathbf{L}_e + \mathbf{L}_e^T).
\end{aligned} \tag{B.6}$$

Insertion of Eq. B.5 into Eq. B.2 yields

$$\dot{W}_{eq} = 2\mathbf{K}_{mech} : \mathbf{D}, \tag{B.7}$$

where

$$\mathbf{K}_{\text{mech}} = \frac{\partial W_{\text{eq}}}{\partial J_{\text{e1}}}\mathbf{B}_{\text{e}} - J_{\text{e3}}\frac{\partial W_{\text{eq}}}{\partial J_{\text{e2}}}\mathbf{B}_{\text{e}}^{-1} + \left(J_{\text{e2}}\frac{\partial W_{\text{eq}}}{\partial J_{\text{e2}}} + J_{\text{e3}}\frac{\partial W_{\text{eq}}}{\partial J_{\text{e3}}}\right)\mathbf{I}. \tag{B.8}$$

Differentiation of Eq. 4.23 is given by

$$\dot{W}_{\text{el}} = \mathbf{E}\cdot\dot{\mathbf{H}} + \frac{1}{2\varepsilon J}\left(\mathbf{H}\cdot\dot{\mathbf{C}}\cdot\mathbf{H} - \frac{\dot{J}}{J}\mathbf{H}\cdot\mathbf{C}\cdot\mathbf{H}\right), \tag{B.9}$$

where (from Eq. 4.20_3)

$$\mathbf{H} = \varepsilon J\mathbf{C}^{-1}\cdot\mathbf{E}. \tag{B.10}$$

Also, the derivative of the right Cauchy-Green deformation tensor reads

$$\dot{\mathbf{C}} = 2\mathbf{F}^{\text{T}}\cdot\mathbf{D}\cdot\mathbf{F}. \tag{B.11}$$

Then, the second term in Eq. B.9 is provided by

$$\frac{1}{2\varepsilon J}\mathbf{H}\cdot\dot{\mathbf{C}}\cdot\mathbf{H} = \frac{1}{\varepsilon J}\mathbf{H}\cdot\mathbf{F}^{\text{T}}\cdot\mathbf{D}\cdot\mathbf{F}\cdot\mathbf{H} = \frac{J}{\varepsilon}\mathbf{h}\cdot\mathbf{D}\cdot\mathbf{h} = \frac{J}{\varepsilon}(\mathbf{h}\otimes\mathbf{h}) : \mathbf{D}. \tag{B.12}$$

knowing that

$$\dot{J} = J\mathbf{I} : \mathbf{D}. \tag{B.13}$$

The third term in Eq. B.9 is expressed by

$$\frac{\dot{J}}{2\varepsilon J^2}\mathbf{H}\cdot\mathbf{C}\cdot\mathbf{H} = \frac{1}{2\varepsilon J}\mathbf{H}\cdot\mathbf{F}^{\text{T}}\cdot\mathbf{F}\cdot\mathbf{H}(\mathbf{I} : \mathbf{D}) = \frac{J}{2\varepsilon}(\mathbf{h}\cdot\mathbf{h})\mathbf{I} : \mathbf{D}. \tag{B.14}$$

Insertion of Eqs. B.12 and B.14 into Eq. B.9 yields

$$\dot{W}_{\mathrm{el}} = \mathbf{E}\cdot\dot{\mathbf{H}} + 2\mathbf{K}_{\mathrm{el}} : \mathbf{D}, \tag{B.15}$$

where

$$\mathbf{K}_{\mathrm{el}} = \frac{J}{2\varepsilon}\left((\mathbf{h}\otimes\mathbf{h}) - \frac{1}{2}(\mathbf{h}\cdot\mathbf{h})\mathbf{I}\right). \tag{B.16}$$

Finally, the derivative of the free energy density Eq. B.1 together with Eqs. B.7 and B.15 is determined by

$$\begin{aligned}
&\Theta_C = \mu^0 + k_B T\left(\ln\frac{Q}{1+Q} + \frac{1}{1+Q} + \frac{\chi}{(1+Q)^2} - \frac{C_{\mathrm{H^+}} + C_{\mathrm{OH^-}} + C_{\mathrm{Cl^-}}}{C}\right),\\
&\Theta_{\mathrm{H^+}} = \mu^0_{\mathrm{H^+}} + k_B T\ln\frac{C_{\mathrm{H^+}}}{C}, \qquad \Theta_{\mathrm{OH^-}} = \mu^0_{\mathrm{OH^-}} + k_B T\ln\frac{C_{\mathrm{OH^-}}}{C},\\
&\Theta_{\mathrm{Cl^-}} = \mu^0_{\mathrm{Cl^-}} + k_B T\ln\frac{C_{\mathrm{Cl^-}}}{C}, \qquad \Theta_\alpha = k_B T\ln\frac{\alpha}{1-\alpha}.
\end{aligned} \tag{B.17}$$

Appendix C

Derivative of free energy density of a polyelectrolyte hydrogel in a basic solution

$$
\begin{aligned}
&\Theta_C = \mu^0 + k_B T\left(\ln\frac{Q}{1+Q} + \frac{1}{1+Q} + \frac{\chi}{(1+Q)^2} - \frac{C_{H^+} + C_{Na^+} + C_{OH^-} + C_{Cl^-}}{C}\right),\\
&\Theta_{H^+} = \mu^0_{H^+} + k_B T \ln\frac{C_{H^+}}{C}, \qquad \Theta_{Na^+} = \mu^0_{Na^+} + k_B T \ln\frac{C_{Na^+}}{C},\\
&\Theta_{OH^-} = \mu^0_{OH^-} + k_B T \ln\frac{C_{OH^-}}{C}, \qquad \Theta_{Cl^-} = \mu^0_{Cl^-} + k_B T \ln\frac{C_{Cl^-}}{C},\\
&\Theta_{\beta_H} = k_B T C_b \ln\frac{\beta_H}{1-\beta_H-\beta_{Na}}, \qquad \Theta_{\beta_{Na}} = k_B T C_b \ln\frac{\beta_{Na}}{1-\beta_H-\beta_{Na}}.
\end{aligned}
\tag{C.1}
$$

Bibliography

[1] Todd R Hoare and Daniel S Kohane. Hydrogels in drug delivery: progress and challenges. *Polymer*, 49(8):1993–2007, 2008.

[2] Thilini K. Mudiyanselage and Douglas C. Neckers. Highly absorbing superabsorbent polymer. *J. Polym. Sci. A Polym. Chem.*, 46(4):1357–1364, 2008.

[3] Jian Ping Gong and Wei Hong. Mechanics and physics of hydrogels. *Soft Matter*, 8(31):8006, 2012.

[4] W Kuhn, B Hargitay, A Katchalsky, and H Eisenberg. Reversible dilation and contraction by changing the state of ionization of high-polymer acid networks. 1950.

[5] A Katchalsky. Solutions of polyelectrolytes and mechanochemical systems. *Journal of Polymer Science*, 7(4):393–412, 1951.

[6] Yoshihito Osada. Conversion of chemical into mechanical energy by synthetic polymers (chemomechanical systems). In *Polymer Physics*, pages 1–46. Springer, 1987.

[7] Jindřich Kopeček. Hydrogels: From soft contact lenses and implants to self-assembled nanomaterials. *Journal of Polymer Science Part A: Polymer Chemistry*, 47(22):5929–5946, 2009.

[8] Toyoichi Tanaka. Collapse of gels and the critical endpoint. *Physical Review Letters*, 40(12):820, 1978.

[9] Yong Qiu and Kinam Park. Environment-sensitive hydrogels for drug delivery. *Adv. Drug Deliv. Rev.*, 53(3):321 – 339, 2001.

[10] Jeanie L Drury and David J Mooney. Hydrogels for tissue engineering: scaffold design variables and applications. *Biomaterials*, 24(24):4337–4351, 2003.

[11] Todd Hoare and Robert Pelton. Impact of microgel morphology on functionalized microgel-drug interactions. *Langmuir*, 24(3):1005–1012, 2008.

[12] Xinqiao Jia and Kristi L. Kiick. Hybrid multicomponent hydrogels for tissue engineering. *Macromol. Biosci.*, 9(2):140–156, 2009.

[13] Kosmas Deligkaris, Tadele Shiferaw Tadele, Wouter Olthuis, and Albert van den Berg. Hydrogel-based devices for biomedical applications. *Sensor Actuat. B-Chem.*, 147(2):765–774, 2010.

[14] O Okay. *Hydrogel Sensors and Actuators*, volume 6 of *Springer Series on Chemical Sensors and Biosensors*. Springer, Berlin, Heidelberg, 2010.

[15] Renate Messing and Annette M. Schmidt. Perspectives for the mechanical manipulation of hybrid hydrogels. *Polym. Chem.*, 2:18–32, 2011.

[16] O Okay and W Oppermann. Polyacrylamide-clay nanocomposite hydrogels: rheological and light scattering characterization. *Macromolecules*, 40(9):3378–3387, 2007.

[17] K Haraguchi and Y Xu. Thermal analyses of poly (n-isopropylacrylamide) in aqueous solutions and in nanocomposite gels. *Colloid and Polymer Science*, 290(16):1627–1636, 2012.

[18] Ch W Peak, J J Wilker, and G Schmidt. A review on tough and sticky hydrogels. *Colloid and Polymer Science*, 291(9):2031–2047, 2013.

[19] Ruixue Liu, Amir H Milani, Tony J Freemont, and Brian R Saunders. Doubly crosslinked ph-responsive microgels prepared by particle inter-penetration: swelling and mechanical properties. *Soft Matter*, 7(10):4696–4704, 2011.

[20] J Meid, S Lehmann, and W Richtering. Temperature-sensitive composite hydrogels: Coupling between gel matrix and embedded nano-and microgels. In *Intelligent Hydrogels*, pages 91–100. Springer, 2013.

[21] Yoshihito Osada and Kanji Kajiwara. *Gels Handbook, Four-Volume Set*, volume 1. Academic Press, 2000.

[22] Walter Richtering and Brian R Saunders. Gel architectures and their complexity. *Soft matter*, 10(21):3695–702, 2014.

[23] I. Y. Galaev and B. Mattiasson. 'smart' polymers and what they could do in biotechnology and medicine. *Trends in Biotechnology*, 17(8):335–340, 1999. cited By 0.

[24] C. De Las Heras Alarcon, S. Pennadam, and C. Alexander. Stimuli responsive polymers for biomedical applications. *Chemical Society Reviews*, 34(3):276–285, 2005. cited By 751.

[25] Dirk Schmaljohann. Thermo- and ph-responsive polymers in drug delivery. *Advanced Drug Delivery Reviews*, 58(15):1655 – 1670, 2006. 2006 Supplementary Non-Thematic Collection.

[26] David J Beebe, Jeffrey S Moore, Joseph M Bauer, Qing Yu, Robin H Liu, Chelladurai Devadoss, and Byung-Ho Jo. Functional hydrogel structures for autonomous flow control inside microfluidic channels. *Nature*, 404(6778):588–590, 2000.

[27] Gorka Orive, Rosa Maria Hernandez, Alicia Rodriguez Gascon, Alfonso Dominguez-Gil, and Jose Luis Pedraz. Drug delivery in biotechnology: present and future. *Current opinion in biotechnology*, 14(6):659–664, 2003.

[28] Andreas Richter, Georgi Paschew, Stephan Klatt, Jens Lienig, Karl-Friedrich Arndt, and HansJürgen P Adler. Review on hydrogel-based ph sensors and microsensors. *Sensors*, 8(1):561–581, 2008.

[29] David R Nisbet, Kylie E Crompton, Malcolm K Horne, David I Finkelstein, and John S Forsythe. Neural tissue engineering of the cns using hydrogels. *Journal of Biomedical Materials Research Part B: Applied Biomaterials*, 87(1):251–263, 2008.

[30] Carmen AlvarezLorenzo and Angel Concheiro. Smart drug delivery systems: from fundamentals to the clinic. *Chemical Communications*, 50(58):7743–7765, 2014.

[31] Yoshitsugu Hirokawa and Toyoichi Tanaka. Volume phase transition in a nonionic gel. *The Journal of chemical physics*, 81(12):6379–6380, 1984.

[32] T Okano, YH Bae, H Jacobs, and SW Kim. Thermally on-off switching polymers for drug permeation and release. *Journal of Controlled Release*, 11(1):255–265, 1990.

[33] Katsuto Otake, Hiroshi Inomata, Mikio Konno, and Shozaburo Saito. Thermal analysis of the volume phase transition with n-isopropylacrylamide gels. *Macromolecules*, 23(1):283–289, 1990.

[34] Seiji Katayama, Yoshitsugu Hirokawa, and Toyoichi Tanaka. Reentrant phase transition in acrylamide-derivative copolymer gels. *Macromolecules*, 17(12):2641–2643, 1984.

[35] Hua Yu and David W Grainger. Thermo-sensitive swelling behavior in crosslinked n-isopropylacrylamide networks: Cationic, anionic, and ampholytic hydrogels. *Journal of applied polymer science*, 49(9):1553–1563, 1993.

[36] Atul R Khare and Nikolaos A Peppas. Swelling/deswelling of anionic copolymer gels. *Biomaterials*, 16(7):559–567, 1995.

[37] Clinton D Jones and L Andrew Lyon. Synthesis and characterization of multiresponsive core-shell microgels. *Macromolecules*, 33(22):8301–8306, 2000.

[38] Karl Kratz, Thomas Hellweg, and Wolfgang Eimer. Influence of charge density on the swelling of colloidal poly (n-isopropylacrylamide-co-acrylic acid) microgels. *Colloids and Surfaces A: Physicochemical and Engineering Aspects*, 170(2):137–149, 2000.

[39] Alberto Fernandez-Nieves, Hans Wyss, Johan Mattsson, and David A Weitz. *Microgel suspensions: fundamentals and applications*. John Wiley & Sons, 2011.

[40] Milton J Rosen and Joy T Kunjappu. *Surfactants and interfacial phenomena*. John Wiley & Sons, 2012.

[41] Jindřich Kopeček. Smart and genetically engineered biomaterials and drug delivery systems. *European Journal of Pharmaceutical Sciences*, 20(1):1–16, 2003.

[42] Allan S Hoffman. Hydrogels for biomedical applications. *Advanced drug delivery reviews*, 64:18–23, 2012.

[43] A Fernández-Nieves, A Fernández-Barbero, and FJ De las Nieves. Salt effects over the swelling of ionized mesoscopic gels. *The Journal of Chemical Physics*, 115(16):7644–7649, 2001.

[44] Mitsuru Satoh, Takehito Kawashima, Jiro Komiyama, and Toshiro Iijima. A new model of counterion condensation in polyelectrolyte solutions i. comparison with other condensation theories and experimental data on counterion activity coefficients. *Polymer journal*, 19(10):1191–1200, 1987.

[45] M Muthukumar. Theory of counter-ion condensation on flexible polyelectrolytes: adsorption mechanism. *The Journal of chemical physics*, 120(19):9343–9350, 2004.

[46] Gary M Eichenbaum, Patrick F Kiser, Andrey V Dobrynin, Sidney A Simon, and David Needham. Investigation of the swelling response and loading of ionic microgels with drugs and proteins: The dependence on cross-link density. *Macromolecules*, 32(15):4867–4878, 1999.

[47] Elena Yu Kramarenko, Alexei R Khokhlov, and Kenichi Yoshikawa. A three-state model for counterions in a dilute solution of weakly charged polyelectrolytes. *Macromolecular theory and simulations*, 9(5):249–256, 2000.

[48] Wensheng Cai and Ram B Gupta. Thermosensitive and ampholytic hydrogels for salt solution. *Journal of applied polymer science*, 88(8):2032–2037, 2003.

[49] Haibao Lu and Shanyi Du. A phenomenological thermodynamic model for the chemo-responsive shape memory effect in polymers based on flory–huggins solution theory. *Polym. Chem.*, 5(4):1155–1162, 2014.

[50] Anjana Jain, Young-Tae Kim, Robert J McKeon, and Ravi V Bellamkonda. In situ gelling hydrogels for conformal repair of spinal cord defects, and local delivery of bdnf after spinal cord injury. *Biomaterials*, 27(3):497–504, 2006.

[51] Anthony Atala, Robert Lanza, James A Thomson, and Robert Nerem. *Principles of regenerative medicine*. Academic Press, 2010.

[52] Mitsuhiro Ebara. *Smart Biomaterials*. Springer, 2014.

[53] Emily R Aurand, Jennifer Wagner, Craig Lanning, and Kimberly B Bjugstad. Building biocompatible hydrogels for tissue engineering of the brain and spinal cord. *Journal of functional biomaterials*, 3(4):839–863, 2012.

[54] Junmin Zhu and Roger E Marchant. Design properties of hydrogel tissue-engineering scaffolds. *Expert review of medical devices*, 8(5):607–626, 2011.

[55] Yinghui Zhong and Ravi V Bellamkonda. Biomaterials for the central nervous system. *Journal of the Royal Society Interface*, 5(26):957–975, 2008.

[56] Brian Holt, Anubhav Tripathi, and Jeffrey R Morgan. Designing polyhema substrates that mimic the viscoelastic response of soft tissue. *Journal of biomechanics*, 44(8):1491–1498, 2011.

[57] Diana-Maria Dragusin, Sandra Van Vlierberghe, Peter Dubruel, Manuel Dierick, Luc Van Hoorebeke, Heidi A Declercq, Maria M Cornelissen, and Izabela-Cristina Stancu. Novel gelatin–phema porous scaffolds for tissue engineering applications. *Soft Matter*, 8(37):9589–9602, 2012.

[58] Shahaf Armon, Efi Efrati, Raz Kupferman, and Eran Sharon. Geometry and mechanics in the opening of chiral seed pods. *Science*, 333(6050):1726–1730, 2011.

[59] Zi Liang Wu, Michael Moshe, Jesse Greener, Heloise Therien-Aubin, Zhihong Nie, Eran Sharon, and Eugenia Kumacheva. Three-dimensional shape transformations of hydrogel sheets induced by small-scale modulation of internal stresses. *Nature communications*, 4:1586, 2013.

[60] Myunghwan Byun, Christian D Santangelo, and Ryan C Hayward. Swelling-driven rolling and anisotropic expansion of striped gel sheets. *Soft Matter*, 9(34):8264–8273, 2013.

[61] RH Pelton. Polystyrene and polystyrene-butadiene latexes stabilized by poly (n-isopropylacrylamide). *Journal of Polymer Science Part A: Polymer Chemistry*, 26(1):9–18, 1988.

[62] L. C. Dong and A. S. Hoffman. A novel approach for preparation of ph- and temperature-sensitive hydrogels for enteric drug delivery. *J. Contr. Rel.*, 15:141–152, 1991.

[63] Tae Gwan Park and Allan S. Hoffman. Synthesis and characterization of ph- and/or temperature-sensitive hydrogels. *Journal of Applied Polymer Science*, 46(4):659–671, 1992.

[64] H Feil, Y. H. Bae, J Feijen, and S. W. Kim. Mutual influence of ph and temperature on the swelling of ionizable and thermosensitive hydrogels. *Macromolecules*, 25(20):5528–5530, 1992.

[65] Daoji Gan and L Andrew Lyon. Synthesis and protein adsorption resistance of peg-modified poly (n-isopropylacrylamide) core/shell microgels. *Macromolecules*, 35(26):9634–9639, 2002.

[66] Ingo Berndt, Walter Richtering, and D Kiel. Doubly temperature sensitive core - shell microgels. *Macromolecules*, pages 8780–8785, 2003.

[67] Martin J Snowden, Babur Z Chowdhry, Brian Vincent, and Gayle E Morris. Colloidal copolymer microgels of n-isopropylacrylamide and acrylic acid: ph, ionic strength and temperature effects. *J. Chem. Soc., Faraday Trans.*, 92(24):5013–5016, 1996.

[68] Molla R Islam, Andrews Ahiabu, Xue Li, and Michael J Serpe. Poly (n-isopropylacrylamide) microgel-based optical devices for sensing and biosensing. *Sensors*, 14(5):8984–8995, 2014.

[69] Karel Dusek. *Responsive gels: volume transitions I*, volume 1. 1993.

[70] Hideya Kawasaki, Shigeo Sasaki, and Hiroshi Maeda. Effect of ph on the volume phase transition of copolymer gels of n-isopropylacrylamide and sodium acrylate. *The Journal of Physical Chemistry B*, 101(26):5089–5093, 1997.

[71] R. A. Stile, E. Chung, W. R. Burghardt, and K. E. Healy. Poly(n-isopropylacrylamide)-based semi-interpenetrating polymer networks for tissue engineering applications. effects of linear poly(acrylic acid) chains on rheology. *Journal of Biomaterials Science, Polymer Edition*, 15(7):865–878, 2004. cited By 18.

[72] Jianfeng Shen, Na Li, and Mingxin Ye. Preparation and characterization of dual-sensitive double network hydrogels with clay as a physical crosslinker. *Applied Clay Science*, 103(0):40 – 45, 2015.

[73] Christine Hiemstra, Leonardus J van der Aa, Zhiyuan Zhong, Pieter J Dijkstra, and Jan Feijen. Rapidly in situ-forming degradable hydrogels from dextran thiols through michael addition. *Biomacromolecules*, 8(5):1548–1556, 2007.

[74] Chun Wang, Russell J Stewart, and JindŘich KopeČek. Hybrid hydrogels assembled from synthetic polymers and coiled-coil protein domains. *Nature*, 397(6718):417–420, 1999.

[75] Stephanie J Bryant, Kelly A Davis-Arehart, Ning Luo, Richard K Shoemaker, Jeffrey A Arthur, and Kristi S Anseth. Synthesis and characterization of photopolymerized multifunctional hydrogels: water-soluble poly (vinyl alcohol) and

chondroitin sulfate macromers for chondrocyte encapsulation. *Macromolecules*, 37(18):6726–6733, 2004.

[76] Jianyu Li, Widusha RK Illeperuma, Zhigang Suo, and Joost J Vlassak. Hybrid hydrogels with extremely high stiffness and toughness. *Acs Macro Letters*, 3(6):520–523, 2014.

[77] Jeong-Yun Sun, Xuanhe Zhao, Widusha RK Illeperuma, Ovijit Chaudhuri, Kyu Hwan Oh, David J Mooney, Joost J Vlassak, and Zhigang Suo. Highly stretchable and tough hydrogels. *Nature*, 489(7414):133–136, 2012.

[78] Michele V Chin-Purcell and Jack L Lewis. Fracture of articular cartilage. *Journal of biomechanical engineering*, 118(4):545–556, 1996.

[79] Brian H Thomas, J Craig Fryman, Kaifeng Liu, and Jim Mason. Hydrophilic–hydrophobic hydrogels for cartilage replacement. *Journal of the mechanical behavior of biomedical materials*, 2(6):588–595, 2009.

[80] Haesun Park and Kinam Park. Hydrogels in bioapplications. In *ACS Symposium Series*, volume 627, pages 2–10. ACS Publications, 1996.

[81] Karl Kratz, Thomas Hellweg, and Wolfgang Eimer. Structural changes in pnipam microgel particles as seen by sans, dls, and em techniques. *Polymer*, 42(15):6631–6639, 2001.

[82] S Cardea, L Baldino, I De Marco, P Pisanti, and E Reverchon. Supercritical gel drying of polymeric hydrogels for tissue engineering applications. *Chem Eng Trans*, 32:1123–8, 2013.

[83] N Pernodet, M Maaloum, and B Tinland. Pore size of agarose gels by atomic force microscopy. *Electrophoresis*, 18(1):55, 1997.

[84] Alan W Decho. Imaging an alginate polymer gel matrix using atomic force microscopy. *Carbohydrate Research*, 315(3):330–333, 1999.

[85] Emilios K Dimitriadis, Ferenc Horkay, Julia Maresca, Bechara Kachar, and Richard S Chadwick. Determination of elastic moduli of thin layers of soft material using the atomic force microscope. *Biophysical journal*, 82(5):2798–2810, 2002.

[86] M Radmacher, RW Tillmann, and HE Gaub. Imaging viscoelasticity by force modulation with the atomic force microscope. *Biophysical journal*, 64(3):735, 1993.

[87] Joseph L Lenhart and Phillip J Cole. Adhesion properties of lightly crosslinked solvent-swollen polymer gels. *The Journal of Adhesion*, 82(10):945–971, 2006.

[88] Daniel TN Chen, Qi Wen, Paul A Janmey, John C Crocker, and Arjun G Yodh. Rheology of soft materials. *Condensed Matter Physics*, 1, 2010.

[89] Manuel Quesada-Peréz, José Alberto Maroto-Centeno, Jacqueline Forcada, and Roque Hidalgo-Alvarez. Gel swelling theories: the classical formalism and recent approaches. *Soft Matter*, 7(22):10536, 2011.

[90] Fariba Ganji, Samira Vasheghani-Farahani, Ebrahim Vasheghani-Farahani, et al. Theoretical description of hydrogel swelling: a review. *Iran Polym J*, 19(5):375–398, 2010.

[91] Mary C Boyce and Ellen M Arruda. Swelling and mechanical stretching of elastomeric materials. *Mathematics and Mechanics of Solids*, 6(6):641–659, 2001.

[92] Toyoichi Tanaka, Lon O Hocker, and George B Benedek. Spectrum of light scattered from a viscoelastic gel. *The Journal of Chemical Physics*, 59(9):5151–5159, 1973.

[93] Chung-Yuen Hui and Vijayanand Muralidharan. Gel mechanics: A comparison of the theories of biot and tanaka, hocker, and benedek. *The Journal of chemical physics*, 123(15):154905, 2005.

[94] Alexei R Khokhlov, Sergei G Starodubtzev, and Valentina V Vasilevskaya. Conformational transitions in polymer gels: theory and experiment. In *Responsive gels: volume transitions I*, pages 123–171. Springer, 1993.

[95] Josiah Willard Gibbs. On the equilibrium of heterogeneous substances. *American Journal of Science*, (96):441–458, 1878.

[96] Maurice A Biot. General theory of three-dimensional consolidation. *Journal of applied physics*, 12(2):155–164, 1941.

[97] Paul J Flory and Jr John Rehner. Statistical mechanics of cross-linked polymer networks ii. swelling. *J. Chem. Phys.*, 11(11):521–526, 1943.

[98] Paul J Flory and Jr John Rehner. Statistical mechanics of cross-linked polymer networks i. rubberlike elasticity. *J. Chem. Phys.*, 11(11):512–520, 1943.

[99] C. J. Durning and K. N. Morman Jr. Nonlinear swelling of polymer gels. *The Journal of chemical physics*, 98(5):4275–4293, 1993.

[100] S Baek and A. R. Srinivasa. Diffusion of a fluid through an elastic solid undergoing large deformation. *International Journal of non-linear Mechanics*, 39(2):201–218, 2004.

[101] John Dolbow, Eliot Fried, and Huidi Ji. Chemically induced swelling of hydrogels. *J. Mech. Phys. Solids*, 52(1):51–84, 2004.

[102] Wei Hong, Xuanhe Zhao, Jinxiong Zhou, and Zhigang Suo. A theory of coupled diffusion and large deformation in polymeric gels. *J. Mech. Phys. Solids*, 56(5):1779–1793, 2008.

[103] Masao Doi. Gel dynamics. *J. Phys. Soc. Jpn.*, 78(5), 2009.

[104] Thomas Wallmersperger, Bernd Kröplin, and Rainer W Gülch. Coupled chemo-electro-mechanical formulation for ionic polymer gels—-numerical and experimental investigations. *Mechanics of Materials*, 36(5):411–420, 2004.

[105] A Shawn Chester and Lallit Anand. A coupled theory of fluid permeation and large deformations for elastomeric materials. *J. Mech. Phys. Solids*, 58(11):1879–1906, 2010.

[106] P Fernando Duda, Angela C Souza, and Eliot Fried. A theory for species migration in a finitely strained solid with application to polymer network swelling. *J. Mech. Phys. Solids*, 58(4):515–529, 2010.

[107] A Lucantonio, P Nardinocchi, and L Teresi. Transient analysis of swelling-induced large deformations in polymer gels. *J. Mech. Phys. Solids*, 61(1):205–218, 2013.

[108] AD Drozdov. Stress–strain relations for hydrogels under multiaxial deformation. *Int. J. Solids Struct.*, 50(22):3570–3585, 2013.

[109] Erik Birgersson, Hua Li, and Shunnian Wu. Transient analysis of temperature-sensitive neutral hydrogels. *J. Mech. Phys. Solids*, 56(2):444–466, 2008.

[110] A Shawn Chester and Lallit Anand. A thermo-mechanically coupled theory for fluid permeation in elastomeric materials: application to thermally responsive gels. *J. Mech. Phys. Solids*, 59(10):1978–2006, 2011.

[111] A. D. Drozdov. Swelling of thermo-responsive hydrogels. *Eur. Phys. J. E Soft Matter*, 37(10):1–13, 2014.

[112] A. D. Drozdov. Volume phase transition in thermo-responsive hydrogels: constitutive modeling and structure–property relations. *Acta. Mech.*, 2014.

[113] Emilio NM Cirillo, Nicoletta Ianiro, Paola Nardinocchi, and Giulio Sciarra. Phase coexistence in temperature-driven volume transition in hydrogels and interface localization. *arXiv:1502.03389*, 2015.

[114] Fatema Afroze, Eric Nies, and Hugo Berghmans. Phase transitions in the system poly (n-isopropylacrylamide)/water and swelling behaviour of the corresponding networks. *J. Mol. Struct.*, 554(1):55–68, 2000.

[115] S Baek and A. R. Srinivasa. Modeling of the ph-sensitive behavior of an ionic gel in the presence of diffusion. *International Journal of Non-linear Mechanics*, 39(8):1301–1318, 2004.

[116] Hua Li, Rongmo Luo, Erik Birgersson, and KY Lam. Modeling of multiphase smart hydrogels responding to ph and electric voltage coupled stimuli. *Journal of Applied Physics*, 101(11):114905–114905, 2007.

[117] Ligang Feng, Yuxi Jia, Xiliang Chen, Xue Li, and Lijia An. A multiphasic model for the volume change of polyelectrolyte hydrogels. *The Journal of chemical physics*, 133(11):114904, 2010.

[118] Romain Marcombe, Shengqiang Cai, Wei Hong, Xuanhe Zhao, Yuri Lapusta, and Zhigang Suo. A theory of constrained swelling of a ph-sensitive hydrogel. *Soft Matter*, 6(4):784–793, 2010.

[119] Wei Hong, Xuanhe Zhao, and Zhigang Suo. Large deformation and electrochemistry of polyelectrolyte gels. *Journal of the Mechanics and Physics of Solids*, 58(4):558–577, 2010.

[120] Jundika C Kurnia, Erik Birgersson, and Arun S Mujumdar. Analysis of a model for ph-sensitive hydrogels. *Polymer*, 53(2):613–622, 2012.

[121] Huixian Yan and Bo Jin. Equilibrium swelling of a polyampholytic ph-sensitive hydrogel. *The European Physical Journal E*, 36(3):1–7, 2013.

[122] Jianyu Li, Zhigang Suo, and Joost J Vlassak. A model of ideal elastomeric gels for polyelectrolyte gels. *Soft matter*, 10(15):2582–2590, 2014.

[123] Seon Jeong Kim, Geoffrey M Spinks, Shona Prosser, Philip G Whitten, Gordon G Wallace, and Sun I Kim. Surprising shrinkage of expanding gels under an external load. *Nature materials*, 5(1):48–51, 2006.

[124] Sébastien Ladet, Laurent David, and Alain Domard. Multi-membrane hydrogels. *Nature*, 452(7183):76–79, 2008.

[125] Wei Hong, Zishun Liu, and Zhigang Suo. Inhomogeneous swelling of a gel in equilibrium with a solvent and mechanical load. *Int. J. Solids Struct.*, 46(17):3282–3289, 2009.

[126] Jiaping Zhang, Xuanhe Zhao, Zhigang Suo, and Hanqing Jiang. A finite element method for transient analysis of concurrent large deformation and mass transport in gels. *J. Appl. Phys.*, 105(9):093522, 2009.

[127] Shengqiang Cai and Zhigang Suo. Mechanics and chemical thermodynamics of phase transition in temperature-sensitive hydrogels. *J. Mech. Phys. Solids*, 59(11):2259–2278, 2011.

[128] Jonas Gernandt, Göran Frenning, Walter Richtering, and Per Hansson. A model describing the internal structure of core/shell hydrogels. *Soft Matter*, 7(21):10327, 2011.

[129] Andreea Balaceanu, Yaroslav Verkh, Dan E. Demco, Martin Moller, and Andrij Pich. Correlated morphological changes in the volume temperature transition of core-shell microgels. *Macromolecules*, 46(12):4882–4891, 2013.

[130] Dong Wang and MS Wu. Analytical solutions for bilayered spherical hydrogel subjected to constant dilatation. *Mech. Mat.*, 58:12–22, 2013.

[131] A D Drozdov. Equilibrium swelling of core-shell composite microgels. *Meccanica*, pages 1–21, 2015.

[132] Hashem Mazaheri, Mostafa Baghani, and Reza Naghdabadi. Inhomogeneous and homogeneous swelling behavior of temperature-sensitive poly-(n-isopropylacrylamide) hydrogels. *J. Intell. Mater. Syst. Struct.*, 2015.

[133] Paulo A. L. Fernandes, Stephan Schmidt, Michael Zeiser, Andreas Fery, and Thomas Hellweg. Swelling and mechanical properties of polymer gels with cross-linking gradient. *Soft Matter*, 6:3455–3458, 2010.

[134] Walter Richtering and Andrij Pich. The special behaviours of responsive core-shell nanogels. *Soft Matter*, 8(45):11423, 2012.

[135] Xuanhe Zhao, Wei Hong, and Zhigang Suo. Inhomogeneous and anisotropic equilibrium state of a swollen hydrogel containing a hard core. *Appl. Phys. Lett.*, 92(5):1904, 2008.

[136] M.S. Wu and H.O.K. Kirchner. Second-order elastic solutions for spherical gels subjected to spherically symmetric dilatation. *Mech. Mater.*, 43(11):721 – 729, 2011.

[137] Hui-Hui Dai and Zilong Song. Some analytical formulas for the equilibrium states of a swollen hydrogel shell. *Soft Matter*, 7(18):8473–8483, 2011.

[138] Bo Li, Guang-Kui Xu, and Xi-Qiao Feng. Tissue–growth model for the swelling analysis of core–shell hydrogels. *Soft Materials*, 11(2):117–124, 2013.

[139] Cheng Lian, Dongyan Zhi, Shouhong Xu, Honglai Liu, and Ying Hu. A lattice model for thermally-sensitive core–shell hydrogels. *J. Colloid Interface Sci.*, 406:148–153, 2013.

[140] P Maarten Biesheuvel, Tatjana Mauser, Gleb B Sukhorukov, and Helmuth Möhwald. Micromechanical theory for ph-dependent polyelectrolyte multilayer capsule swelling. *Macromolecules*, 39(24):8480–8486, 2006.

[141] Kaspar Loeffel and Lallit Anand. A chemo-thermo-mechanically coupled theory for elastic–viscoplastic deformation, diffusion, and volumetric swelling due to a chemical reaction. *Int. J. Plasticity*, 27(9):1409–1431, 2011.

[142] A. D. Drozdov and J deClaville Christiansen. Swelling of ph-sensitive hydrogels. *Physical Review E*, 91(2):022305, 2015.

[143] Paul J Flory. *Principles of polymer chemistry*. Cornell University Press, 1953.

[144] COMSOL. Multiphysics 5.0. 2014. http://www.comsol.com.

[145] Takaharu Okajima, Ichiro Harada, Kazufumi Nishio, and Shunsuke Hirotsu. Kinetics of volume phase transition in poly (n-isopropylacrylamide) gels. *J. Chem. Phys*, 116(20):9068–9077, 2002.

[146] Min Kyoo Kang and Rui Huang. A variational approach and finite element implementation for swelling of polymeric hydrogels under geometric constraints. *J. Appl. Mech.*, 77(6):061004, 2010.

[147] S Baek and T. J. Pence. Inhomogeneous deformation of elastomer gels in equilibrium under saturated and unsaturated conditions. *J. Mech. Phys. Solids*, 59(3):561–582, 2011.

[148] Ingo Berndt, Jan Skov Pedersen, and Walter Richtering. Temperature-sensitive core-shell microgel particles with dense shell. *Angew. Chem. Int. Ed. (English)*, 45(11):1737–41, 2006.

[149] Ingo Berndt, Jan Skov Pedersen, Peter Lindner, and Walter Richtering. Influence of shell thickness and cross-link density on the structure of temperature-sensitive poly- n -isopropylacrylamide - poly- n -isopropylmethacrylamide core - shell microgels investigated by small-angle neutron scattering. *Langmuir*, (22):459–468, 2006.

[150] Maurice L Huggins. Solutions of long chain compounds. *J. Chem. Phys*, 9(5):440–440, 1941.

[151] Paul J Flory. Thermodynamics of high polymer solutions. *J. Chem. Phys*, 10(1):51–61, 1942.

[152] Shunsuke Hirotsu. Softening of bulk modulus and negative poissons ratio near the volume phase transition of polymer gels. *J. Chem. Phys*, 94(5):3949–3957, 1991.

[153] Hideaki Shirota, Noriko Endo, and Kazuyuki Horie. Volume phase transition of polymer gel in water and heavy water. *Chem. Phys.*, 238(3):487–494, 1998.

[154] Ken Sekimoto and Kyozi Kawasaki. Elastic instabilities and phase coexistence of gels. *Physica A*, 154(3):384–420, 1989.

[155] Leslie Ronald George Treloar. *The physics of rubber elasticity*. Oxford University Press, 1975.

[156] Etsuo Kokufuta. Polyelectrolyte gel transitions: experimental aspects of charge inhomogeneity in the swelling and segmental attractions in the shrinking. *Langmuir*, 21(22):10004–10015, 2005.

[157] A. D. Drozdov. Swelling of ph-responsive cationic gels: Constitutive modeling and structure–property relations. *International Journal of Solids and Structures*, 6465(0):176 – 190, 2015.

[158] Paola Nardinocchi, Matteo Pezzulla, and Luca Placidi. Thermodynamically based multiphysic modeling of ionic polymer metal composites. *Journal of Intelligent Material Systems and Structures*, page 1045389X11417195, 2011.

[159] WN Charman, DP Christy, EP Geunin, and DC Monkhouse. Interaction between calcium, a model divalent cation, and a range of poly (acrylic acid) resins as a function of solution ph. *Drug development and industrial pharmacy*, 17(2):271–280, 1991.

[160] Todd Hoare and Robert Pelton. Highly ph and temperature responsive microgels functionalized with vinylacetic acid. *Macromolecules*, 37(7):2544–2550, 2004.

[161] Robert Lanza, Robert Langer, and Joseph P Vacanti. *Principles of tissue engineering*. Academic press, 2011.

[162] Brandon V Slaughter, Shahana S Khurshid, Omar Z Fisher, Ali Khademhosseini, and Nicholas A Peppas. Hydrogels in regenerative medicine. *Adv Mater*, 21(32-33):3307–3329, 2009.

[163] Wyatt Potter, Ronald E Kalil, and Weiyuan J Kao. Biomimetic material systems for neural progenitor cell-based therapy. *Front Biosci*, 13(806):21, 2008.

[164] Šárka Kubinová and Eva Syková. Nanotechnology for treatment of stroke and spinal cord injury. *Nanomedicine*, 5(1):99–108, 2010.

[165] Giuseppe Perale, Filippo Rossi, Erik Sundstrom, Sara Bacchiega, Maurizio Masi, Gianluigi Forloni, and Pietro Veglianese. Hydrogels in spinal cord injury repair strategies. *ACS chemical neuroscience*, 2(7):336–345, 2011.

[166] Syed KH Gulrez. *Hydrogels: methods of preparation, characterisation and applications*.

[167] Jun-Ying Xiong, Janaky Narayanan, Xiang-Yang Liu, Tan Kok Chong, Shing Bor Chen, and Tai-Shung Chung. Topology evolution and gelation mechanism of agarose gel. *The Journal of Physical Chemistry B*, 109(12):5638–5643, 2005.

[168] Valéry Normand, Didier L Lootens, Eleonora Amici, Kevin P Plucknett, and Pierre Aymard. New insight into agarose gel mechanical properties. *Biomacromolecules*, 1(4):730–738, 2000.

[169] Joseph Sambrook et al. *Molecular cloning*, volume 2.

[170] Janaky Narayanan, Jun-Ying Xiong, and Xiang-Yang Liu. Determination of agarose gel pore size: Absorbance measurements vis a vis other techniques. In *Journal of Physics: Conference Series*, volume 28, page 83. IOP Publishing, 2006.

[171] Philip Serwer. Agarose gels: properties and use for electrophoresis. *Electrophoresis*, 4(6):375–382, 1983.

[172] Erin M Johnson, David A Berk, Rakesh K Jain, and William M Deen. Hindered diffusion in agarose gels: test of effective medium model. *Biophysical journal*, 70(2):1017–1023, 1996.

[173] Geraint P Roberts and Howard A Barnes. New measurements of the flow-curves for carbopol dispersions without slip artefacts. *Rheologica Acta*, 40(5):499–503, 2001.

[174] Felix K. Oppong, Laurent Rubatat, Barbara J. Frisken, Arthur E. Bailey, and John R. de Bruyn. Microrheology and structure of a yield-stress polymer gel. *Phys. Rev. E*, 73:041405, 2006.

[175] JO Carnali and MS Naser. The use of dilute solution viscometry to characterize the network properties of carbopol microgels. *Colloid and Polymer Science*, 270(2):183–193, 1992.

[176] Lubrizol. *Molecular Weight of Carbopol and Pemulen Polymers*, 9 2008. Rev. 2.

[177] Iris A Gutowski. *The effects of pH and concentration on the rheology of Carbopol gels*. PhD thesis, Department of Physics, Simon Fraser University, 2010.

[178] Lubrizol. *Viscosity of Carbopol Polymers in Aqueous Systems*, 8 2010. Rev. 3.

[179] Lubrizol. *Neutralizing Carbopol and Pemulen Polymers in Aqueous and Hydroalcoholic Systems*, 9 2009. Rev. 3.

[180] Fabien Mahaut, Xavier Chateau, Philippe Coussot, and Guillaume Ovarlez. Yield stress and elastic modulus of suspensions of noncolloidal particles in yield stress fluids. *Journal of Rheology (1978-present)*, 52(1):287–313, 2008.

[181] Giuseppe Perale, Carmen Giordano, Fabio Bianco, Filippo Rossi, Marta Tunesi, Francesco Daniele, Filippo Crivelli, Michela Matteoli, and Maurizio Masi. Hydrogel for cell housing in the brain and in the spinal cord. *The International journal of artificial organs*, 34(3):295–303, 2011.

[182] Giuseppe Perale, Pietro Veglianese, Filippo Rossi, Marco Peviani, Marco Santoro, Dorina Llupi, Edoardo Micotti, Gianluigi Forloni, and Maurizio Masi. In situ agar–carbomer hydrogel polycondensation: A chemical approach to regenerative medicine. *Materials letters*, 65(11):1688–1692, 2011.

[183] Filippo Rossi, Giuseppe Perale, and Maurizio Masi. Biological buffered saline solution as solvent in agar-carbomer hydrogel synthesis. *Chemical Papers*, 64(5):573–578, 2010.

[184] Filippo Rossi, Giuseppe Perale, Giuseppe Storti, and Maurizio Masi. A library of tunable agarose carbomer-based hydrogels for tissue engineering applications: The role of cross-linkers. *Journal of Applied Polymer Science*, 123(4):2211–2221, 2012.

[185] Filippo Rossi, Pietro Veglianese, Marco Santoro, Simonetta Papa, Cristina Rogora, Valentina DellOro, Gianluigi Forloni, Maurizio Masi, and Giuseppe Perale. Sustained delivery of chondroitinase abc from hydrogel system. *Journal of functional biomaterials*, 3(1):199–208, 2012.

[186] Ian N Sneddon. The relation between load and penetration in the axisymmetric boussinesq problem for a punch of arbitrary profile. *International Journal of Engineering Science*, 3(1):47–57, 1965.

[187] Heinrich Hertz. Über die berührung fester elastischer körper. 1882.

[188] Emiliano Fernández, Carmen Mijangos, Jean-Michel Guenet, M Teresa Cuberes, and Daniel López. New hydrogels based on the interpenetration of physical gels of agarose and chemical gels of polyacrylamide. *European Polymer Journal*, 45(3):932–939, 2009.

[189] A. D. Drozdov and J. Declaville Christiansen. Modeling the effects of ph and ionic strength on swelling of polyelectrolyte gels. *Journal of Chemical Physics*, 142(11), 2015.

[190] Salvador Mafé, José A Manzanares, Anthony E English, and Toyoichi Tanaka. Multiple phases in ionic copolymer gels. *Physical review letters*, 79(16):3086, 1997.

[191] Andrey V Dobrynin and Jan-Michael Y Carrillo. Swelling of biological and semiflexible polyelectrolytes. *Journal of Physics: Condensed Matter*, 21(42):424112, 2009.

[192] Gabriel S Longo, Monica Olvera de La Cruz, and I Szleifer. Molecular theory of weak polyelectrolyte gels: the role of ph and salt concentration. *Macromolecules*, 44(1):147–158, 2010.

[193] Jing Hua, Mithun K Mitra, and M Muthukumar. Theory of volume transition in polyelectrolyte gels with charge regularization. *The Journal of chemical physics*, 136(13):134901, 2012.

[194] Sudipto K De, NR Aluru, B Johnson, WC Crone, David J Beebe, and J Moore. Equilibrium swelling and kinetics of ph-responsive hydrogels: Models, experiments, and simulations. *Microelectromechanical Systems, Journal of*, 11(5):544–555, 2002.

[195] Shuiqin Zhou and Benjamin Chu. Synthesis and volume phase transition of poly (methacrylic acid-co-n-isopropylacrylamide) microgel particles in water. *The Journal of Physical Chemistry B*, 102(8):1364–1371, 1998.

[196] Gerald S Manning. Limiting laws and counterion condensation in polyelectrolyte solutions i. colligative properties. *The journal of chemical Physics*, 51(3):924–933, 1969.

[197] Huixian Yan, Bo Jin, Songhua Gao, and Liwei Chen. Equilibrium swelling and electrochemistry of polyampholytic ph-sensitive hydrogel. *International Journal of Solids and Structures*, 51(23):4149–4156, 2014.

[198] Fukun Lai and Hua Li. Modeling of effect of initial fixed charge density on smart hydrogel response to ionic strength of environmental solution. *Soft Matter*, 6(2):311–320, 2010.

[199] Sarthok Sircar, James P Keener, and Aaron L Fogelson. The effect of divalent vs. monovalent ions on the swelling of mucin-like polyelectrolyte gels: Governing equations and equilibrium analysis. *The Journal of chemical physics*, 138(1):014901, 2013.

[200] Lubrizol. *Pharmaceutical Polymers Typical Properties and Specifications*, 10 2013. Rev. 1.

[201] SJ Curran, RE Hayes, A Afacan, MC Williams, and PA Tanguy. Properties of carbopol solutions as models for yield-stress fluids. *Journal of food science*, 67(1):176–180, 2002.